SC71046.FR

Copy No. 4

Fundamental Studies of Diamond Growth and Surface Reactions

Final Report
for February 01, 1991 through May 31, 1994

CONTRACT NO. N00014-91-C-0048

Prepared for:

Scientific Officer
Division Head, Materials Division
Office of Naval Research
800 North Quincy Street
Arlington, VA 22217-5000
Attn: Dr. Pohanka

Prepared by:

Alan B. Harker

July 1994

Rockwell International
Science Center

The Contractor, Rockwell International Corporation Science Center, hereby certifies that, to the best of its knowledge and belief, the technical data delivered herewith under Contract No. _____ is complete, accurate, and complies with all requirements of the contract.

8/4/94
Date

/AB Harker
Name and Title of Certifying Official

Table of Contents

LIST OF FIGURES

1.0 Introduction

This report summarizes the research carried out during the period March 1991 through May 1994 at Rockwell Science Center under ONR contract No. N00014-91-C-0048. This contract was part of the ONR directed effort on the development of polycrystalline diamond as an optical material. A primary focus of the research was investigating the relationships between the microstructure of polycrystalline diamond and its optical and mechanical properties. The program also involved a considerable effort in the development of characterization techniques for observing the fundamental properties of thick and thin diamond films. A secondary goal of the research was the investigation of the surface reactions of diamond to evaluate their potential for reactive polishing applications. Polishing is critical not only to the ultimate application of diamond as an optical material, but also to the characterization of its detailed microstructure.

Also included in this program was an additional task, funded by the Naval Air Warfare Center Aircraft Division (NAWCAD) at Warminster, PA. The additional task was to devise a methodology for bonding diamond with an integral gradient index antireflective surface (moth-eye) to germanium and zinc sulfide and to provide samples of the bonded composites to NAWCAD for liquid jet impact testing.

The research conducted under this program resulted in a number of technical articles describing the detailed findings. Reprints of these articles are appended to this report, which summarizes the significant results.

2.0 Effects of Growth Conditions on Microstructure

Much of our reported activities have dealt with developing an understanding of the empirical relationships between microwave plasma assisted chemical vapor deposition (MPACVD) growth chamber conditions and the resultant microstructure of the polycrystalline diamond films. The program findings have been largely published in a series of articles relating growth conditions and the competition between etching and growth to the observed microstructure. The primary findings as they relate to the development of optical quality polycrystalline diamond are that the conditions which produce the least (100) facets in the films provide the highest optical transparency[5].

Not clear is if the conditions that produce the (100) orientation in the films also lead to sp2 and hydrogen impurities or whether the (100) facets themselves provide host sites for the

impurities. We have observed several features associated with (100) facet development that indicate that this orientation is both formed under conditions unfavorable to high purity diamond growth and that this facet itself promotes inclusions and impurity stabilization. These include:

a) Step Growth: Films that have the diamond (100) axis largely normal to the growth plane exhibit a strong step growth (Figure 1). This produces a high number of growth sites in which multiple bonds are involved in the addition of new carbon radicals to the growth surface, thus providing increased opportunities for impurity stabilization.

SCP.0487C.072594

Fig. 1. Scanning electron micrograph of (100) textured diamond crystallites showing strongly defined step or ledge growth.

b) Non-Diamond Carbon At Grain Boundaries: In our plasma torch single crystal growth studies with (100) seeds, we have routinely observed that the rapid out-of-plane growth of (100) facets produces a high level of renucleation at the grain edges (Fig. 2). Thus, though the exposed (100) face appears highly crystalline, the grain edges show distinct non-diamond morphology either due to physical shielding of the grain edges from the plasma or the stabilization of renucleation centers.

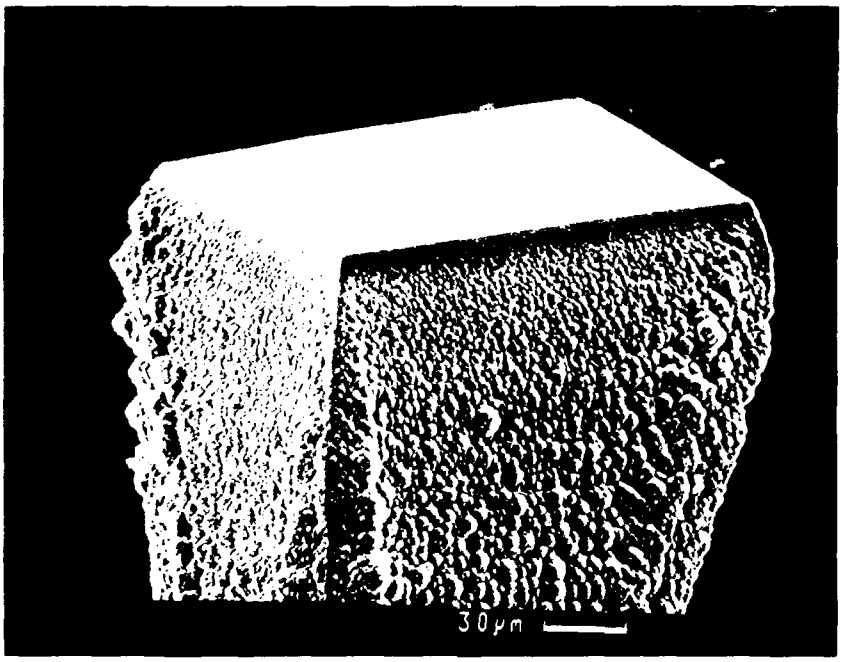

SCP.0488C.072594

Fig. 2. A diamond single crystal growing in the (100) direction, which shows very heavy renucleation at the grain edges not directly exposed to the primary plasma.

c) (100) Growth Conditions: The (100) facets are the first to appear when growth conditions move away from amorphous carbon and into the diamond formation regime (i.e., high carbon content, low etchant concentration).

d) Growth Rates: The highest rates of growth appear associated with (100) crystallites, indicating a very high level of stabilization of ad-atoms versus etching.

At the extreme of low carbon reactant concentration, diamond crystallite growth only slightly exceeds the rate of surface etching by H atoms and other reactive species. Under these conditions (220) axis normal oriented films are prevalent. The dominant exposed facet is the triangular (111) face of diamond and individual grains grow to termination. Renucleation and twin defects provide the dominant method of continued grain development. The rapidly etched (100) grains are generally absent from films grown under these conditions (Fig. 3).

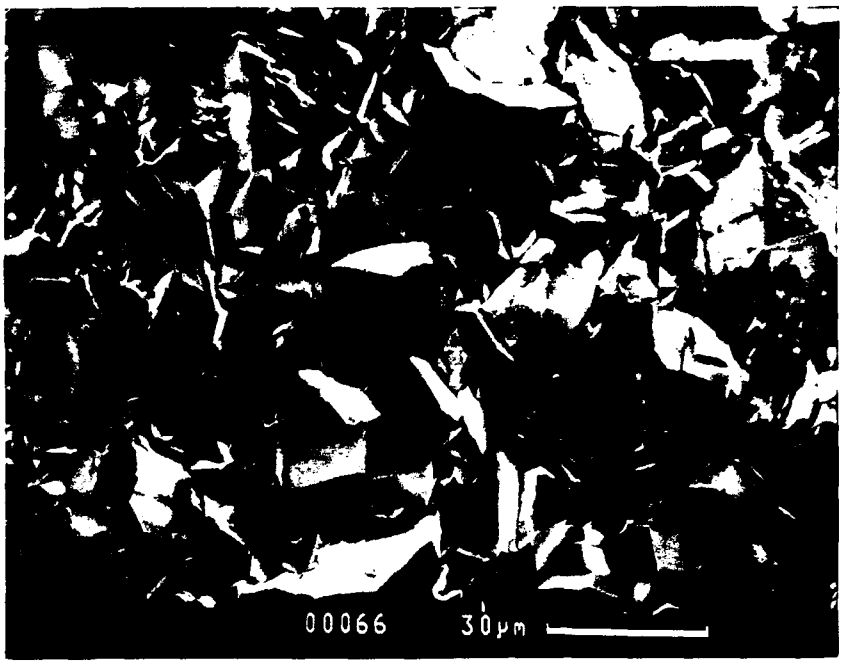

SCP.0486C.072594

Fig. 3. Scanning electron micrograph of a polycrystalline diamond surface with low hydrogen impurity content. The microstructure has preferential (220) and (111) texture.

Of the preferentially oriented films grown in this program, those with the (220) and related (331) axis normal to the growth plane have exhibited the highest optical transparency. This is consistent with the properties of films produced by other organizations that we have had the opportunity to characterize. These films are generally grown at hydrocarbon concentrations of 0.25 to 0.5% at temperatures of 750 to 1050°C and with the presence of oxygen or water. High etching levels to remove impurities is critical to producing the films with minimum hydrogen impurities.

3.0 Microlithography of Diamond Surfaces

During the study of diamond microstructures, it became clear that the presence of scratches and other surface features greatly influenced both the nucleation and adhesion of the growing diamond film. To further explore this phenomenon, a number of different grid and line patterns were generated on the surfaces of silicon and fused silica substrates, and films were grown under conditions that produced significant levels of tensile stress at the diamond-substrate interfaces. Films grown on substrates without etch patterns often showed loss of adhesion. Those films

grown on etched substrates remained adhered up to and past the point where the interfacial stresses caused subsurface fractures in the substrates.

The presence of fine scale (1 to 3 micron) features etched into a substrate surface also produced much more dense nucleation and often created highly regular grain shapes in the initial film. These results established the basis for improving the adhesion of diamond films to dissimilar substrates such as germanium and zinc sulfide and provided the necessary technology to produce the first diamond moth-eye, gradient optical index of refraction, antireflective surfaces. These results were reported in several scientific publications[4,10,11].

4.0 Polishing

To examine the detailed microstructure of the polycrystalline diamond it is necessary to remove the gross surface features. This permits the use of optical microscopy to probe the depth of the transparent material and the investigation of detailed defect structure through the use of the charge contrast electron backscatter imaging technique developed under this contract[16]. High quality polishing is also required to obtain an absorption coefficient as a function of wavelength and to investigate the temperature dependence of the absorptions in the material.

In the diamond gem industry, mechanical polishing procedures have been developed to obtain an optical quality finish on small-scale diamond surfaces. The general process involves either mechanical abrasion on high speed laps with oil and diamond grit, or single point turning with a diamond tip. Mechanical polishing has been the initial method of choice for use with polycrystalline diamond plates; however, with larger sized parts becoming available, the time scales and yields involved become increasingly undesirable.

Alternative approaches to diamond polishing that have been evaluated include reactive ion etching, ion implantation, laser ablation, and direct contact at high temperature with metals and SiOx surfaces. Each of these processes has some potential, but suffer in ease of adaptation for the optical finishing of both flat and curved surfaces.

Primary attention in this program was given to exploring reactive techniques that have the potential for ease of scaling to larger sizes and shaped surfaces. Specific systems investigated included hot iron and manganese plate lapping, molten rare earth contact, reactive ion etching in oxygen and hydrogen, and molten salt exposure. Each technique achieved some degree of success, and each had rather severe limitations.

Metal Plate Lapping

A series of experiments were carried out to evaluate the use of iron and steel alloy plates as lapping surfaces for the removal of the coarse roughness of CVD diamond surfaces. The experiments were run at temperatures from 650 to 900°C and used plates made of base iron, base manganese, cast iron, and several soft steel alloys. The results of the experiments with iron plate lapping were reported in the literature [7,9].

The critical observation was that the direct contact diamond-iron lapping process was extremely temperature dependent. At the alpha to gamma phase transition point, 723°C, carbon solubility of iron increases by a factor of 40 to 0.8%. At temperatures above this, the dissolution of diamond into iron is significantly accelerated. The reaction is solubility limited but can be run continuously if a hydrogen atmosphere is maintained to reactively convert the dissolved carbon to methane.

The same basic reaction occurs with other transition metals with carbon solubility; however, temperatures above 725°C are generally required. The primary limitation of the process then becomes one of maintaining the desired physical contact and orientation between the lapping plate and diamond surface.

Our primary success in the use of the metal-diamond contact polishing came through the use of a heated metal stylus tracing over the surface of a rotating diamond plate. The schematic in Fig. 4 shows the basic mechanical arrangement. With a stepping motor controlling the sway rate and amplitude, the stylus could be passed over the surface with a controlled load and maintain contact at all times. This approach is capable of producing an extremely fine surface finish with a roughness less than 0.4 nm by atomic force microscopy. This approach is also capable of following contours and is perhaps best suited to final lapping rather than to general area surface facet removal.

Reactive oxygen ion etching was also studied and reported in the literature[7]. The basic process consisted of using a heated substrate holder to immerse the diamond part in a reactive oxygen plasma operating at about 100 watts and 300 millitorr. The greatest limitation was the exaggerated rate of etching at grain boundaries. This was overcome by initially coating the diamond surface with a thin gold layer and then mechanically abrading the surface to expose the tallest diamond facets. The part could then be etched until the full surface was exposed and gross roughness was removed. This process was, however, fairly slow, with the rate decreasing with

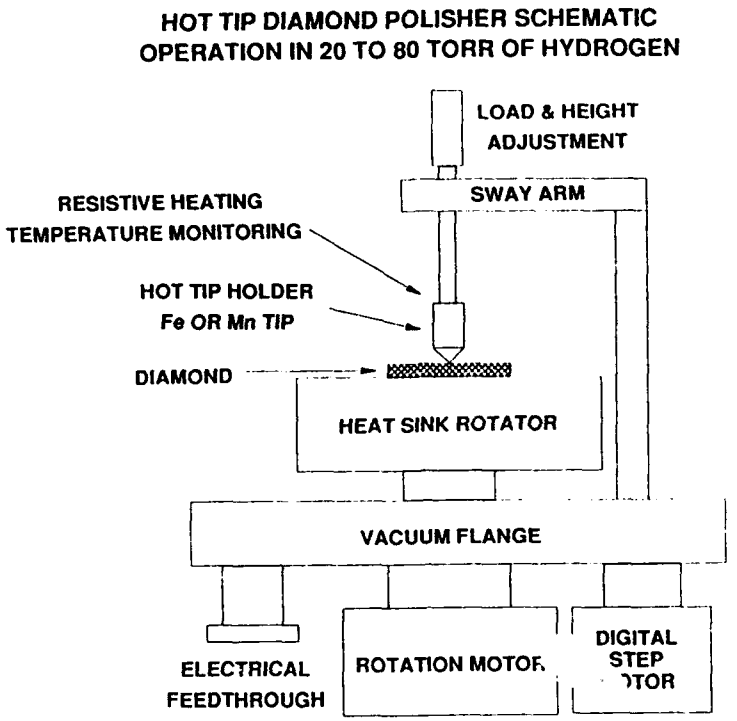

Fig. 4. Schematic of heated metal stylus diamond lapping apparatus.

time to about 1 micron per hour after exposure for a period of 4 hours. The initial rates seemed to be much higher due to the localization of the plasma near the exposed high facets. These initial rates were as high as 20 microns/hr, but were not sustained.

Molten Metal Dissolution

Studies with molten metal dissolution were limited to lanthanum and cerium metals. In both cases the viscosity of the melt required that the diamond be submerged. The result was a rounding of all surfaces during the dissolution, with saturation of the liquid metal by carbon being the limiting feature. High rates of dissolution, 50 to 200 microns/hour, were achieved with small parts in an inert atmosphere by this approach. The limitations of scaling are those associated with trying to establish controlled contact with a viscous molten metal.

Molten Salt Exposure

A range of molten salts including nitrates, hydroxides, chlorides, and fluorides was evaluated for their use as reactive polishing agents. The primary disadvantage of the salt approach

was the slow rates and the preferential etching of grain boundaries and defect zones. Figure 5 shows before and after micrographs of a large grained sample exposed to molten lithium fluoride for 24 hours. The facets show general area etching; however, grain boundaries and etch pits have been opened up to a far greater degree.

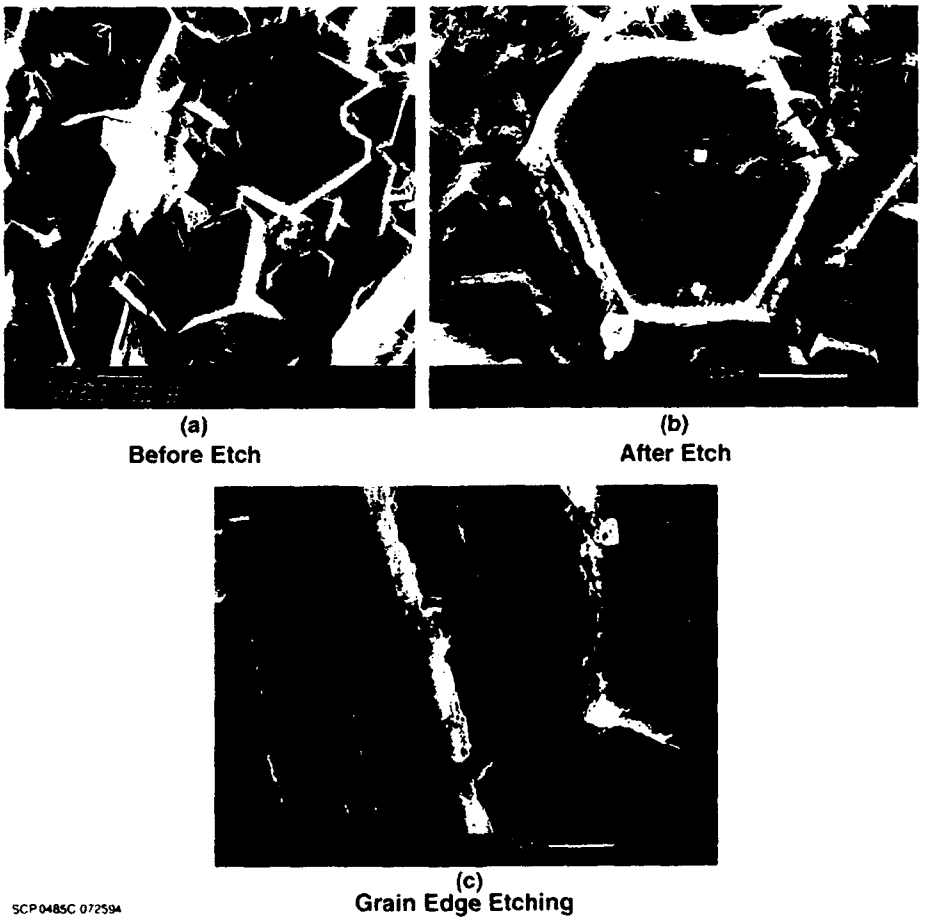

Fig. 5. Scanning electron micrographs of a polycrystalline diamond surface before and after etching by lithium fluoride.

Based on the above results, we focused primarily on the development of the metal stylus tip polishing approach during the ONR program. The polishing levels achieved were so near to the atomic level that new levels of microstructural characterization by electron microscopy became possible.

Since the end of technical efforts on this program, we have extended the metal polishing technology under IR&D. These experiments have resulted in the discovery of a combined metal–metal salt polishing approach that relies on the salt to transport metal cations to the diamond surface for reaction. The reaction rate (mg/hr of etching) has been shown to be linear with time to beyond 24 hours exposure, and the process appears to provide isotropic etching with (220) oriented films. The mechanism is still under study; results will be reported in the literature as they become available.

5.0 Charge Induced Electron Contrast Imaging

The high levels of surface smoothness made possible by the metal tip polishing technique led to the discovery that diamond samples placed in the electron microscope without a conductive coating showed very uneven charging effects, which were most noticeable in the secondary electron imaging mode. Detailed studies revealed that the charging phenomenon was associated with variable rates of local charge dissipation through highly local conductive pathways in the sample. The variable charge dissipation rates produce areas of dark and light contrast in the samples, which provide a direct image of the near-surface crystalline defect structure.

Details such as grain boundaries, twin boundaries, and the unique five–fold multiple twin defect can be observed on the surface of the diamond films. Extension of the technique to samples polished by other techniques showed that the Edge Technologies, Inc., reactive diamond polishing approach provided sufficient surface smoothness to observe the effect as did large as-grown facets of individual crystallites with unpolished samples. The methodology for the technique is described in two journal articles[16,17].

6.0 Characterization of Spectroscopic Properties of Diamond

To relate the microstructure of the diamond films to their spectroscopic properties, a number of temperature dependent infrared and microwave measurements were carried out with samples supplied by the major diamond fabricators. These measurements consisted of infrared transmission and emission measurements between 2 and 15 microns wavelength and a direct spectroscopic measurement of the dielectric constant and loss tangent of polycrystalline diamond at 37 GHz in the millimeter wave region. The temperature dependence of these properties was observed between 300 and 750K.

The principal results of these measurements have been reported at the annual program reviews and made available to Dr. Daniel Harris, the program technical contract monitor. Three publications also resulted from these efforts[9,12,20]. The measurements showed a strong correlation between the observed spectroscopic properties and sample microstructures. The microwave loss tangent measurements correlated directly with the impurity levels in the samples, which acted as absorption centers. The dielectric constant was, however, fairly consistent for all samples and agreed well with the single crystal value.

In the highest optical quality samples, the absorption coefficient and emission at 10–12 microns wavelength was near the limit of detection for the dual and single beam spectrometers used in the measurements. Only at the highest temperatures investigated, 600–750K, was signal sufficient to obtain accurate measurements. The best quality samples had room temperature extinction coefficients ranging from 0.1 to 0.3 cm^{-1} at 10 microns wavelength and had preferred (220) and (111) crystalline orientations. The highest quality sample ((220) oriented) had a measured emissivity of 0.02 at 10 microns wavelength at 748K at a thickness of 0.914 mm, corresponding to an extinction coefficient of 0.22 cm^{-1} at that temperature.

7.0 Bonded Diamond Composite Windows

As an additional task to the basic ONR program, a more directed technical effort was carried out for NAWCAD, Warminster, PA. The added task was to evaluate techniques for achieving diamond hardening layers on germanium infrared windows and to deliver such samples to NAWCAD for impact damage testing. This program evaluated both the growth of diamond on germanium and the bonding of diamond plates to germanium using a long wave infrared transparent adhesive developed at the Science Center.

The initial work in growing diamond on germanium took advantage of previous efforts in using lithography to control and induce the nucleation and adhesion of diamond on dissimilar surfaces[4]. This work resulted in the first-ever diamond moth-eye antireflective surface being grown on an IR transparent substrate[11]. The diamond moth-eye on germanium had excellent optical properties (> 95% transmission) and abrasion resistance, but was not thick enough for high impact damage resistance.

The first diamond layers bonded to germanium and zinc sulfide were prepared and tested by liquid jet water drop impact. The initial results were quite encouraging, showing that damage levels in both germanium and zinc sulfide could be improved by at least 150 m/s with a diamond

layer of about 50 microns[8,13]. Later work focused more on the optimization of the physically graded index of refraction moth-eye surfaces (Fig. 6) to provide an all-diamond optical surface for high impact resistance applications. These results were the first experimental verification of the basic design rules for the microscopically textured surfaces, and the results were reported in the literature[15,19].

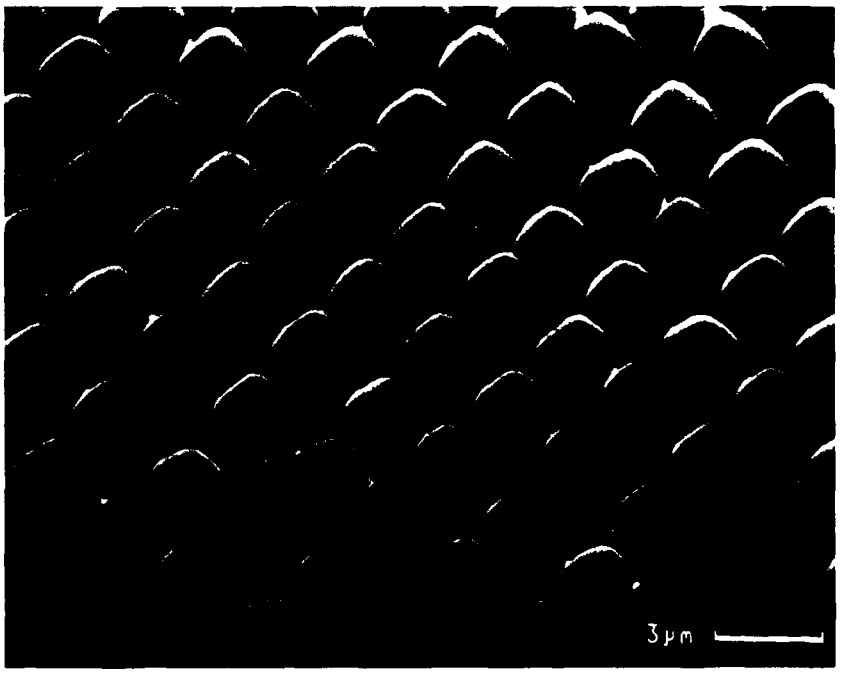

Fig. 6. Scanning electron micrograph of a diamond moth-eye textured surface.

The use of the moth-eye antireflection surfaces in diamond and the concept of using adhered layers for improved rain erosion resistance is being furthered developed under Air Force sponsorship[22]. Under this continued development effort, a 340 micron thick diamond plate bonded to zinc sulfide has been demonstrated to withstand 650 mph rain impacts in the Wright Materials Laboratory whirling arm facility; and the moth-eye surface features can survive this level of erosion exposure[23].

8.0 Residual Stress Characterization

Much of the later work in the program was centered on determining stress levels in growing polycrystalline diamond films and attempting to determine the extrinsic and intrinsic

sources. Much of the work involved establishing characterization tools for both observing the samples during growth and carrying out post-growth lattice strain measurements. The in-situ temperature and plasma observation studies involved the use of digital CCD cameras with sensitivity from the visible to 1.1 microns wavelength in the near infrared (Fig. 7.). Sample temperature distributions were observed and related to macroscopic strain in the silicon substrates. These studies showed that substrate distortion was related both to the absolute temperature and the temperature distribution on the growing surface. Competition between the differential thermal expansion stress and the tensile growth stresses could produce measurable residual stresses of 200 to 300 MPa in the surface on the diamond films on silicon. These stresses are greatly relieved when the sample is removed from the substrate. Even more significant was the observation that anisotropic distortion in the substrate and growing diamond film could be observed in 2–inch diameter samples when surface temperatures varied by more than 10K across the surface.

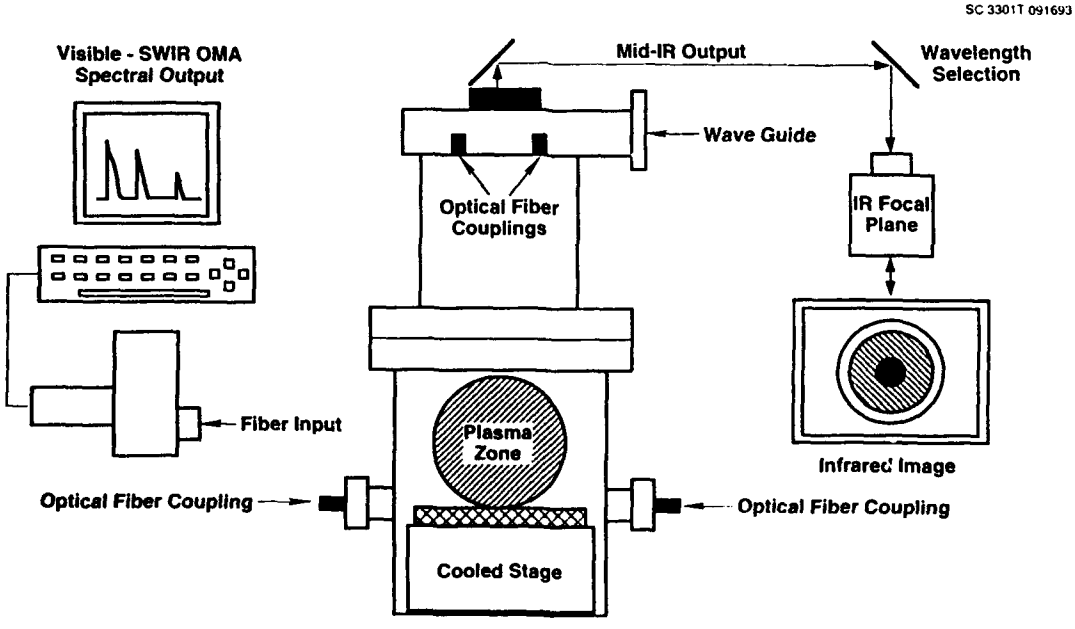

Fig. 7. Schematic of the multicamera arrangement developed to observe the growth plasma emission and the temperature distribution on the diamond growth surface in an MPACVD chamber.

Since the growth stresses were sufficient to induce surface cracks in the growing samples (Fig. 8), more detailed studies of stress distribution were carried out. The basic analysis tool was

electron channeling in a scanning electron microscope (SEM) equipped with the beam rocking feature for this technique. Measurements of the line spacings and crossing angles in these highly symmetric patterns provide data on lattice strain and direction. Using the electron channeling technique for mapping showed that the strains were balanced within the individual grains, and that the strain distributions conformed to the general shape of the grains and the presence of defect boundaries. Measurements at twin defects showed lower levels of strain near the twin boundary. Strains equivalent to stress levels of 500 to 800 MPa can be resolved in diamond by this technique, and such strains were observed to be present in individual grains[18,21].

Fig. 8. Scanning electron micrograph of growth stress induced surface cracking in a (220) oriented polycrystalline diamond.

9.0 Summary

The research conducted in this program covered a fairly wide area and was reoriented several times to address the emerging technical issues in diamond growth. Progress in this and other laboratories often made current studies less pertinent as diamond growth techniques matured. Issues that are still of great concern are the need to control growth stresses and to improve post growth polishing techniques. We are addressing these areas through attempting to produce more

equiaxial grain morphologies for stress control and the use of metal + metal salt reactive etching. The issues of growth rates, area coverage, and expense are being addressed in numerous laboratories as commercialization of the technology occurs.

The investigators in this program are grateful to the Office of Naval Research for sponsoring this very exciting research program and acknowledge the technical input and helpful direction provided by Dr. Robert Schwartz, Dr. Daniel Harris, and Mr. Michael Wilson, the program technical contract monitors.

10.0 References

1. A.B. Harker, "Properties of Low Temperature Plasma CVD Diamond Films", in *Proceedings of Diamond Optics II,* SPIE 33rd Annual International Symposium on Optical and Optoelectronic Applied Science and Engineering, San Diego, CA (August 6–11, 1989) pp. 152–158 (1989).

2. A.B. Harker and J.F. DeNatale, "Temperature and Reactive Etching Effects on the Microstructure of Microwave Plasma Deposited Diamond Films", *J. Mater. Res.*, Vol 5, No. 4, pp. 818–823 (1990).

3. A.B. Harker, J.F. DeNatale, and J.F. Flintoff, "Microstructure of Diamond Films as a Function of Deposition Conditions", *Proceedings of the Diamond III Symposium,* SPIE vol 1325, pp. 202–209 (1990).

4. J.F. DeNatale, J.F. Flintoff, and A.B. Harker, "Microstructural Control of Diamond Thin Films by Microlithographic Patterning", *J. Appl. Phys.* **68(8)**, 4014–4019 (1990).

5. J.F. DeNatale, A.B. Harker, and J.F. Flintoff, "Microstructure and Orientation Effects in Diamond Films", *J. Appl. Phys.* **69(9)**, 6456–6460 (1991).

6. A.B. Harker and J.F. DeNatale, "Pressure Effects in the Microwave Plasma Growth of Polycrystalline Diamond", *Proceedings Diamond Optics IV, Diamond Optics IV,* SPIE Volume 1534, pp. 2–8 (1991).

7. A.B. Harker, "The Polishing of Polycrystalline Diamond Films" *Proceedings of the Diamond III Symposium,* SPIE vol 1325, pp. 222–229 (1990).

8. M. Wilson, I. Perez, M. Thomas, J.B. Boodey, W.R. Scott, and A.B. Harker, "Liquid Jet Impact Measurements in Diamond Coated Ge Substrates", Materials Science Monographs, 73, *Applications of Diamond Films and Related Materials,* Y. Tzeng, M. Yoshikawa, M. Murakawa, and A. Feldman, eds. (Elsevier Science Pub. B.V., Amsterdam, 1991), pp. 217–220 (1991).

9. A.B. Harker, "Reactive Polishing of Polycrystalline Diamond and Measured Spectroscopic Properties", in *Applications of Diamond Films and Related Materials,* Y. Tzeng, M. Yoshikawa, M. Murakawa, and A. Feldman, eds. (Elsevier Science Pub. B.V., Amsterdam, 1991), pp. 223–226 (1991).

10. J.F. DeNatale, J.F. Flintoff, and A.B. Harker, "Effects of Interfacial Modification on Diamond Film Adhesion", *Diamond Optics IV,* SPIE Proceedings 1534, pp. 44–48 (1991).

11. J.F. DeNatale, P.J. Hood, J.F. Flintoff, and A.B. Harker, "Fabrication and Characterization of Diamond Moth Eye Antireflective Surfaces on Ge", *J. Appl. Phys.* **71(3)**, 1388 (1992).

12. A.B. Harker and W.W. Ho, "Dielectric Properties of Synthetic Polycrystalline Diamond", *Proceedings of the 4th Electromagnetic Windows Symposium,* Monterey, CA, 1991. *Limited Distribution*

13. A.B. Harker, J.F. DeNatale, M. Thomas, and M. Wilson, "Polycrystalline Diamond Anti-Erosion Coatings for IR Optics", *Proceedings* of the IRIS IR Materials and Detectors Symposium, Moffet Field, CA, pp. 10–14, (August 1992). *Limited Distribution*

14. J.F. DeNatale, J.F. Flintoff, and A.B. Harker, "Adhesion Improvement in Diamond Films by Microlithographic Patterning", *J. Mat. Sci.* **27**, 553–556 (1992).

15. A.B. Harker and J.F. DeNatale, "Diamond Gradient Index 'Moth Eye' Antireflective Surfaces for LWIR Windows", in *Window and Dome Technologies and Materials III*, ed P. Klocek, SPIE Volume 1760, pp. 261–267 (1992).

16. A.B. Harker, J.F. DeNatale, J.F. Flintoff, and J.J. Breen, "Direct Observation of the Defect Structure of Polycrystalline Diamond by Scanning Electron Microscopy", *Applied Physics Letters*, **62(24)**, 3105–3107 (1993).

17. A.B. Harker, D.G. Howitt, J.F. DeNatale, and J.F. Flintoff, "Charge Sensitive Secondary Electron Imaging of Diamond Microstructures", *Scanning*, Vol. 16, 87–90 (1994).

18. A.B. Harker, M.R. James, D.G. Howitt, J.F. DeNatale and J.F. Flintoff, "Residual Stress Measurements on Polycrystalline Diamond", to be published in the SPIE proceedings of Window and Dome Technologies IV, San Diego, CA (July 1994).

19. A.B. Harker, J.F. DeNatale, and J.F. Flintoff, "Optical and Mechanical Performance of Diamond Moth-Eye Antireflective Surfaces for LWIR Windows", *Proceedings of the 5th DoD Electromagnetic Windows Symposium*, Boulder CO, Wright Laboratory Technical Report, WL-TR-93-4117, p. 425 (1993). *Limited Distribution*

20. M.E. Thomas, A.B. Harker, and J. Trombetta, "Temperature Dependence of Absorption in CVD Diamond", to be published in the SPIE proceedings of Window and Dome Technologies IV, San Diego, CA (July 1994).

21. A.B. Harker, presented at "Workshop of Characterizing Diamond Films III", February 23–24, 1994, Gaithersburg, MD. NISTIR 5418 (1994).

22. Diamond Interface Studies, USAF Wright Materials Laboratory contract No. F33615-92-C-5968 (1992–1996)

23. A.B. Harker, "Diamond Optical Surfaces for IR Windows", presented at IRIS Specialty Group on IR Materials, Boulder, CO, August 15–16, 1994. *Limited Distribution*

Appendix 1

Properties of Low Temperature Plasma CVD Diamond Films

Properties of low temperature plamsa CVD diamond films

Alan B. Harker

Rockwell International Science Center
Thousand Oaks, CA 91360

ABSTRACT

In the microwave plasma deposition (PECVD) of diamond from methane, the variables available for controlling the microstructure of the resulting films are the plasma composition and density, the substrate surface properties, and the temperature. It has been demonstrated that the competition between nucleation site formation and the rate of reactive plasma etching is the critical feature in the development of the film microstructure. Through reducing the deposition temperature and enhancing the etching rates of sp2 carbon, fine grained optical quality diamond films have been produced.

INTRODUCTION

A critical limitation in the exploitation of synthetic diamond films is the need to control their microstructure. Wide band-gap semiconductor applications require hetero-epitaxial films while highly smooth, fine grained polycrystalline films are needed for tribological and optical applications. In this work a parametric study has been carried out to determine the process variables controlling the microstructure and crystallinity of sp3 bonded diamond films produced from a microwave-induced plasma composed of methane, hydrogen, and oxygen. The primary analytical tools used in the study were infrared spectroscopy, electron microscopy, and Raman scattering spectroscopy.

In the formation of diamond films the initial process involves the formation of chemical bonds between the substrate and carbon-carbon and carbon-hydrogen bonded molecules. These nucleation centers than act as sites for the bonding of additional adatoms and clusters. This typical film growth process is limited, however, by the reactive etching of the growing film by the excited hydrogen, oxygen, and radical species such as OH present in the plasma environment. The ability to produce pure crystalline diamond relies on the process conditions being established in which the sp2 bonded, graphitic carbon, and carbon-hydrogen bonds are etched away at a rate sufficiently fast that only the more strongly bonded metastable sp3 diamond carbon remains in the growing film. Hence, the process of attempting to control the microstructure in the diamond films must be considered as one of balancing the rates of the nucleation, growth, and etching processes occurring in the system.

EXPERIMENTAL

The deposition experiments were carried out in a turbomolecular pumped stainless steel vacuum chamber equipped with an Applied Science and Technology 1000 W magnetron plasma source. The chamber had a baked base pressure of 10^{-8} torr. Experimental conditions ranged from pressures of 12 to 50 torr with substrate temperatures of 450 to 1150°C as measured by infrared pyrometry. In all cases the pyrometric measurements were made on Si wafers with an assumed emission of 0.96. Gas mixtures were typically hydrogen containing 1 volume percent methane and 0.25 volume percent oxygen. Substrates used in the experiments were (100) oriented silicon wafers, fused quartz, random oriented sapphire, (100) germanium, and (100) natural diamond.

in Proceedings of Diamond Optics II", SPIE 33rd Annual International Symposium on Optical and Optoelectronic Applied Science & Engineering, San Diego, CA (Aug. 6-11, 1989) pp. 152-158, (1989).

Microstructural characterization of the films was carried out by electron microscopy using a Phillips 400 and CM-30 for transmission electron microscopy (TEM) and selected area electron diffraction (SAD) analysis. Scanning electron microscopy (SEM) and selected area electron channeling were also used. Spectroscopic analysis included infrared transmission and reflection measurements with a scanning dual beam spectrophotometer, integrating sphere light scattering measurements at 3.39 μm, and micro-Raman scattering. The micro-Raman scattering measurements were made with a nominal 5 μm spot size, which could be defocused to obtain broader area analysis.

RESULTS AND DISCUSSION

As previously reported by other investigators,[1,2,3] a plasma discharge of 1% CH_4 in H_2 at low pressures and temperatures between 800 and 1200°C produces the nucleation and growth of diamond and diamond-graphite films. These films are typically polycrystalline, highly faceted, and have individual grains with linear dimensions ranging from 3 to 10 μm as shown in the scanning electron micrograph in Figure 1. The film microstructure in Figure 1 is from a region of film growing directly below the visible discharge in the chamber at 1040°C. The grains are strongly faceted and show the dominance of individual grain growth over nucleation. The major limitation in the out-of-plane growth of the individual crystallites is the high density of twinning and stress induced defects. These defects cause continual reorientation of the crystalline faces during deposition, inhibiting grain growth and reducing any orientation of the film to the substrate. The size of the individual grains is determined in part by the density of the initial nucleation centers and in part by the development of new growth directions in the individual crystallites.

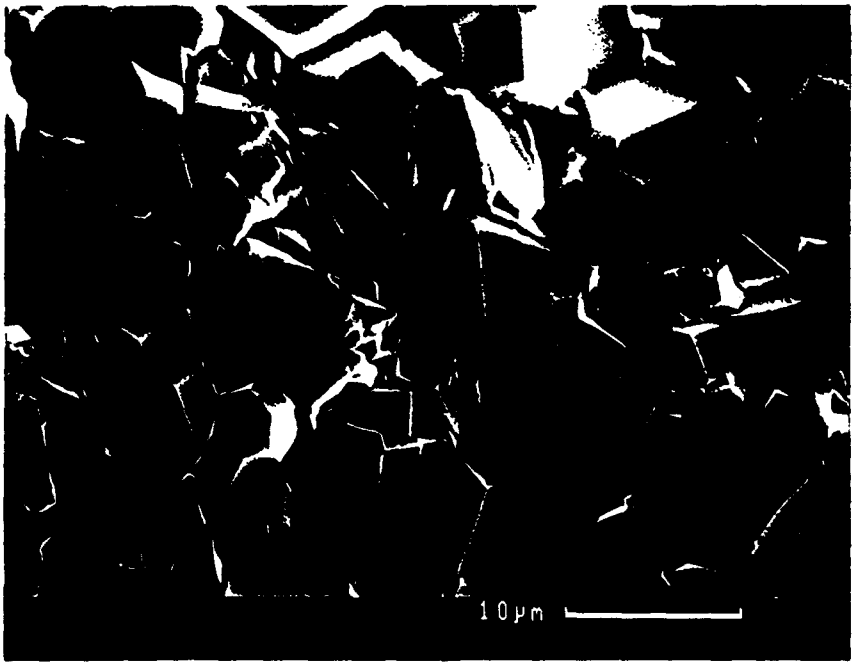

Fig. 1. Scanning electron micrograph of a highly faceted diamond film deposited at 1040°C.

The density of nucleation sites is relatively low due to the high mobility of the plasma generated species arriving at the substrate, and the high temperature of the substrate itself. Lattice matching and several surface pretreatments, such as scratching with diamond grit, can enhance the density of nucleation centers, but such high temperature films typically have super-micron grain size and rough faceted surfaces which cause light scattering.

Oriented Grain Growth

For optical and electronic applications epitaxial film growth or at least grain-oriented polycrystalline films with smooth surfaces are desired. In order to achieve such growth, both the lattice match between the diamond film and substrate and the etching versus deposition rate must be maximized. High lattice match optimizes the potential nucleation site formation with direct relationship to the substrate lattice, while increasing the etching process favors the removal of less stable defect based growth sites. Further enhancement in orientation comes from reducing the deposition temperature to limit stacking faults, twinning, and other stress related defects.

By maintaining all conditions the same as described above, but dropping the deposition temperature to nominally 450°C, a significant reduction in the degree of stress related defects can be achieved as shown by TEM analysis. The result of the lower density of defects in the nucleating grains is that existing grains have the opportunity to grow while maintaining their original orientation to the substrate.

The effect of reducing the stress in the growing film, while enhancing the formation of nucleation centers at lower temperatures is the formation of finer grained, oriented films on (100) Si substrates and the formation of stress free homo-epitaxial films on (100) natural diamond substrates. Figure 2 shows SEM micrographs of two films formed on (100) silicon substrates at a nominal substrate temperature of 450°C at different distances from the plasma ball. The finer grained film, formed 1.5 cm from the plasma is randomly oriented. The slightly coarser film, formed directly beneath the plasma ball, is oriented with 220 plane parallel to the 100 plane of the substrate. The orientation of the textured film can be seen by the significant enhancement of the 220 Bragg reflection in Figure 3.

When a natural (100) oriented diamond substrate was coated under the same conditions as used for the oriented film on silicon (30 torr, 1% CH_4 in H_2, 0.25% O_2 450°C) a homo-epitaxial film was formed. The epitaxial nature of the film was confirmed by X-ray diffraction and electron channeling in the SEM. The channeling pattern in Figure 4 which shows the diamond cubic symmetry propagated throughout the film, would be totally absent if any significant stress or lack of orientation was present in upper 100 nm of the film. Raman and IR analysis of the films shows them to be true diamond with little sp2 bonding contribution (Figure 5). Figure 6 shows the calculated (assuming a refractive index of 2.4) and observed transmission from a 1.9 μm thick diamond film on silicon formed at 450°C. The good agreement shows the lack of scattering and adsorption in the 6 to 50 μm spectral region of the IR.

CONCLUSIONS

The microstructure and orientation in diamond films formed on silicon substrates from a microwave-induced plasma of CH_4 in H_2 can be highly modified by the addition of reactive etchants such as oxygen, altering the deposition temperature, and altering the distance of the substrate from the plasma center. Higher temperatures favor low nucleation rates, enhanced grain growth and high defect levels. Lower temperatures favor nucleation, lower stress, and sustained orientation to the substrate. The presence of oxygen in the plasma serves to enhance faceted growth through the preferential etching of non sp3 bonded species forming on the film

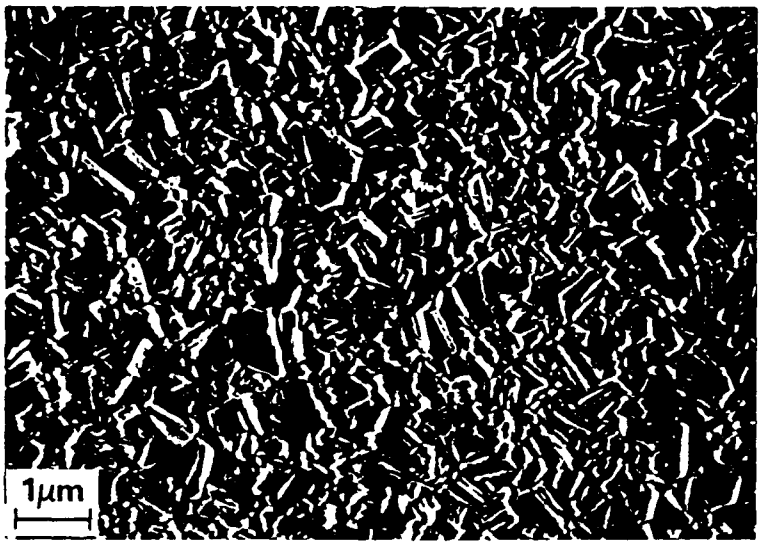

(a)

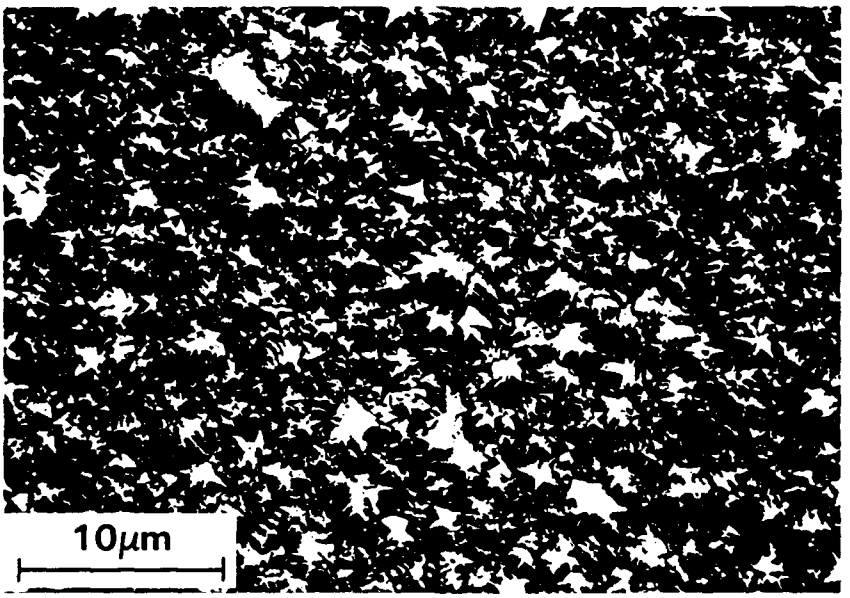

(b)

Fig. 2. Scanning electron micrographs of (a) a fine grain randomly oriented diamond film on (100) silicon and (b) a oriented diamond film on (100) silicon, both deposited at a nominal surface temperature of 450°C.

surface. At substrate temperatures below 500°C fine grained oriented diamond films have been produced upon (100) silicon and full epitaxy has been achieved on natural (100) diamond.

ACKNOWLEDGEMENT

Portions of this work were sponsored by the United States Office of Naval Research under Contract No. N00014-85-C-0140.

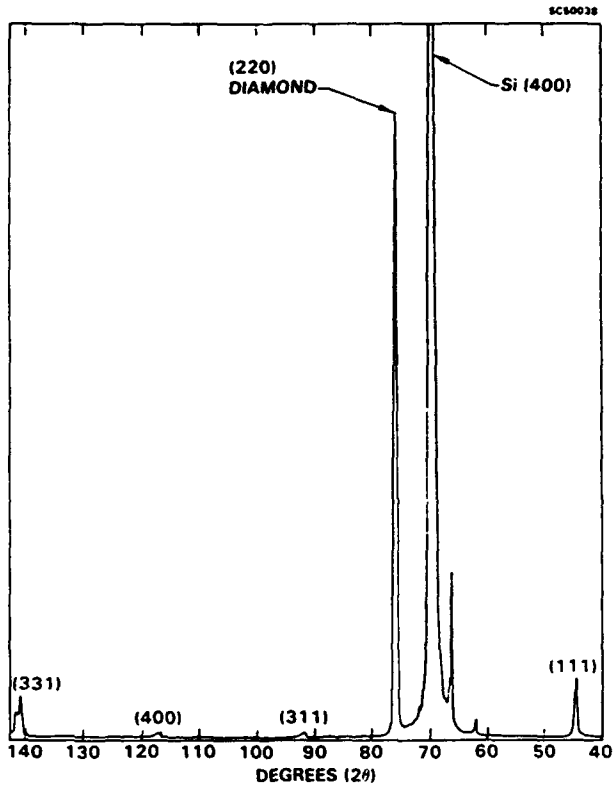

Fig. 3. Scanning x-ray diffraction pattern of a (220) oriented diamond film formed on (100) silicon.

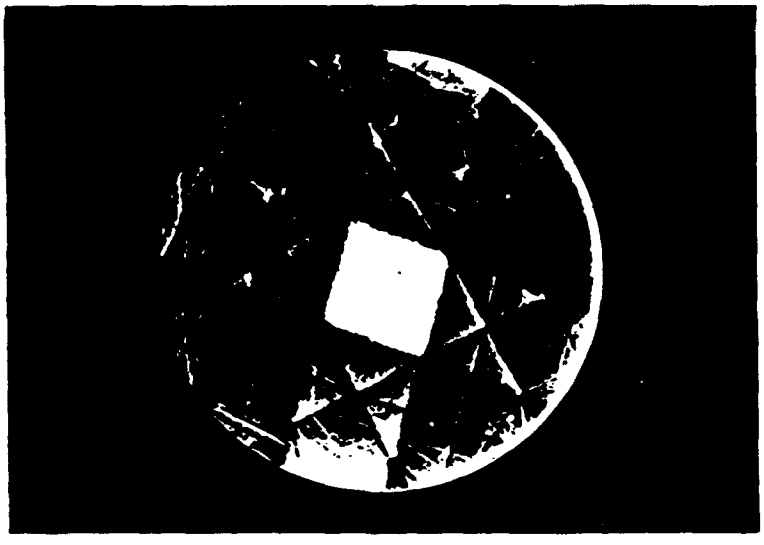

Fig. 4. An electron channeling pattern produced from a 2 μm thick homo-epitaxial diamond film formed on a type 2A (100) natural diamond.

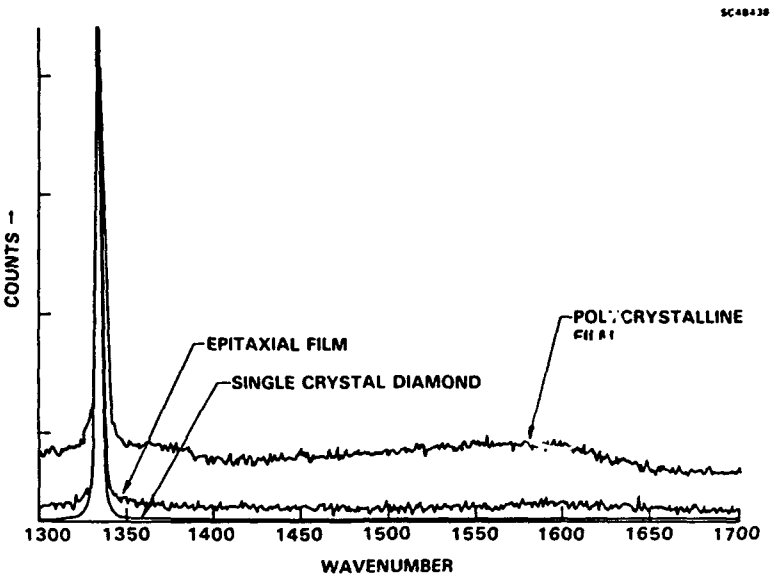

Fig. 5. Micro-Raman spectra taken from a homo-epitaxial diamond film and a polycrystalline random diamond film formed at 450°C.

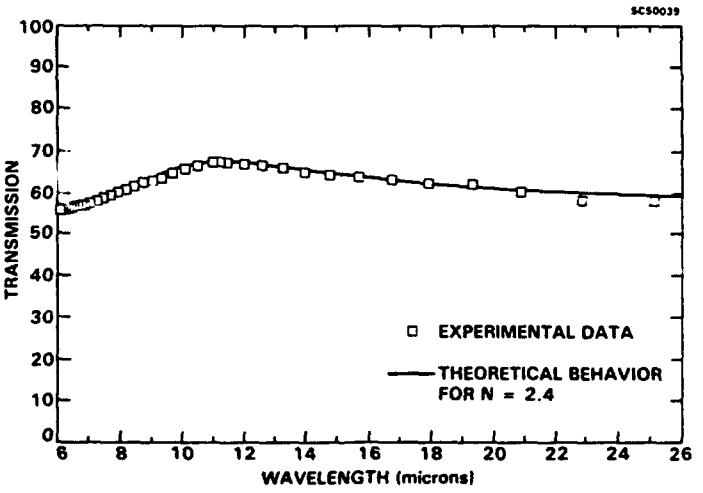

Fig. 6. The calculated and observed (squares) transmission of a diamond film on silicon. The film is 1.9 μm thick with an assumed optical index of refraction of 2.4.

REFERENCES

1. M. Kamo, Y. Saito, S. Matsumoto, and N. Setaka, "Diamond Synthesis for Gas Phase in Microwave Plasma," J. Crystal Growth, vol. 62, pp. 642-644 (1983).
2. A.R. Badzian, T. Badzian, R. Roy, R. Messier, and K.E. Spear,"Crystallization of Diamond Crystals and Films By Microwave Assisted CVD (Part II)," Mat. Res. Bull. 23(4), pp. 531-548 (1988).
3. Y. Saito, K. Sato, K. Gomi, and H. Miyadera, "Synthesis and Application of Diamond or Diamond-Like Films from CO-H2 Plasma," Proc. Symp. Plasma Chem., Vol. 1, pp. 303-308 (1988).

Appendix 2

Temperature and Reactive Etching Effects on the Microstructure of Microwave Plasma Deposited Diamond Films

Temperature and reactive etching effects on the microstructure of microwave plasma deposited diamond films

Alan B. Harker and Jeffery F. DeNatale
Rockwell International Science Center, Thousand Oaks, California 91362

(Received 22 September 1989; accepted 21 December 1989)

In the microwave induced plasma deposition of diamond from methane-hydrogen-oxygen mixtures, the variables available for controlling the microstructure of the resulting films are the plasma composition and density, the substrate surface properties, and the temperature. It has been demonstrated that the competition between nucleation site formation and the rate of reactive plasma etching is the critical feature in the development of the film microstructure on silicon substrates. On diamond substrates, the favorable lattice match dominates and homo-epitaxial films are formed over a wide temperature range. Raman scattering studies also demonstrate that the reactive etching of the diamond surface by oxygen-containing species is critical to the removal of non-diamond carbon species over the temperature range 450–1050 °C.

I. INTRODUCTION

A critical limitation in the exploitation of synthetic diamond films is the need to control their microstructure. Wide band-gap semiconductor applications require single crystal films while highly smooth, polycrystalline films are needed for tribological and optical applications. In this work a parametric study has been carried out to determine the process variables controlling the microstructure and crystallinity of sp3 bonded diamond films produced from a microwave induced discharge of mixtures of methane, hydrogen, and oxygen. The primary analytical tools used in the study were infrared spectroscopy, electron microscopy, and Raman scattering spectroscopy.

In the formation of diamond films the initial process involves the formation of chemical bonds between the substrate and crystallized clusters of carbon-carbon and carbon-hydrogen bonded molecules. These nucleation centers then act as sites for the bonding of additional adatoms and clusters. This typical film growth process is limited, however, by the reactive etching of the growing film by the excited species present in the plasma environment. The ability to produce pure crystalline diamond relies on the process conditions being established in which the sp2 bonded, graphitic carbon, and carbon-hydrogen bonds are etched away at a rate sufficiently fast that only sp3 diamond bonded carbon remains in the growing film. Hence, the process of attempting to control the microstructure in the diamond films must be considered as one of balancing the rates of the nucleation, growth, and etching processes occurring in the system.

II. EXPERIMENTAL

The deposition experiments were carried out in a turbomolecular pumped stainless steel vacuum chamber equipped with an Applied Science and Technology 1500 W magnetron plasma source. The chamber had a baked base pressure of 10^{-8} Torr. Experimental conditions ranged from pressures of 3 to 50 Torr with substrate temperatures of 450 to 1150 °C as measured by infrared pyrometry. In all cases the pyrometric measurements were made on Si wafers with an assumed emission of 0.96. Gas mixtures were typically hydrogen containing 0.3 to 1 vol.% methane and up to 1 vol.% oxygen. Substrates used in the experiments were (100) oriented silicon wafers and (100) type 2A natural diamond.

Microstructural characterization of the films was carried out by electron microscopy using a Phillips CM-30 for transmission electron microscopy (TEM) and selected area electron diffraction (SAD) analysis. Scanning electron microscopy (SEM) and selected area electron channeling were also used. Spectroscopic analysis included infrared transmission and reflection measurements with a scanning dual beam spectrophotometer, and micro-Raman scattering. The micro-Raman scattering measurements were made with a nominal 5 micron spot size, which could be defocused to obtain broader area analysis.

III. RESULTS AND DISCUSSION

As previously reported by other investigators,[1-4] a microwave induced plasma of CH_4 and O_2 in H_2 at low pressures and temperatures between 800 and 1200 °C produces the nucleation and growth of diamond and diamond-graphite films on a range of substrate materials. These films are typically polycrystalline, highly faceted, and have individual grains with linear dimensions ranging from 3 to 50 micrometers. The large grain size is indicative of a low density of nucleation sites in the films formed at high temperatures. This can be caused by poor lattice match to the substrate and by the

high mobility of the plasma generated species arriving at the substrate. Lattice matching and several surface pretreatments, such as scratching with diamond grit, can enhance the density of nucleation centers. In the microwave induced plasma films produced in this work at temperatures of 850 to 1050 °C with low nucleation densities, nearly isotropic growth in the developing grains and polycrystalline particles was observed. As shown in the SEM micrographs in Fig. 1, the developing diamond particles on silicon produce regular, near spherical overall shapes induced by high levels of crystallographic twinning and defects. The individual crystalline particles show uniform growth rates and ultimately form a continuous film as proximity leads to particle overlap.

When surface pretreatments such as diamond grit scratching are applied to the substrate surface, the density of nucleation sites is typically increased. In these cases a continuous film forms when the growing particles impinge upon one another. The degree of faceting in the individual diamond particles in the continuous films has been found to be a function of the growth versus reactive etching rates in the system. In Fig. 2, the SEM micrographs give a comparison between the morphology of continuous films produced at 1 vol.% CH_4, with and without the presence of 0.25 vol.% O_2. In the absence of oxygen the individual diamond particles have very high defect densities and are nearly spherical. With oxygen present the reactive etching leads to strongly faceted individual grains. In these films

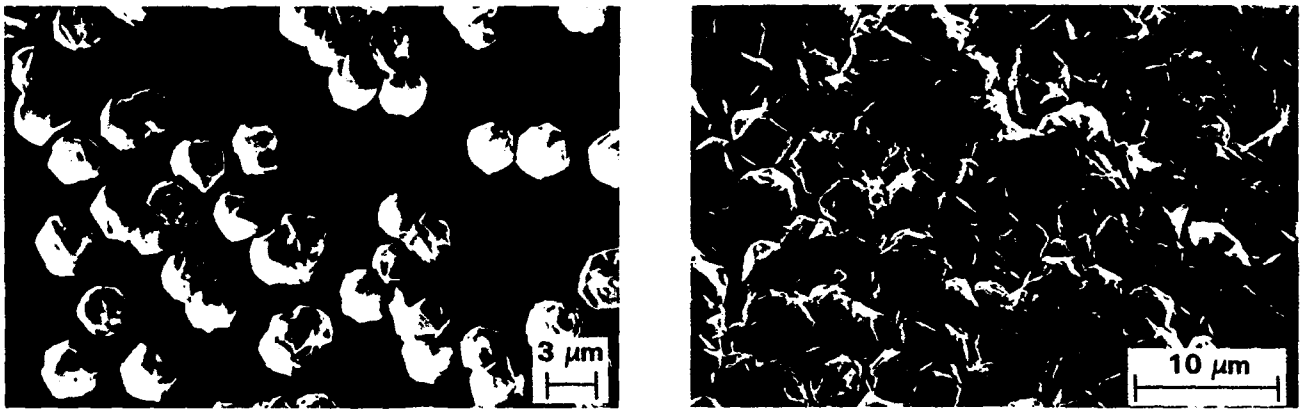

(a) (b)

FIG. 1. (a) Scanning electron micrograph of discrete, faceted diamond particles forming on (100) Si at 1040 °C which show near isotropic growth. (b) Scanning electron micrograph of a continuous diamond film forming from the overlap of discrete particles.

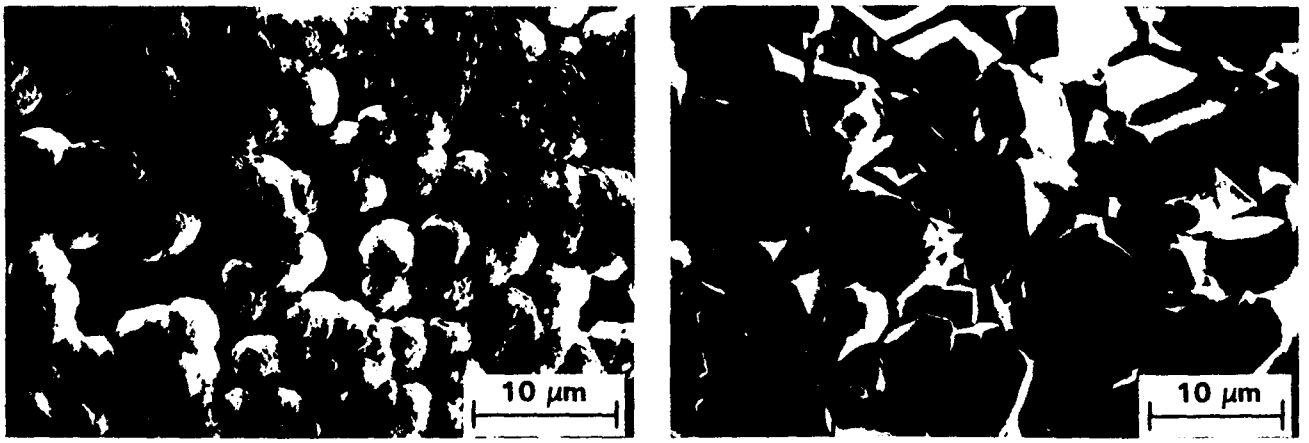

(a) (b)

FIG. 2. (a) SEM micrograph of the microstructure of diamond film formed at 1040 °C on Si with no O_2. (b) SEM micrograph of a highly faceted diamond film formed at 1040 °C with 0.25% O_2.

[Fig. 2(b)] the individual crystallite growth is limited by proximity effects and the formation of new growth directions at twin and defect sites on the crystalline facets.

The high density of defects plays a dominant role in determining the morphology of the diamond films at the higher temperatures. These defects appear very early in the film deposition process and may be stress related. The major crystallographic defect observed in the films is a multiple twinning on the {111} planes in ⟨211⟩ directions. This can lead to extremely high defect densities in the grains, as illustrated by the TEM micrograph, Fig. 3. Successive generation of this twin structure around the ⟨011⟩ axes can generate the fivefold defect structure, shown in Fig. 4, which is commonly reported to be present in the high-temperature diamond films.[5] This defect forms early in the individual grain development, as can be seen in the extremely fine-scale crystallites in the TEM micrograph. This defect was found to be present in a large fraction of the grains in the high-temperature formed films. Once formed, the fivefold defect structure is able to propagate and determine the shape of some of the crystalline grains even as they develop to super-micron size, as previously shown in Fig. 1.

Interestingly, while the polycrystalline films show a high level of defects, single crystal homo-epitaxial films can be formed under the same conditions. Figure 5 shows an electron channeling pattern of a 2-micron thick epitaxial diamond film produced on a (100) type 2A diamond surface. The pattern shows the cubic symmetry of the substrate to be fully propagated through the single crystal film. The film thickness was determined by masking an edge of the substrate with a second diamond. The channeling pattern would not be produced from the diamond film surface if there were any appreciable stress or loss of long-range order in the top 100 nm. Infrared transmission measurements showed no increase in absorption in the 250-micron thick diamond from the presence of the film.

While the homo-epitaxial films formed at 800–1100 °C are suitable for electronic studies, the high defect densities and very rough surfaces of the polycrystalline films formed in this temperature range do not have properties suitable for electronic, optical, or tribological applications. In order to obtain smoother film surfaces, finer grained polycrystalline films are required. To achieve this, both the lattice match between the diamond film and substrate and the etching versus deposition rate must be maximized. High lattice match optimizes the potential nucleation site formation, while increasing the rate of the etching processes favors the removal of less stable defect based growth sites. Further enhancement comes from reducing the deposition temperature to limit stacking faults, twinning, and other stress related defects.

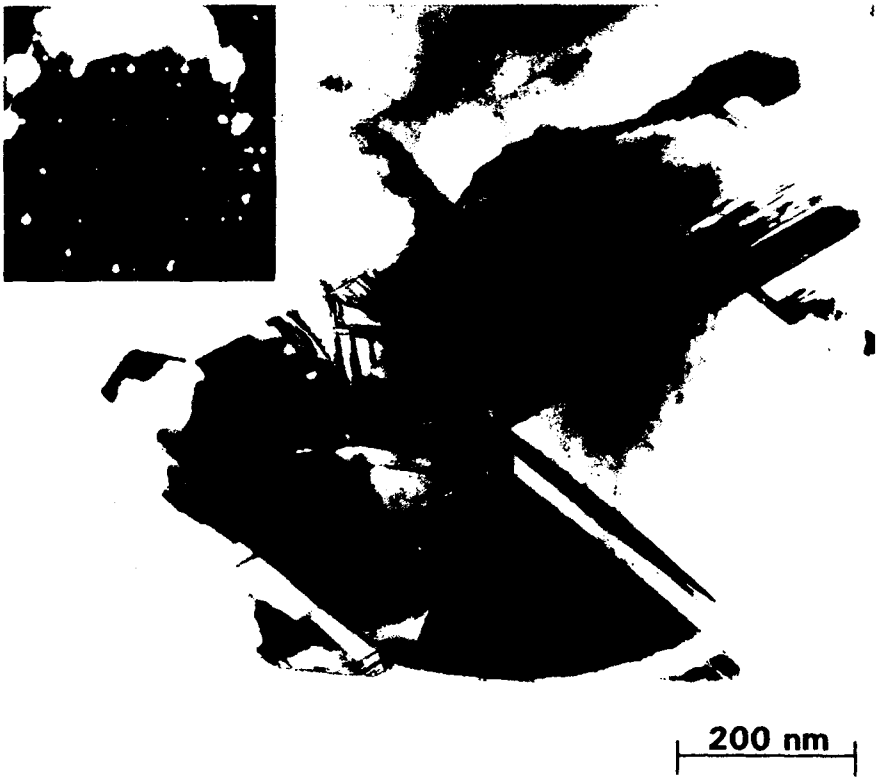

FIG. 3. Transmission electron micrograph and selected area electron diffraction pattern illustrating the high defect densities from multiple twinning in high temperature formed diamond films.

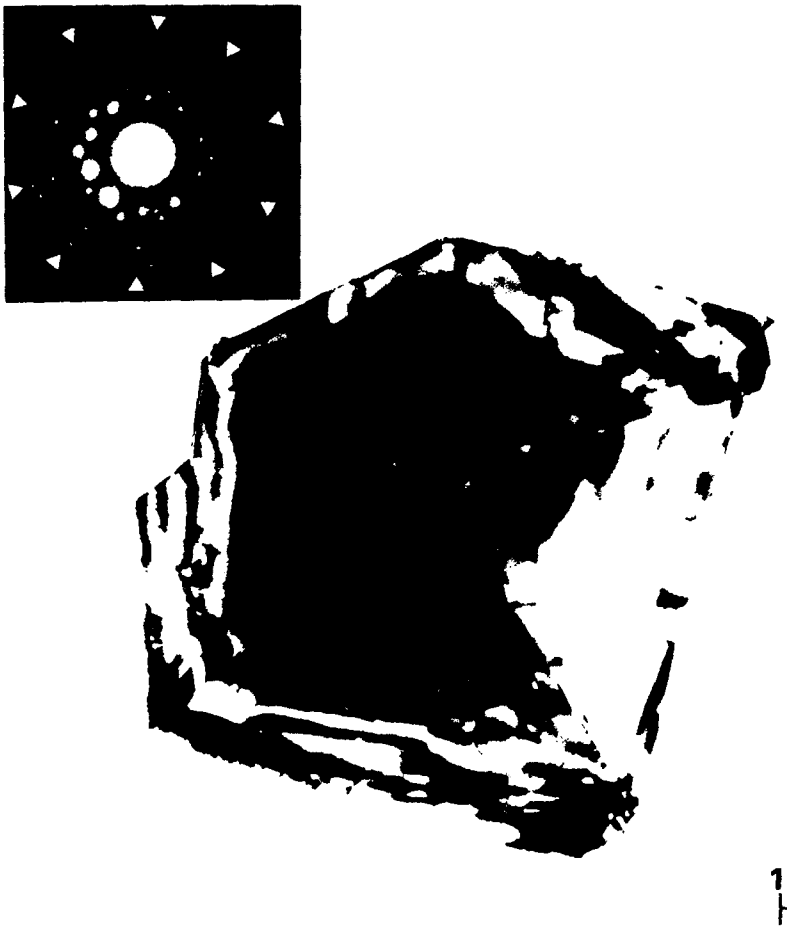

FIG. 4. Transmission electron micrograph and electron diffraction pattern of the fivefold twin defect structure commonly occurring in high temperature formed diamond films.

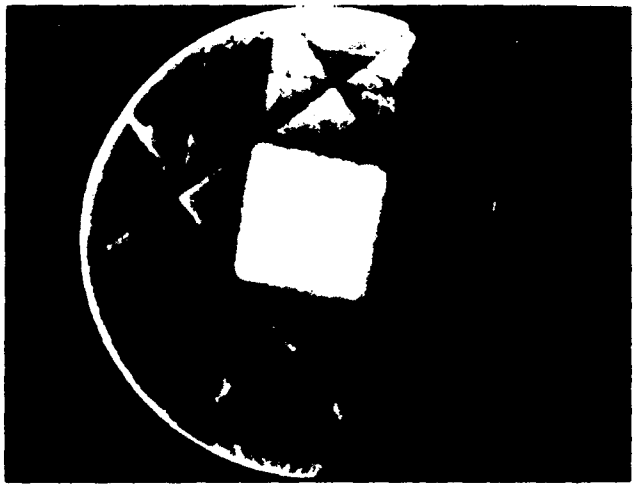

FIG. 5. A scanning electron channeling pattern formed from a homo-epitaxial diamond film grown on (100) type 2A diamond at 1040 °C.

The role of temperature in determining the nucleation, defect structure, and growth morphology of the diamond films can be seen by TEM. Figure 6(a) shows a TEM micrograph of a diamond film deposited at 1040 °C on Si. The bulk of the grains contains defects of the type described earlier, with the film microstructure defined by the impingement of large grains originating from highly separated nucleation centers. The morphology of these films is also characterized by the extensive out-of-plane growth shown in Figs. 1–3. By maintaining all conditions the same, but dropping the deposition temperature to 450 °C, a significant improvement in the film morphology can be achieved [Fig. 6(b)]. The lower temperature deposited films exhibit planar twinning similar to the higher temperature films, but little of the fivefold twin structure is present. The finer grain size and more uniform nucleation in these lower temperature films leads to higher film densities and reduced surface irregularities from out-of-plane growth.

The major effect of lowering the diamond deposition temperature is the formation of finer grained polycrystalline films and oriented films on (100) Si substrates. Figure 7 shows SEM micrographs of two films formed on (100) Si at a nominal substrate temperature of 450 °C at different distances from the

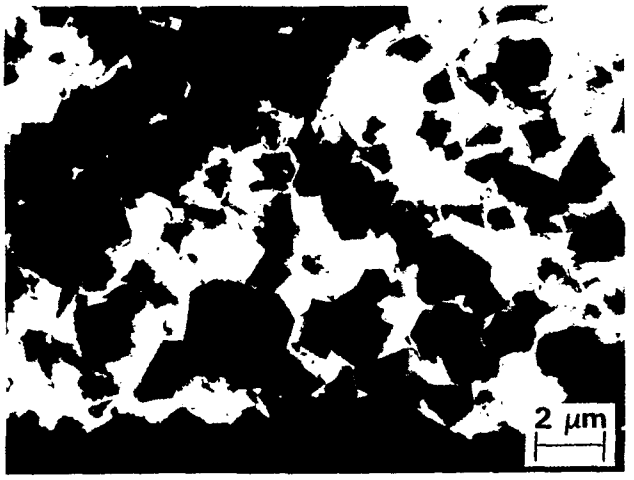

(a)

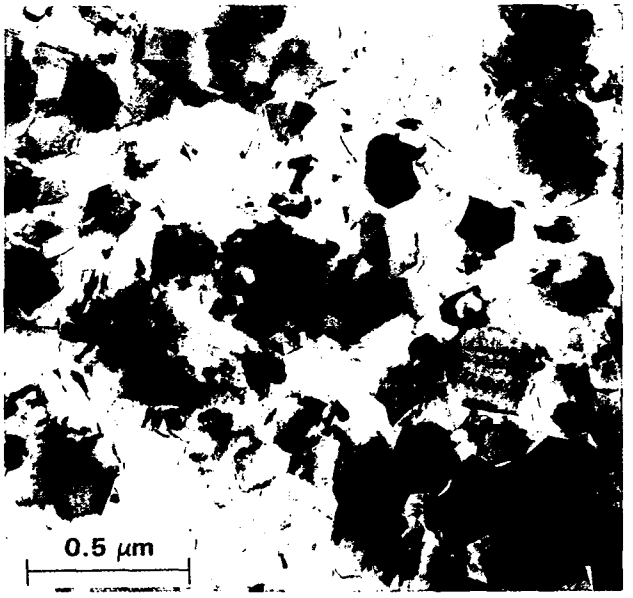

(b)

FIG. 6. (a) Transmission electron micrograph showing the coarse microstructure and high defect densities of a diamond film grown at 1040 °C on Si. (b) Transmission electron micrograph of a fine grained diamond film grown at 450 °C on Si.

plasma ball. The finer grained film, formed 1.5 cm from the plasma, is randomly oriented. The slightly coarser film, formed directly beneath the plasma ball, is oriented with (220) plane parallel to the (100) plane of the substrate. The orientation of the textured film can be seen by the significant enhancement of the (220) Bragg reflection in Fig. 8. When a natural (100) oriented diamond substrate was coated under the same conditions as used for the oriented film on silicon (30 Torr, 1% CH_4 and 0.25% O_2 in H_2, 450 °C), a homoepitaxial film was formed.

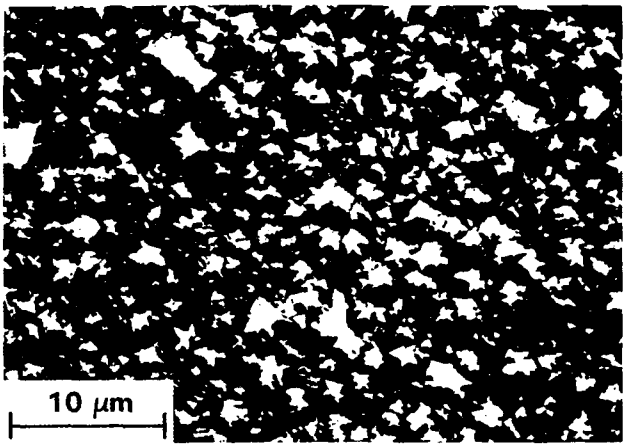

(a)

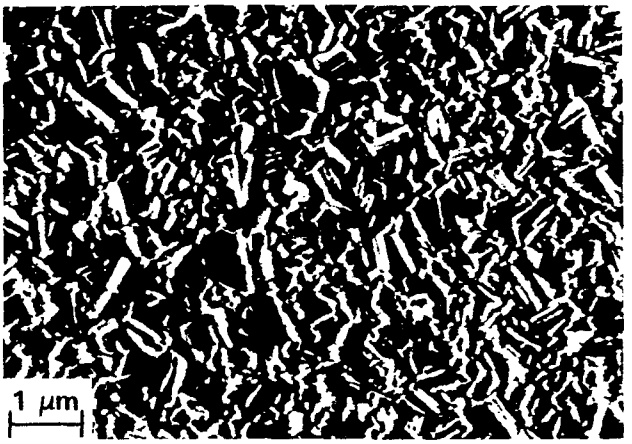

(b)

FIG. 7. (a) Scanning electron micrograph of a (220) oriented diamond film grown at 450 °C on (100) Si. (b) A random oriented fine-grain diamond film grown on (100) Si at 450 °C.

The role of oxygen at these lower temperatures seems primarily to be the etching away of sp2 bonded carbon. Raman spectra of films grown at the lower temperatures without oxygen showed the broad scattering line at 1550 cm^{-1} characteristic of sp2 bonded carbon.[6] Conversely, with oxygen present, the spectra were dominated by the diamond Raman line observed at 1334.5 cm^{-1}. The Raman scattering spectra in Fig. 9 are from the (100) face of a natural diamond, a homoepitaxial film, and a fine grained (220) oriented diamond film on (100) Si formed at 450 °C. The polycrystalline film has a slightly broader sp3 scattering peak than the natural diamond and epitaxial film; however, it shows only a minor contribution of sp2 bonded carbon

IV. CONCLUSIONS

The microstructure and orientation in diamond films formed on Si substrates by microwave induced

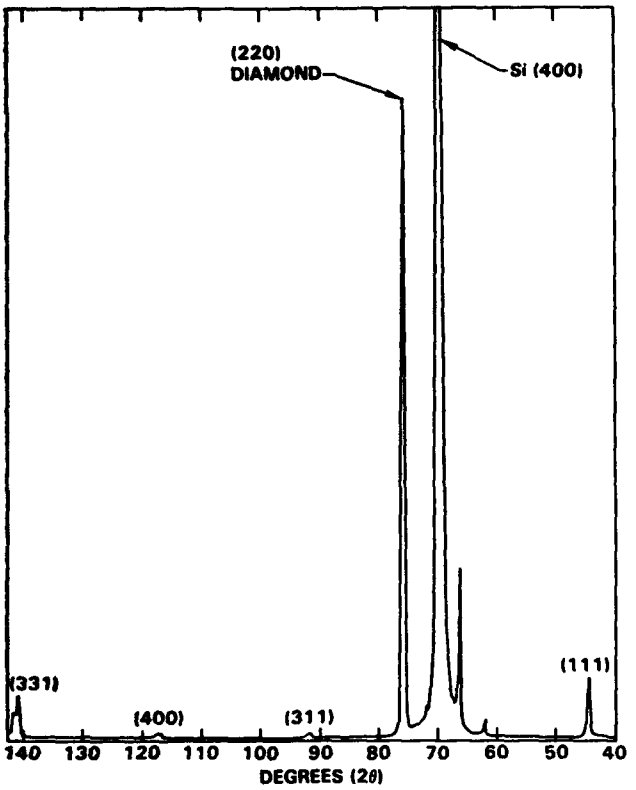

FIG. 8. X-ray diffraction pattern of the oriented diamond film on (100) Si shown in the SEM micrograph in Fig. 7(a).

plasma discharge of CH_4 in H_2 can be highly modified by the use of reactive etchants such as O_2, altering the deposition temperature, and altering the distance of the substrate from the plasma center. Higher temperatures favor low nucleation rates, enhanced grain growth, and high defect levels. Lower temperatures favor nucleation and sustained orientation to the substrate. The presence of O_2 in the plasma serves to enhance faceted growth through the preferential etching of non sp3 bonded species forming on the film surface. At substrate temperatures below 500 °C fine-grained oriented diamond films have been produced upon (100) silicon and full epitaxy has been achieved on natural (100) diamond.

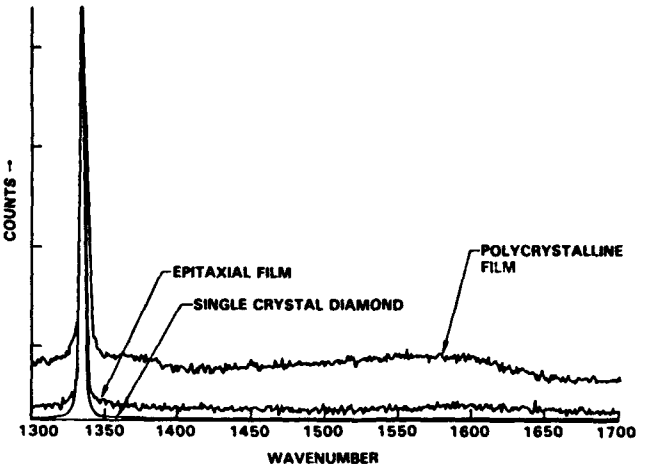

FIG. 9. Raman scattering spectra of a homo-epitaxial diamond film and a polycrystalline diamond film grown at 450 °C compared to that of type 2A diamond.

ACKNOWLEDGMENTS

This research was sponsored in part by the Office of Naval Research. The authors also acknowledge the contribution of Mr. John F. Flintoff who performed the scanning electron microscopy for this work.

REFERENCES

[1]M. Kamo, Y. Saito, S. Matsumoto, and N. Setaka, J. Cryst. Growth **62**, 642–644 (1983).
[2]A. R. Badzian, T. Badzian, R. Roy, R. Messier, and K. E. Spear, Mater. Res. Bull. **23** (4), 531–548 (1988).
[3]Y. Saito, K. Sato, K. Gomi, and H. Miyadera, Proc. Symp. Plasma Chem. **1**, 303–308 (1988).
[4]A. B. Harker, "Proceedings of Diamond Optics II," SPIE 33rd Annual Int. Symp. on Optical and Optoelectronic Applied Science & Engineering, San Diego, CA (Aug. 6–11, 1989).
[5]J. Narayan, A. R. Srivatsa, M. Peters, S. Yokota, and K.V. Ravi, Appl. Phys. Lett. **53** (19), 1823 (1988).
[6]D. S. Knight and W. B. White, *Raman Scattering, Luminescence, and Spectroscopic Instrumentation in Technology*, SPIE **1055**, 144–151 (1989).

Appendix 3

Microstructure of Diamond Films as a Function of Deposition Conditions

PROCEEDINGS REPRINT

SPIE—The International Society for Optical Engineering

Reprinted from

Diamond Optics III

9-11 July 1990
San Diego, California

Volume 1325

Microstructure of diamond films as a function of deposition conditions

A.B. Harker, J.F. DeNatale, and J.F. Flintoff

Rockwell International Science Center
P.O. Box 1085
1049 Camino Dos Rios
Thousand Oaks, CA 91360

ABSTRACT

The microstructure of polycrystalline diamond films grown by microwave plasma assisted chemical vapor deposition (PACVD) have been observed as a function of growth temperature, substrate identity and surface condition. Our highest microwave PACVD growth rates have been achieved in (110) axis normal oriented polycrystalline diamond films. Results indicate that at growth temperatures below 650°C kinetically dominated processes induce the formation of a preferential (110) axis normal orientation in diamond films with micron scale microstructure. This orientation can be sustained on silicon, boron nitride, and silicon nitride substrates to film thicknesses in excess of 60 microns through the occurrence of (111) twin defects. Such films have the high density and generally uniform microstructure required for optical applications.

1. INTRODUCTION

The rate of growth of PACVD diamond films is intimately tied to the availability of low energy growth sites. Such low energy sites will be associated with the most rapidly growing crystalline faces. In general, those crystalline faces having the highest growth rates rapidly fill their available bonding sites and cease growth. Hence, the exposed facets on a randomly oriented crystalline film would be expected to be those exhibiting the slowest growth. In the case of diamond films, the dominance of (100) and (111) faceting on the exposed surfaces indicates that these are the slow growth faces (Fig. 1) and explains the need to have continued renucleation to sustain reasonable growth rates. In order to achieve a situation in which the film development is controlled by a growth rather than a renucleation mechanism it would be necessary to provide a continuous source of the most favored growth sites. In this work it has been shown that such a situation can be achieved through the continued propagation of a highly twinned (110) axis normal oriented diamond film.

Fig. 1 Scanning electron micrograph of a random polycrystalline diamond film surface grown at 1000°C by microwave PACVD.

In this research we have investigated the degree to which the microstructure of PACVD polycrystalline diamond films can be modified and controlled through the use of various substrates, substrate surface preparations, and deposition conditions. The primary deposition variable investigated was temperature, with films being deposited over the range 450 to 1000°C. Substrates investigations included (100), (110), and (111) Type 2A diamond single crystals, pyrolytic polycrystalline boron nitride (PBN), polycrystalline silicon nitride, (100) silicon, and fused silica.

2. EXPERIMENTAL

All films were grown in a standard stainless steel ASTEX 1.5 KW microwave reactor with an inductively heated graphite sample holder. The chamber is equipped with windows to permit sample surface temperature monitoring by optical pyrometry. The gas composition used for growth was 99% hydrogen, 0.7% methane, and 0.3% oxygen. Films were analyzed by scanning electron microscopy, micro-Raman scattering, and x-ray diffraction. Growth rates were determined by infrared reflectance measurements.

3. RESULTS

The initial growth temperature variation experiments were conducted with (100) silicon substrates polished with submicron diamond paste. These experiments, previously reported,[1] revealed that (110) axis normal oriented diamond films could be produced at growth temperatures of 450 to 650°C when the samples were located in the plasma region of highest growth rate. Outside of the direct plasma impingement zone, only randomly oriented films have been observed.

Our study has shown that such (110) oriented films can be produced upon polycrystalline silicon nitride and boron nitride substrates as well as on (100) silicon with growth rates of 0.5 to 1.0 μm per hour at 650°C. Figure 2 shows an electron micrograph of a 25 μm thick (110) oriented diamond film on polycrystalline silicon nitride. The microstructure of the one-dimensionally oriented film is generally more regular than that of a random film. The surface appearance is dominated by the exposed edges of crystallites multiply twinned along the (111) planes. The observation that such oriented films can be grown on polycrystalline substrates as well as single crystal (100) silicon indicates that under these growth conditions the crystal structures of the non-lattice matched substrates do not significantly affect the nucleation energetics. This observation is consistent with the high surface energy of diamond.

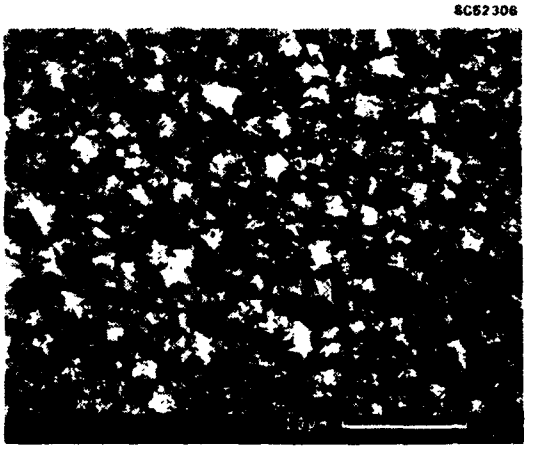

Fig. 2 Scanning electron micrograph of a (110) axis normal polycrystalline diamond film grown on diamond polished polycrystalline silicon nitride at 650°C.

To observe the effects of substrate identity in the growth process, diamond films were produced by PACVD under identical conditions at 650°C on a range of single crystal, polycrystalline, and amorphous substrates. The resulting film properties are tabulated below.

The microstructures of some of the films are shown in the electron micrographs in Fig. 3. The similarities of the microstructures in the (110) oriented films on Si, PBN, and Si_3N_4 are apparent, as are the dramatic differences between the films grown on the Si samples polished with boron nitride and diamond. To provide a consistent description of the various microstructures one must consider surface energies, the types of expected crystalline defects, and the metastable nature of the low pressure diamond synthesis environment in which etching is occurring concurrently with film growth.

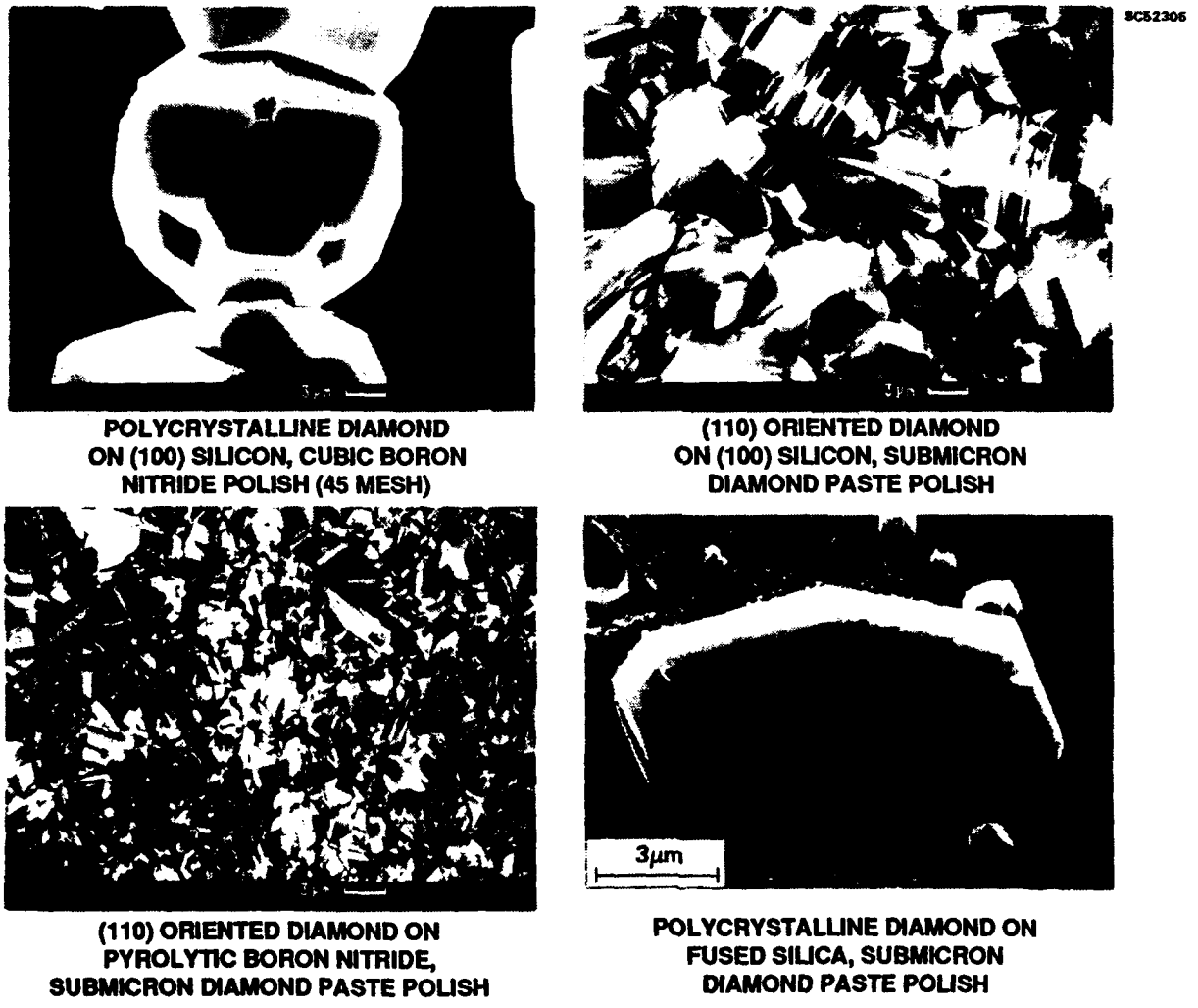

Fig. 3 Scanning electron micrographs showing the morphology of poly-polycrystalline diamond films grown on a range of substrates.

Table 1

Microstructure of Diamond Films as a Function of Substrate Identity and Surface Preparation. Boron Nitride Polishes Were Done with a Cubic 45 Mesh Powder

SUBSTRATE	FILM PROPERTIES
(100) Type 2A Diamond	Epitaxial Film, very low defects
(111) Type 2A Diamond	Epitaxial Film, surface defects
(110) Type 2A Diamond	Grain Oriented Polycrystalline (Highest Growth Rate)
(100) Silicon (BN polish)	Well Formed Low Defect Crystallites
(100) Silicon (Dia. Polish)	(110) Oriented Polycrystalline Film
Fused Silica (Dia. Polish)	Well Formed Low Defect Crystallites
Silicon Nitride* (Dia. Polish)	(110) Oriented Polycrystalline
Boron Nitride* (Dia. Polish)	(110) Oriented Polycrystalline

* - Polycrystalline Material

Since the three single crystal diamond substrates all produced fully orientated films, it is clear that substrate crystallograpy can be significant to homoepitaxy under the deposition conditions of this work. The high surface energy of the (100) crystal and the absence of any periodic bonding chains[2] correlates well with its epitaxial nature and low defect density surface.[3,4] Similarly, the appearance of triangular defects on the generally epitaxial (111) growth surface is consistent with the lower surface energy of that plane and the presence of three periodic bonding chains[3] that can produce triangular growth hillocks on that face. However, the more rapid growth rate and grain oriented polycrystalline nature of the film on the (110) diamond crystal require that the nature of the defects generated in the film be considered to explain the results.

The (110) plane of diamond is intersected by the (111) planes that generate the single periodic bonding chain on the (110) face. The (111) planes are subject to both stacking and slip plane faults that are known to produce striations in natural diamond crystals.[5] Similarly, fairly regular twinning defects along the (111) plane produce the striated or layered morphology seen in the grains of the (110) oriented polycrystalline films (Fig. 4). Hence, we conclude that the formation of defects along the (111) planes on the (110) diamond growth surface provides both a low energy state for preferential bonding of the radical species producing growth and a very high surface area of unsatisfied chemical bonds to enhance the growth rate. Additionally, Zheng et al.[5] have reported that the (110) face of diamond shows a lower oxidation rate than either the (100) or (111) face, which would favor (110) film growth.

The generation of oriented films on the non-diamond substrates is consistent with the observed homo-epitaxial film growth behavior. The global (110) orientation on is believed due to the interplay between anisotropic growth modes and anisotropic etching, favoring the (110) oriented growth. For small diamond seed crystals, the plasma etching occurring during the initial stages of growth will tend to alter the crystallographic distribution of seed crystals towards (110) orientation. Coupled with this is the enhanced growth rates observed on the (110) single crystal diamond surface. The combination of these two factors imposes a strong preference for (110) oriented polycrystalline film development under the low temperature conditions used in this work. For higher growth temperatures, it is likely that the energetic differences associated with crystallographically favored growth modes will be much less significant, and the nucleation time associated with "seed" etching will be reduced, favoring random film development. This transition to random growth morphologies at higher temperatures has indeed been experimentally demonstrated.

Fig. 4 Higher resolution electron micrographs of the twin defects generated at the intersection of the octahedral and dodecahedral planes of diamond in a (110) oriented diamond film on (100) silicon.

The samples not exhibiting this type of growth at T <650°C were the films grown on fused silica and (100) silicon polished with a coarse 45 mesh cubic boron nitride powder. On these samples growth of individual faceted particles dominated. In the boron nitride polished samples, growth was occurring upon the faceted super-micron boron nitride crystal surfaces. In this growth dominated regime little nucleation was occurring and very smooth faceted particles were produced. Similarly, in the case of fused silica, the reaction of the surface with the plasma (producing pitting in the micrograph in Fig. 3) releases significant oxygen near the surface. This not only etches the smaller diamond particles left by the abrasion process, but also inhibits the general nucleation of polycrystalline diamond. In this case, growth is again limited to the larger diamond particulate seeds on the surface and well defined particle growth morphologies result.

4. CONCLUSIONS

The preferential growth of (110) oriented polycrystalline diamond films, at temperatures below 650°C by microwave PACVD can be ascribed to a combination of defect enhanced anisotropic growth and anisotropic etching. The oriented film microstructure is fairly regular and is dominated by the presence of layered planar micron scale crystallites and striations induced by multiple twinning defects on the (111) plane. These defects lead to continuous propagation of the a (110) oriented growth surface and permit the orientation to persist with increasing film thickness. The generation of large grained, low defect diamond crystals by PACVD under the growth conditions of this work is limited to those cases in which larger seed crystals grow while general polycrystalline diamond nucleation is inhibited by the absence of sufficient small diamond "seeds" or through the reactive etching of the nucleation sites.

5. ACKNOWLEDGEMENTS

Portions of this research were sponsored by the Office of Naval Research.

6. REFERENCES

1. A.B. Harker and J.F. DeNatale, "Temperature and Reactive Etching Effects on the Microstructure of Microwave Plasma Deposited Diamond Films," J. Mater. Res. 5, pp. 818-823 (1990).
2. P. Hartmon and W.G. Perdok, "On the Relations Between Structure and Morphology of Crystals, III," Acta Cryst. 8, p. 49, 521, 525 (1955).
3. I. Sunagawa, "Growth and Morphology of Diamond Crystals Under Stable and Metastable Conditions," J. Crystal Growth 99, pp. 1156-1161 (1990).
4. M. Moore, "Optical Studies of Diamonds and Their Surfaces," in Properties of Diamond, ed. J.E. Field (Academic Press, London, 1979) 261.
5. Z. Zheng, H. Kanda, T. Ohsawa, S. Yamaoka, "Inhomogeneous Oxidation Rate Measured on the (110) Cross-Section of Synthetic Diamonds," J. Mat. Sci. Lett. 9, pp. 331-333, 1990.

Appendix 4

Microstructure Control of Diamond Thin Films by Microlithographic Patterning

Microstructural control of diamond thin films by microlithographic patterning

J. F. DeNatale, J. F. Flintoff, and A. B. Harker
Rockwell International Science Center, Thousand Oaks, California 91360

(Received 7 May 1990; accepted for publication 22 June 1990)

Microlithographic patterning has been used to elucidate the mechanisms controlling diamond film nucleation and grain growth. The approach is capable of establishing a degree of control over diamond nucleation on the substrate, which can be used to improve film uniformity and enhance fine grained microstructure. The observed microstructures in the patterned films are consistent with an intrinsic growth mechanism based upon defect-initiated renucleation.

I. INTRODUCTION

The application of current synthetic diamond films as optical and friction-reduction coatings is greatly limited by the surface roughness of the as-deposited polycrystalline material. The high degree of defects in the faceted crystalline films as well as the supermicron grain size characteristic of most plasma and filament chemical vapor deposition (CVD) diamond films produces a surface roughness on the order of 500–5000 nm.[1–3] Such roughness causes a high degree of optical scattering extending from the visible through the long wavelength infrared,[4] and produces a surface which is too abrasive for direct application as a bearing surface for wear reduction.

Methods currently exist and are being further developed for the post-deposition polishing of the polycrystalline diamond surfaces,[5,6] but these processes are made more difficult to implement by the surface roughness in the films due to the large, irregular grain sizes. Hence, it is highly desirable for specific applications to not only limit grain growth in the diamond films, but also to produce a dense, uniform microstructure amenable to post-deposition surface polishing.

Deposition of the polycrystalline diamond thin films is inherently different from that of conventional optical thin film materials. For the diamond films, the film morphology is controlled by the nucleation and growth of the individual crystalline diamond grains on the substrate surface. To achieve microstructures consistent with optical applications, one must generate uniform, fine-grained nucleation geometries and restrict out-of-plane growth of large diamond particulates. Microlithographic patterning is being investigated in this laboratory as a means of establishing such a uniform distribution of nucleation centers on the film and a degree of control over the film microstructure. Both Kirkpatrick *et al.*[7] and Ma *et al.*[8,9] have demonstrated that selective nucleation can be achieved using micropatterning of the substrate before deposition. Both groups achieved point nucleation of large (>10 μm) diamond particulates, whose growth was primarily limited by physical impingement. This paper demonstrates microlithographic processing techniques that provide both the fine grain size and spatial uniformity desired for the optical and wear-reduction applications of diamond films. A general mechanism for the controlled grain growth is also discussed.

II. EXPERIMENT

Single-crystal silicon wafers were patterned by standard photolithography techniques prior to growth using a proprietary high-temperature resist. The pattern used for the initial experiments was a square grid of 1-μm-wide lines exposing the bare silicon substrate, separated by 10 μm of resist. Investigations of the linewidth-dependence used a pattern of parallel lines ranging between 0.5 and 1.5 μm wide. The films were grown using microwave-plasma-assisted CVD (PACVD) with a source gas composition of 1% CH_4, 0.5% O_2, and the balance H_2. Substrate growth temperatures of 650 °C were used as determined by optical pyrometry. The substrates were prepared both with and without the use of a diamond polish pretreatment to establish the relative roles of topology and "seeding" on nucleation behavior. Growths were first conducted for a short time to establish diamond formation in the grid lines. The substrates were then removed, the resist was stripped, and the substrates were returned to the chamber for additional film growth.

III. RESULTS

Preliminary experiments were conducted to determine the appropriate length of time for the initial growth on the patterned substrate. The development of the microstructure with increasing time is illustrated in the sequence of scanning electron micrographs in Fig. 1. The diamond was found to nucleate preferentially on the exposed silicon substrate as opposed to the resist. This allowed a significant particle density to be achieved in the lithographed pattern prior to removal of the resist, with a crystallite size of approximately 200 nm. After the three-hour initial deposition, the diamond crystallites in the grid had already impinged upon each other, and growth was extending beyond the pattern. This overgrowth of the diamond film made removal of the resist difficult; and so for the later experiments, a two-hour initial growth was used prior to resist removal. Experiments using thicker resist layers, however, demonstrated that substantial pattern thicknesses can be

 0021-8979/90/204014-06$03.00

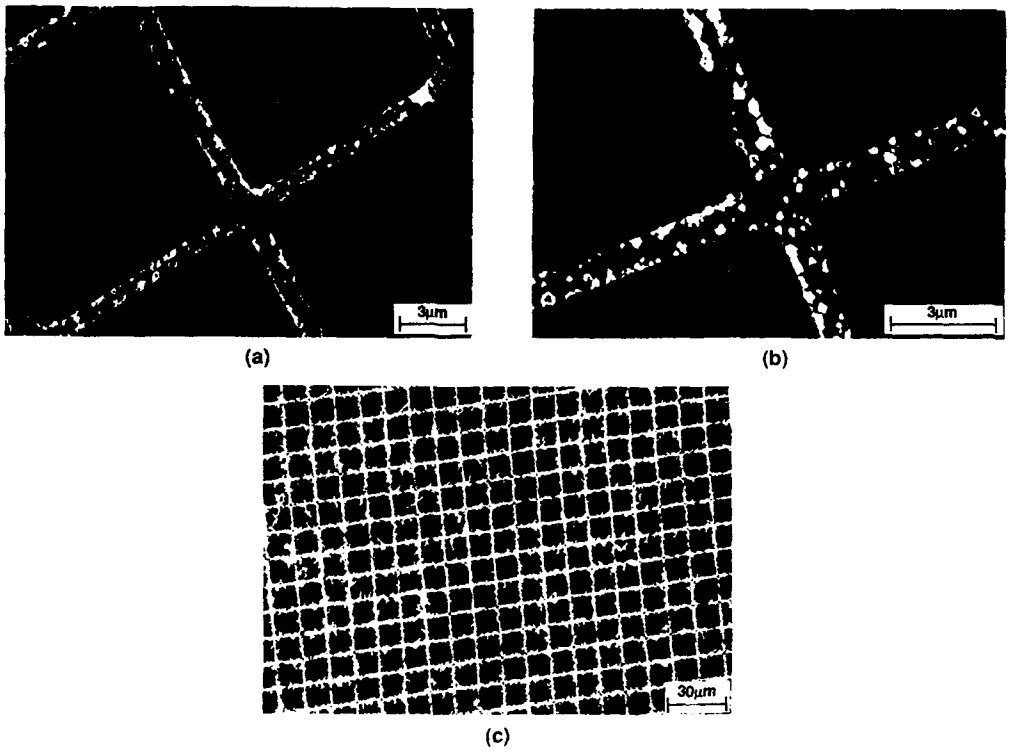

FIG. 1 Diamond crystallite growth on microlithographed Si substrates with increasing growth time (a) 1 h; (b) 2 h; (c) 3 h.

generated by this technique (Fig. 2), while maintaining an extremely fine grain structure.

Experimental control substrates patterned but prepared without the diamond polish pretreatment exhibited no appreciable diamond nucleation on either the resist or the silicon over a period of approximately 20 h.

After grid nucleation, resist removal, and additional growth, the open areas between the grid lines filled in completely to form a continuous film. The diamond film maintained the fine grain structure of the initial nucleated particles, and the pattern was still evident on the surface (Fig. 3). With continued growth, however, this surface pattern became less distinct (Fig. 4).

The effect of the microlithographic pretreatment on the microstructure of the film was clearly demonstrated by comparison of the patterned and unpatterned regions of the substrate. The unpatterned regions provide a reference for the microstructural development that occurs on the bare substrate under the identical growth conditions. The boundary of the patterned region is clearly evident in the scanning electron micrograph in Fig. 5, taken after 24 h of diamond growth. In the unpatterned areas of the silicon substrate, the diamond morphology is characteristic of large, faceted crystal growth and low net particle number densities. These diamond particle microstructures are characteristic of low nucleation density films formed on silicon under the PACVD growth conditions used in this study.[3] In contrast, the patterned areas are characterized by finer grains and higher particle densities, more consistent with the requirements of optical applications. With further growth, the larger particles on the unpatterned regions eventually impinge, as shown in Fig. 6. However, the film growth in the unpatterned region continues with the larger grain size. The transition from the fine-grained structure to the coarse-grained structure at the pattern boundary is extremely abrupt, with the microstructural differences arising within 1–2 μm as seen in the micrograph in Fig. 7.

Extended microscopic examination of the patterned region of the diamond films showed a very uniform micro-

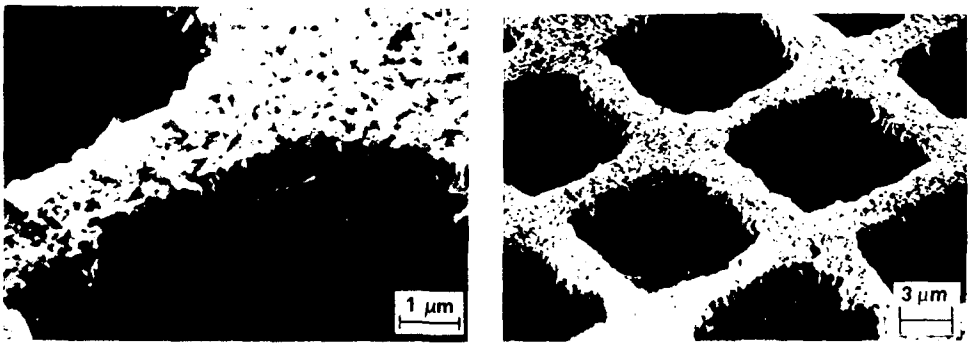

FIG. 2 Microlithographed diamond grid structure grown using thick resist layer.

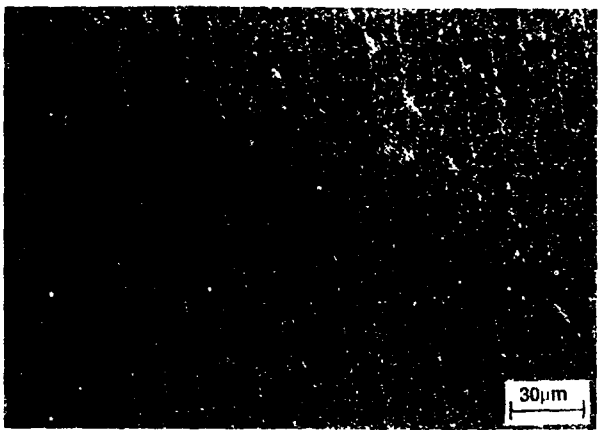

FIG. 3. Development of continuous diamond film on microlithographed Si after resist removal and subsequent growth

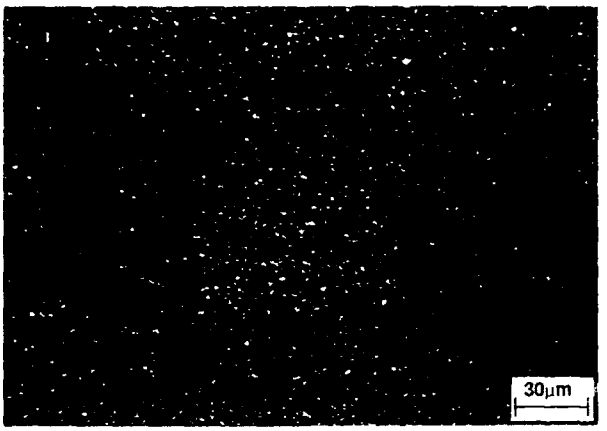

FIG. 4. Surface morphology of initially patterned Si after continued diamond film growth

structure over the entire 2.5 × 2.5 cm pattern size. Often, spatial nonuniformities in sample temperature or plasma distribution lead to significant variations in film microstructure over this scale. Cross-sectional analysis in the scanning electron microscope (SEM) showed this diamond film to have no observable porosity in its microstructure in the patterned region, including both the microlithographed grid area and the initially masked areas (Fig. 8). The individual grains are distinctly columnar in nature over the entire thickness of the film.

The effect of the initial line width on the nucleation morphology was studied using a microlithographed pattern containing lines ranging from 0.5 to 1.5 μm wide. The initial stages of growth, prior to resist removal, are shown in Fig. 9. As was seen in Fig. 1, nucleation preferentially occurred at the edges of the lines in all cases. For the 0.5 μm line, a single row of crystallites was generated. For the line widths greater than 0.5 μm, the crystal size remained constant, with an additional row forming at the opposite line edge. As the pattern linewidth was increased beyond this point, the crystallite particle size remained constant, with the spacing between the deposited rows of diamond particles progressively increasing with the lithographed linewidth.

IV. DISCUSSION

The importance of surface pretreatment to nucleation behavior in diamond thin films is well established. This work is consistent with the bulk of the literature which demonstrates a large increase in diamond nucleation density associated with a diamond abrasive preparation of the substrate surface. The action of surface polishing of a substrate with diamond paste both adds surface topology (by scratching) for diamond nucleation and "seeds" the surface with imbedded diamond particles. In the current experiments, the microlithographic patterns provide numerous sites for nucleation independent of the diamond

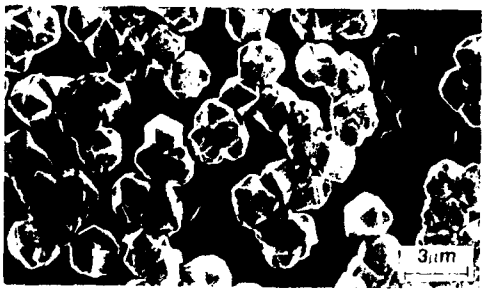

NOT PATTERNED

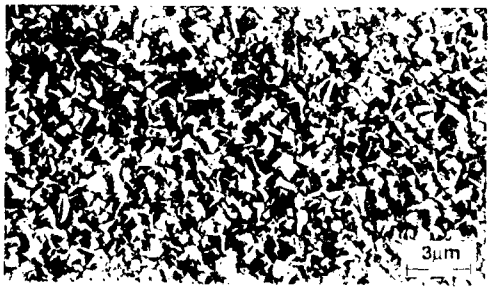

PATTERNED

FIG. 5. Comparison of microstructural development on patterned and nonpatterned regions of Si substrate after 24 h of growth

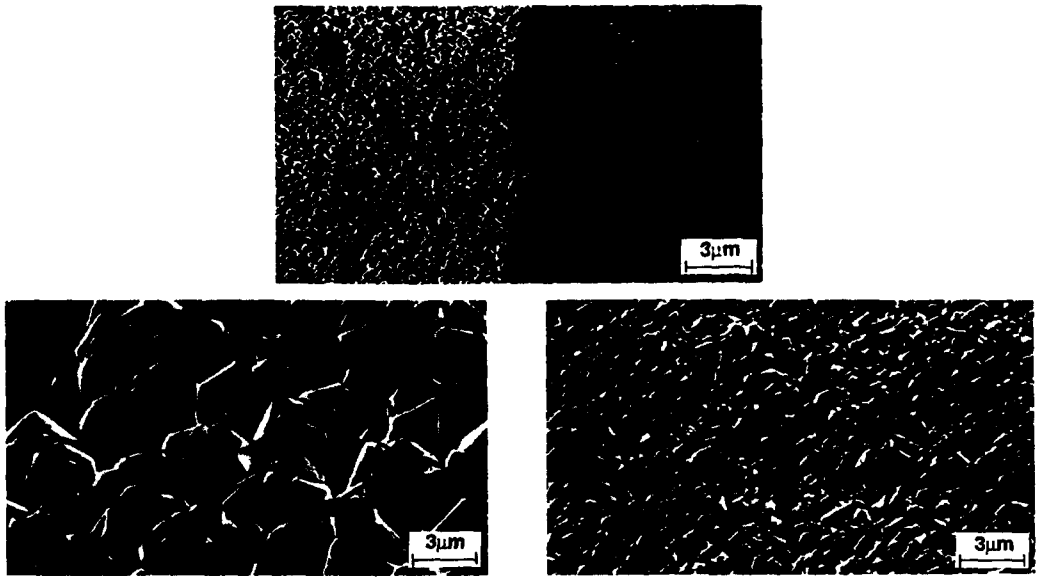

FIG. 6. Comparison of microstructural development in patterned and nonpatterned regions of Si substrate after continued diamond film growth.

polishing, and yet the diamond pretreatment was still required to induce significant film nucleation. This is in contrast to the results of Kirkpatrick *et al.*,[7] who observed preferential nucleation of carbonaceous material at the sites of ion milled craters in silicon without seeding, although the nature of the deposited material is not reported. Bachmann *et al.*[10] used polished Si substrates oriented slightly off the ⟨100⟩ axis, and noted that the crystallographic ledges so produced had no impact on diamond nucleation. This is consistent with the observations reported here using much larger scale topologic features. The current work supports the conclusion that the presence of the diamond particles from the surface pretreatment, i.e., the "seeding," is the critical step in enhancing the film nucleation. The work of Bachmann *et al.*,[10] performed at higher growth temperatures, supports this conclusion and further indicates that nondiamond particles can also lead to significant increases in film nucleation.

The nucleation morphologies of Figs. 1 and 9 indicate that the diamond particles "seeded" by the surface treatment are located at the edges within the microlithographed channels, and that growth of subsequent film grains initially propagate in a similar manner along the same edges until impingement occurs. This is reasonable, since these sites provide two surfaces for film attachment. This is the same morphology observed by Ma *et al.*,[8,9] although their Ar^+ irradiation step limited the nucleation to the edge region shadowed from the ion beam. The observed morphologies in this work are consistent with the residual diamond particles from the initial surface preparation being attached to the inside edges of these channels. Whether this attachment is electrostatic or not has not been determined. The work of Geis[11] reports comparable diamond seed texture development on Si, fused quartz, and chrome-coated substrates, which would tend to discount electrostatic attachment. The selective removal of the seed crystals by Ma *et al.*[8,9] by Ar^+ ion irradiation, however, could be due to either physical sputtering or electronic processes. The absence of significant nucleation in the resist-covered areas in this work (i.e., prior to resist removal) indicates that significant numbers of particles are not being physically em-

FIG. 7. Detail of boundary between patterned and nonpatterned regions of Si substrate.

FIG. 8. Cross-sectional SEM micrograph illustrating dense, columnar structure.

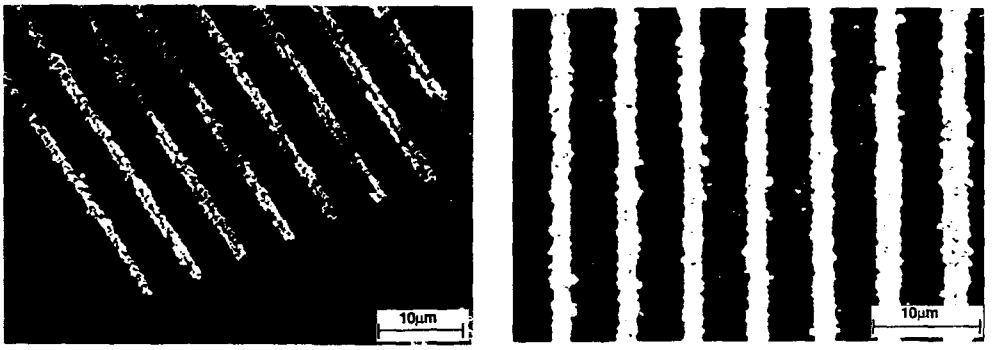

FIG. 9. Effect of pattern linewidth on diamond crystallite nucleation geometry. (a) early stage development; (b) later stage development

bedded in the surface, as these would give rise to uniform diamond nucleation. In contrast, the diamond nucleation was found to be highly selective, forming almost exclusively within the microlithographed grid lines. Such attatchment would undoubtably depend on particle size, and it is likely that the grids are retaining the finer particles in the overall distribution. Indeed, previous work has reported differences in film nucleation and growth associated with the use of different size diamond grit for the surface pretreatment.[10,12] Thus, both the geometry and scale of the pattern, as well as the size and distribution of the seeding material, will affect the final film microstructure, thus providing a degree of control over the film development.

In addition to illustrating the nature of nucleation in the diamond films, this work also elucidates critical factors inherent to diamond film growth. Most striking is the apparent propagation of grain size with continued film growth. Under identical growth conditions, the (patterned) fine grained regions of the sample remained fine and the (unpatterned) coarse-grained regions remained coarse. When a grain renucleates a new crystal adjacent to it, that new crystal appears to achieve the same size as the original one. For a film with a uniform microstructure, such constant grain size could be attributed to control by the growth conditions. However, in this instance different microstructures coexist under the same growth conditions and appear to be self-propagating. This self-propagation of grain size was observed both in the initial growth stages, where growth is occurring in plane, and also in the later stages when full coverage has occurred and out-of-plane growth is occurring. Examination of the early stage growth morphologies, both for the coarse-grained and fine-grained regions, indicates that this effect is not produced by proximity effects due to simple impingement of similar sized crystals. In the initial stages of growth, before significant impingement occurs, the crystal renucleation process appears distinctly linear in nature; i.e., the crystals tend to form in continuous chains, with each uniformly sized crystallite nucleating another in succession.

A mechanism to describe the reproducibility of the diamond crystal particle size during growth must be based on crystallographic factors. Here, nucleation of a new crystal from an existing one must be favored on a particular site on the existing crystal. Under the growth conditions of this work, the nucleation of the new crystal must on average consume an equal number of these sites as it produces. Such behavior would produce growth in a chainlike fashion. Otherwise, if each new crystal provided multiple nucleation sites, the total number of available sites would rapidly grow and produce isotropic growth geometries. This would suggest that the renucleation step preferentially occurs at a defect site. Furthermore, the establishment of a steady state number of these sites would tend to indicate that the defect is linear, rather than planar, in nature. Such a growth mechanism in which there is an energetically favored site would likely be significant only at the lower growth temperatures used in this work. It is expected that at the higher temperatures of 850–1050 °C normally reported for diamond film growth, the nucleation process would be dominated by thermal energetics. Indeed, the increase in film nucleation and growth rates with increasing temperature is well established.[10]

The observed reproducibility in the diamond crystallite particle size, even in unconstrained growth conditions, would indicate that the initial defect density of the particle acts to establish an upper limit on its size. Work in this laboratory as well as by others has shown that under proper experimental conditions, diamond crystals can be grown to considerable sizes. An example given in Fig. 10 is

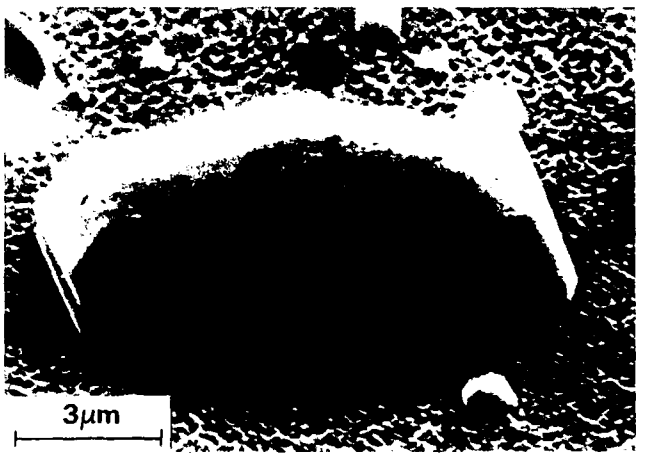

FIG. 10. Large, planar diamond crystal formed on SiO_2 by plasma enhanced CVD

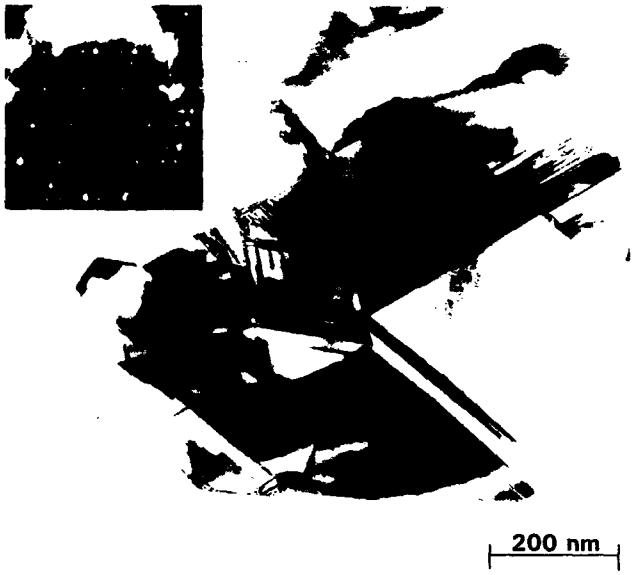

FIG. 11. Multiple twinning occurring in diamond film on Si.

of a regular, faceted platelet grown on SiO_2 by plasma-enhanced CVD. It is likely that the achievement of this large size is controlled to a significant degree by the crystalline perfection of the lattice. Films that were grown under alternate conditions and that developed much smaller crystal dimensions were found to be highly defective,[13] containing significant amounts of crystallographic twinning. An example of this multiple twinning is shown in Fig. 11, which can give rise to the apparent five-fold faceting commonly reported. Thus, while growth conditions are of unquestionable importance in developing appropriate microstructures in diamond thin films, the nucleation and early stages of growth also appear critical in defining the defect concentration, and hence the microstructure, of the final film.

V. CONCLUSIONS

Microlithographic patterning of substrate surfaces can enhance film uniformity over a large spatial area and can assist the formation of fine-grained microstructures. This is especially useful for optical applications, where fine-grained films are preferred for reduced scatter losses. If post-deposition polishing is required, then the patterned growth serves as a useful precursor by improving spatial uniformity and reducing the initial surface roughness.

Examination of the nature of the nucleation and growth of the microlithographed films indicates that the intrinsic film growth mechanism is controlled by renucleation on crystallographic defects. This gives rise to a constant number of growth sites and results in generation of a steady state grain size that is controlled by the early stage film structure. The microlithographic patterning is believed to retain the smallest diamond particles in the initial surface pretreatment, predisposing the later stage film growth to a fine-grained morphology.

ACKNOWLEDGMENTS

The authors are grateful to Dr. D. G. Howitt at the University of California, Davis, for valuable discussions on crystal growth mechanisms. This work was supported in part through the Office of Naval Research.

[1] M. Kamo, Y. Saito, S. Matsumoto, and N. Setaka, J. Cryst. Growth **62**, 642 (1983).
[2] A. R. Badzian, T. Badzian, R. Roy, R. Messier, and K. E. Spear, Mater. Res. Bull. **23**, 531 (1988).
[3] A. B. Harker and J. F. DeNatale, J. Mater. Res., April 1990.
[4] Tom Feng, in Diamond Optics II, SPIE Proceedings Vol. 1146, 159 (1989).
[5] H. Diao, T. Kobata, S. Morimoto, J. Satoh, and M. Yoshikawa, "Diamond Low Resistance Polishing Method," Preprint from Showa Electrical Engineering and Tokyo Engineering University, Tokodai, Japan (1989).
[6] A. B. Harker, J. F. Flintoff, and J. F. DeNatale, in the Proceedings of Diamond Optics III, SPIE Meeting, San Diego, CA, July, 1990 (to be published).
[7] A. R. Kirkpatrick, B. W. Ward, and N. P. Economou, J. Vac. Sci. Technol. B **7**, 1947 (1989).
[8] Jing Sheng Ma, Hiroshi Kawarada, Takao Yonehara, Jun-Ichi Suzuki, Jin Wei, Yoshihiro Yokota, and Akio Hiraki, Appl. Phys. Lett. **55**, 1071 (1989).
[9] Jing Sheng Ma, Hiroshi Kawarada, Takao Yonehara, Jun-Ichi Suzuki, Yoshihiro Yokota, and Akio Hiraki, J. Cryst. Growth **99**, 1206 (1990).
[10] P. K. Bachmann, W. Drawl, D. Knight, R. Weimer, and R. F. Messier, in *Diamond and Diamond-Like Materials Synthesis*, EA-15, edited by A. Badzian, M. Geis, and G. Johnson (Material Research Society, Pittsburgh, PA, 1988), pp. 99–102.
[11] M. W. Geis, Appl. Phys. Lett. **55**, 550 (1989).
[12] S.-C. Yu, H.-S. Chun, and F.-S. Guo, J. Cryst. Growth **99**, 1196 (1990).
[13] A. B. Harker, R&D Magazine **32**, 84 (1990).

Appendix 5

Microstructure and Orientation Effects in Diamond Thin Films

Microstructure and orientation effects in diamond thin films

J. F. DeNatale, A. B. Harker, and J. F. Flintoff
Rockwell International Science Center, Thousand Oaks, California 91358

(Received 13 December 1990; accepted for publication 6 February 1991)

The microstructure and orientation of diamond thin films grown by plasma assisted chemical vapor deposition have been studied as functions of growth temperature, substrate identity, and substrate pre-treatment. Results indicate that for growth temperatures below 650 °C, competition between film growth and etching can lead to preferential (110) oriented films on a variety of substrate materials. This orientation can be globally sustained during growth by the occurrence of (111) planar defects.

INTRODUCTION

The growth of diamond thin films by low-pressure techniques occurs through a complex kinetic balance between the nucleation, growth, and etching of both diamond and nondiamond species. The importance of these competing processes to the final film properties has been documented extensively in the literature, detailing the strong effect film deposition conditions have on the microstructures and Raman signatures of the resulting films.

In this work, we have investigated the degree to which the microstructure and orientation of plasma assisted chemical vapor deposition (PACVD) diamond films can be modified by the use of various substrates, substrate surface preparations, and deposition conditions. This has illuminated the role of crystalline defects in the growth and morphology of polycrystalline and homoepitaxial diamond thin films.

EXPERIMENT

Films were grown by PACVD using an ASTEX 1.5-kW microwave reactor operated at 1.2 kW. The source gas composition used for this work was 99% hydrogen, 0.7% methane, and 0.3% oxygen. The total gas flow rate was approximately 1 slm, with chamber pressure kept constant at 30 Torr using downstream pressure control. Sample heating was accomplished using an inductively heated graphite sample holder, with film temperature determined by optical pyrometry. Films were grown on both diamond and nondiamond substrates. The diamonds were natural type 2A single crystals, oriented with (100), (110), and (111) surfaces, respectively. The nondiamond substrates included (100) single crystal silicon, fused silica, polycrystalline silicon nitride, and (hexagonal) polycrystalline pyrolitic boron nitride (PBN). Surface pretreatment with submicron diamond paste was performed on the nondiamond substrates to enhance film nucleation. In addition, a (100) silicon substrate which had been polished with a 45 mesh cubic boron nitride powder was included in the deposition.

Films were analyzed by scanning electron microscopy (SEM), micro-Raman scattering, and x-ray diffraction. Growth rates were established by infrared reflectance spectroscopy.

RESULTS

A growth temperature of 650 °C was used for the depositions on the single-crystal diamond substrates. The resulting films on all three substrate orientations produced fully oriented films, as evidenced by x-ray diffraction and SEM electron channeling contrast (Fig. 1). Imaging of both the (100) and (111) films indicated them to be epitaxial, although they differed in their surface morphologies (Fig. 2). The (100) film had a low level of observable structural defects, although it did show some fine scale texture development. The (111) film exhibited well-defined triangular defects on an otherwise exceedingly smooth surface. The Raman spectra of these films showed a sharp peak at 1332.5 cm^{-1} (Fig. 3), characteristic of natural single-crystal diamond.

In contrast to the morphologies of the previous two substrates, the film on the (110) diamond substrate exhibited a high degree of fairly coarse surface texture (Fig. 2). In addition, the (110) film was characterized by a growth rate approximately twice that of the other two orientations.

The initial experiments investigating the effects of growth temperature on the nondiamond substrates were conducted using (100) Si substrates polished with submicron diamond paste. These experiments, previously reported,[1] revealed that (110)-oriented polycrystalline diamond films could be produced at growth temperatures of 450–650 °C when the samples were located in the plasma region of highest growth rate. At higher growth temperatures or outside of the direct plasma impingement zone, only randomly oriented films have been observed. Based on these results, a growth temperature of 650 °C was used for the experiments reported here.

The current experiments revealed that similar (110)-oriented films can be produced on polycrystalline boron nitride and silicon nitride substrates as well as on (100) Si with growth rates of 0.1–0.5 μm per hour. X-ray diffraction analysis indicated that the ratio of the peak intensity of the diamond 220 reflection to that of the 111 reflection was approximately a factor of 25 higher than in a random film.

The microstructures of the one-dimensionally oriented films on the various substrate materials all exhibited certain similarities. These films were generally more regular than the random films, with their surface appearance dom-

 0021-8979/91/096456-05$03.00

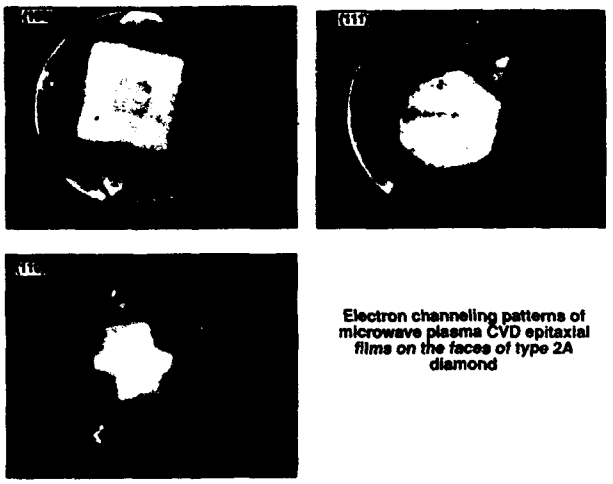

FIG. 1. Electron channeling patterns of PACVD epitaxial diamond films on single-crystal type 2A diamond.

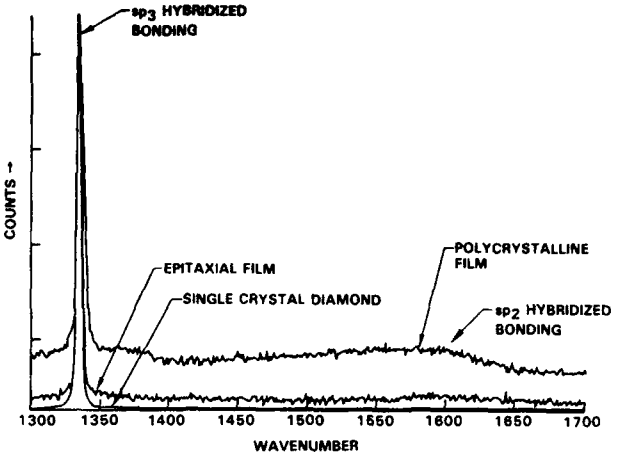

FIG. 3. Raman spectra comparing homoepitaxial diamond film and type 2A diamond substrate. Also shown is spectra of polycrystalline film on Si.

inated by the presence of large numbers of planar growth twins (Figs. 4 and 5). In contrast, the films on fused silica and BN-polished (100) Si showed no tendency for preferred orientation.

The observations of film morphology and properties for the various substrates and surface preparations are summarized in Table I.

DISCUSSION

The homoepitaxial growth of the diamond films on the various diamond substrates indicates that substrate crystallography can significantly affect the microstructure and growth kinetics of the films. The observed surface morphologies and growth rates in these experiments are consistent with the directional bonding of the diamond structure. As noted by Hartman and Perdok[2] and Sunagawa,[3] the (110) face contains one periodic bond chain (PBC) in plane. In addition, by symmetry, one PBC vector also exists normal to the surface. This provides continuously available bonding sites for both in-plane propagation of the surface by atomic attachment as well as strong bonding sites for the attachment of subsequent layers. The observed growth rate and rough surface morphology of the homoepitaxial film on (110) diamond is attributed to the presence of (equivalently) favorable growth modes for both in-plane and out-of-plane growth.

The (111) face of diamond, on the other hand, contains three PBC's.[3] This predicts smooth growth faces with relatively low displacement velocities, as observed experimentally in the homoepitaxial films. The relatively smooth (100) face, in contrast, would not be expected to occur in a perfect diamond structure based solely on PBC analysis.[3] Surface reconstruction, however, can allow this face to develop into a habit-controlling face, and these cube faces are commonly observed in synthetic diamonds fabricated by a variety of techniques.[3] The lower number of PBC's on this face, and the possibility of local distortions in the surface reconstruction may contribute to the greater surface texture observed on the (100) homoepitaxial film as compared with the (111) film.

The observations of substantially higher growth rates for the (110) oriented polycrystalline films on the nondiamond substrates are consistent with their observed growth morphologies as well as with the observed behavior of the homoepitaxial films. The rate of growth of a thin film is intimately associated with the availability of low-energy bonding sites. Such sites will in turn be associated with the most rapidly growing faces. In general, the crystalline faces having the highest growth rates rapidly fill their available bonding sites and cease growth. At this point, growth can continue only on the slower growing faces or by renucleation of a new crystallite, and this becomes the rate-limiting step in the growth kinetics. Hence, the exposed facets on a randomly oriented crystalline film would be expected to be those exhibiting the slowest growth. The dominance of (100) and (111) faceting on the exposed surfaces of random diamond films [Fig. 6(a)] and isolated particles [Fig. 6(b)] suggests these are the

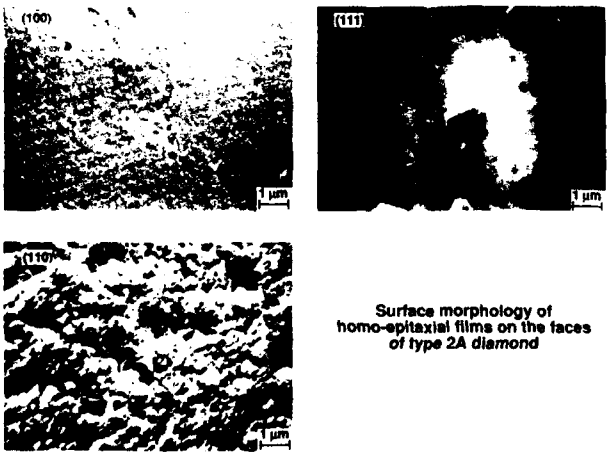

FIG. 2. Surface morphology of homoepitaxial films on type 2A diamond.

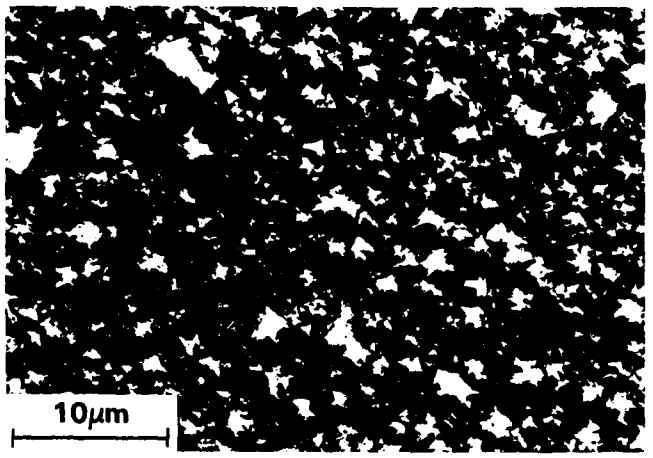

(a)

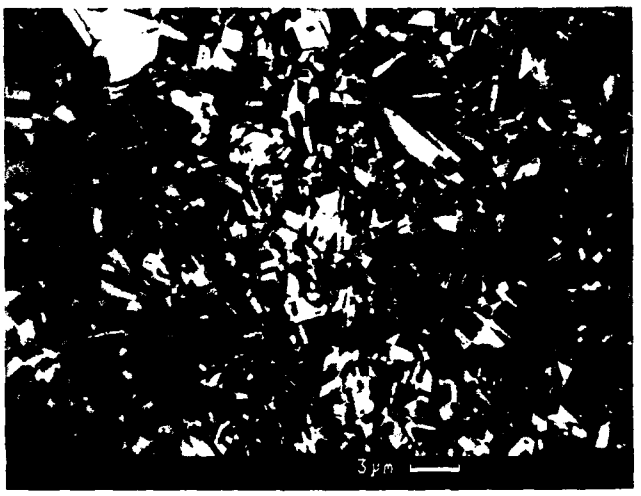

(110) ORIENTED DIAMOND ON PYROLYTIC BORON NITRIDE, SUBMICRON DIAMOND PASTE POLISH

(b)

(110) ORIENTED DIAMOND ON (100) SILICON, SUBMICRON DIAMOND PASTE POLISH

(c)

FIG. 4. Surface microstructures of (110) oriented polycrystalline diamond films. (a) Silicon nitride substrate; (b) boron nitride substrate; (c) (100) Si substrate.

FIG. 5. Detail of multiply twinned grain in (110) oriented diamond film on (100) Si.

slow growth faces. Indeed, Zheng *et al.*[4] have reported that the (110) face of natural diamond shows a lower oxidation rate than either the (100) or (111) faces, suggesting that the atoms on this face have a higher bonding energy. The dominance of (100) and (111) faceting in natural diamond crystals further establishes this, and is consistent with the PBC analysis of Hartmon and Perdok[2] and Sunagawa.[3]

The (110) plane of diamond is intersected by the (111) planes, generating the periodic bonding chains on the (110) faces. The (111) planes are subject to both stacking and slip plane faults that are known to produce striations in natural diamond crystals.[3] Similarly, these regular planar growth twin defects on (111) planes produce striated morphologies in the grains of the oriented polycrystalline diamond films.

We propose that the formation of (111) twin defects on the (110) diamond growth surface provides low-energy sites for preferential bonding of the radical species, leading to an enhancement of the growth rate. Similarly, the presence of these defects leads to a continued propagation of the low-energy bonding sites. This is illustrated in Fig. 7. For a faceted perfect crystal oriented with a (110) surface plane, rapid growth along the (110) faces consumes all the available sites, leading to a crystal bounded by the slower growing faces. At this stage, crystal growth is stopped and renucleation of a new crystallite must occur for bulk film growth to continue. This step is known to be comparatively slow at low temperatures for PACVD diamond films. In the presence of the planar (111) twin defects, however, the growth along the (110) faces does not lead to a consump-

TABLE I. Microstructure of diamond films as a function of substrate identity and surface preparation.

Substrate	Film properties
(100) Type 2A diamond	Epitaxial, low defect, textured
(111) Type 2A diamond	Epitaxial, smooth, isolated defects
(110) Type 2A diamond	Epitaxial, rough surface, highest growth rate
(100) Si (diamond polish)	(110) oriented polycrystalline
(110) Si (c-BN polish)	Random polycrystalline
Fused silica (diamond polish)	Random polycrystalline
Silicon nitride (diamond polish)	(110) oriented polycrystalline
Boron nitride (diamond polish)	(110) oriented polycrystalline

(a)

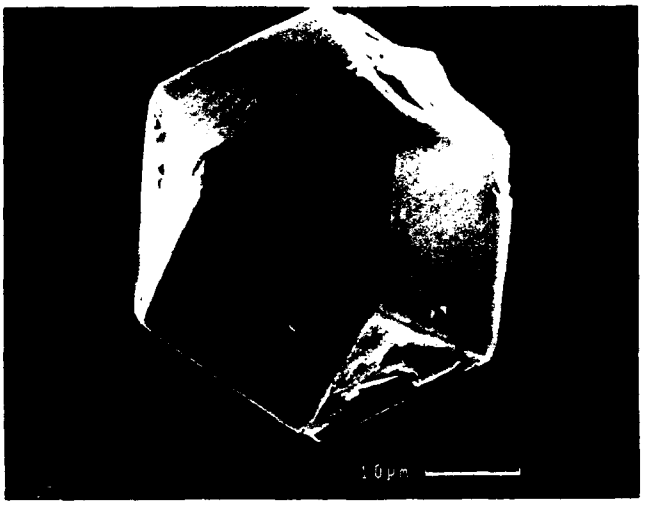

(b)

FIG. 6. (a) SEM micrograph of grain development in a random diamond film grown by PACVD; (b) Faceted morphology of isolated diamond particle grown under random growth conditions.

tion of the preferred bonding sites due to the lack of crystallographic equivalence across the defect boundary. This leads to a propagation of the defective structure, with the net growth rate controlled now by the rate of radical attachment instead of by crystal renucleation.

The generation of oriented films on the nondiamond substrates is consistent with the observed homoepitaxial film growth behavior. The global (110) orientation on the nondiamond substrates is believed due to the interplay between anisotropic growth modes and anisotropic etching, with both factors favoring the (110) growth. For small diamond seed crystals, the plasma etching occurring during the initial stages of film formation will tend to alter the crystallographic distribution of the seeds towards a (110) orientation. Coupled with this are the enhanced growth rates observed on the (110) single-crystal diamond surface. The combination of these two factors imposes a strong preference for global (110) oriented polycrystalline film development under the low deposition temperatures used in this work. For higher growth temperatures, it is likely that the energetic differences associated with the crystallographically favored growth modes will be much less significant, and the nucleation time during which seed etching occurs will be reduced, favoring random film development. This transition to random growth morphologies at higher growth temperatures has indeed been experimentally demonstrated. Furthermore, the observation that such oriented films can be grown on a variety of polycrystalline substrates as well as on single-crystal (100) silicon indicates that under these growth conditions the crystal structure of the nonlattice matched substrates do not significantly affect the nucleation energetics. This observation is consistent with the high surface energy of diamond.[5] For high surface energy substrates, such as diamond itself, substrate crystallography has been shown to play a role.

The samples not exhibiting the oriented growth at these low temperatures ($< 650\,^{\circ}C$) were the (100) Si polished with coarse cubic boron nitride powder and the fused silica substrate. On the silicon sample, growth was initiated on the individual boron nitride crystal surfaces (Fig. 8). While smaller particles did initiate some growth on the Si surface, the morphology was dominated by large, isolated

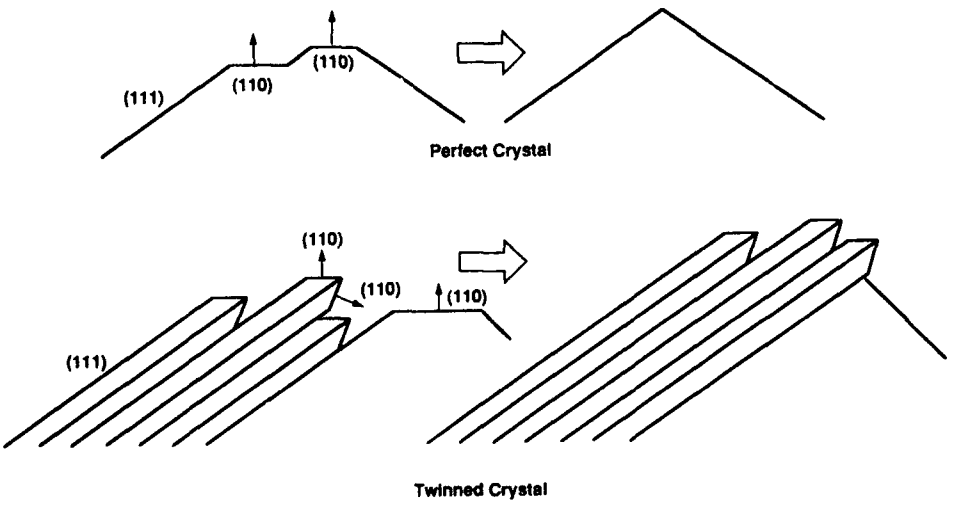

FIG. 7. Schematic of (110) growth surface propagation in a multiply twinned diamond crystal.

FIG. 8. Preferential growth of diamond crystals on coarse cubic boron nitride particles.

diamond crystals with smooth faceted geometries (Fig. 9). The lack of global orientation and the reduced growth rate in this sample were consistent with the proposed mechanisms for oriented growth in the diamond seeded films.

For the fused silica substrate, the different growth behavior is attributed to oxygen release during surface reduction. The interaction of the plasma with the substrate surface is clear, as evidenced by the pitting observed in the micrograph of Fig. 10. Oxygen released during this reaction will not only etch the smaller diamond particles embedded by the polishing process, but will also inhibit the general nucleation of the polycrystalline diamond film by surface disruption. In this case, growth is again limited to the larger diamond particulate seeds on the surface, and well-defined particle growth morphologies result. It has been noted in this laboratory that diamond films grown on fused silica are extremely white, containing little of the graphitic components which tend to darken the films. This is consistent with a higher local oxygen content at the reaction surface, which preferentially removes the sp^2 bonded carbons.[6]

POLYCRYSTALLINE DIAMOND ON (100) SILICON, CUBIC BORON NITRIDE POLISH (45 MESH)

FIG. 9. Faceted diamond crystal morphology observed on BN-seeded (100) Si.

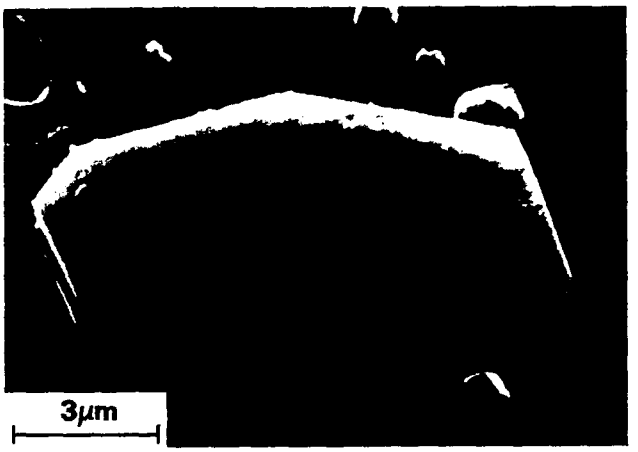

POLYCRYSTALLINE DIAMOND ON FUSED SILICA, SUBMICRON DIAMOND PASTE POLISH

FIG. 10. Diamond particle morphology for random film grown on fused silica.

CONCLUSIONS

The preferential growth of globally oriented (110) polycrystalline diamond films below 650 °C can be ascribed to a combination of anisotropic etching of diamond nuclei and anisotropic growth enhanced by the presence of crystallographic planar defects. These films tend to be described by regular microstructures dominated by multiple (111) growth twins. These defects provide a source of preferred attachment sites for the growing film and lead to a propagation of a (110) oriented growth surface. This tends to maintain the film in a growth-limited mode as opposed to a renucleation-limited mode, resulting in a significant increase in the net film growth rate.

ACKNOWLEDGMENT

Portions of this research were sponsored by the Office of Naval Research.

[1] A. B. Harker and J. F. DeNatale, J. Mater. Res. **5**, 818 (1990).
[2] P. Hartmon and W. G. Perdok, Acta. Cryst. **8**, 49 (1955).
[3] I. Sunagawa, J. Cryst. Growth **99**, 1156 (1990).
[4] A. Zheng, H. Kanda, T. Ohsawa, and S. Yamaoka, J. Mat. Sci. Lett. **9**, 331 (1990).
[5] R. Kern, G. Le Lay, and J. J. Metois, *Basic Mechanisms in the Early Stages of Epitaxy*, in *Current Topics in Materials Science*, edited by E. Kaldis (North Holland, New York, 1979), Vol. 3.
[6] S. J. Harris and A. M. Weiner, Appl. Phys. Lett. **55**, 2179 (1989).

Appendix 6

Pressure Effects in the Microwave Plasma Growth of Polycrystalline Diamond

Pressure effects in the microwave plasma growth of polycrystalline diamond

A. B. Harker and J. F. DeNatale

Rockwell International Science Center
1049 Camino Dos Rios, Thousand Oaks, CA 91360

ABSTRACT

Microwave plasma deposition of polycrystalline diamond is being investigated over the pressure range 1 to 100 kPa. The conditions of growth, microstructure, and spectroscopic properties of the resulting materials are being compared. A phenomenological description of the dependence of diamond microstructure upon growth conditions has been developed.

1. INTRODUCTION

Microwave plasma assisted CVD (MPACVD) deposition of polycrystalline diamond has been studied extensively in this and other laboratories in low pressure growth systems at temperatures from 250 to 1100°C with a range of hydrocarbon sources (e.g., CH_4, CO, CH_3OH, C_3H_4O, etc).[1,2,3] These 2.45 GHz systems typically produce a fairly diffuse plasma at pressures of 1 to 5 kPa, providing CVD type growth. At higher plasma pressures, the three body recombination of electrons with ions becomes dominant, greatly limiting the geometric area of the plasma. Visually, the plasma shrinks to the center of the chamber with increasing pressure and eventually cannot be sustained.

To produce a microwave plasma at higher pressures, other cavity designs which produce sufficient energy density to achieve and sustain gas breakdown must be used. We have investigated the use of a custom designed TM_{010} cylindrical 2.45 GHz cavity to develop sustained plasmas and diamond growth at pressures in excess of one atmosphere. At higher pressures, diamond particles nucleate with line of sight relationship to the plasma source with a higher temperature dependence for diamond growth than observed under lower pressure CVD conditions. The microstructures of the diamond films produced in the low and high pressure systems can be related in the same manner to the growth controlling parameters.

2. EXPERIMENTAL

Diamond films were grown in two different flow systems both using an Applied Science 1.5kW, 2.45GHz magnetron source and waveguide arrangements. All substrate surfaces were prepared by diamond paste abrasion before deposition.

The low pressure cavity is an all-metal sealed, water cooled, 15.5 cm inner diameter stainless steel chamber with radiantly heated graphite sample holder. The radiation is coupled into the chamber with a TM_{01} rectangular to circular waveguide adapter through a silica window. The chamber operates at 1 to 5 kPa, with typical gas mixtures being 0.5% CH_4 in H_2. Growth temperatures ranged from 450 to 980°C (IR pyrometer), with variation of 50 to 75°C across the 10 cm silicon substrate.

The higher pressure system (20 to >100 kPa) uses the same 1.5 kW magnetron head coupled through a three stub tuner into a custom designed cylindrical high pressure TM_{010} 2.45gHz cavity. The microwave power is coupled directly into the gas flowing through a 12 mm quartz flow tube passing through the center of the cavity. This system couples 1.2 to 1.5 kW into the flowing gas and produces a plasma flame. The flame is forced out of the quartz tube by flows of 20 to 50 l/min of a 2/1 Ar/H_2 mixture with CH_4 held at the same ratio to H_2 as with the MPACVD chamber. The substrates in this system were typically 4x4x25mm rectangular polycrystalline Si_3N_4 bars held at right angles to the plasma front or 0.5 cm radius molybdenum hemispheres. All substrates were mounted on a water-cooled fixture and temperatures were monitored by an IR pyrometer.

Polycrystalline particles and films were examined by scanning electron microscopy and Raman scattering spectroscopy.

0-8194-0662-7/91/$4.00

3. RESULTS AND DISCUSSION

Nucleation and microstructure effects in the low pressure (1.6 to 5.3 kPa) microwave plasma assisted diamond chamber have been described by a number of researchers. The most generally reported trends are the observation of (100) exposed faces on the diamond grains at higher hydrocarbon concentrations, switching to primarily (111) exposed crystalline planes at lower hydrocarbon concentrations for a fixed deposition temperature.[1,2] A significantly different microstructure occurs when the film growth becomes defect renucleation dominated and highly twinned (110) global orientation is obtained[3]. Such (110) oriented films have been obtained by a number of researchers under conditions with low hydrocarbon concentrations and added oxygen.[3,4] In this work these same trends in diamond film microstructure have been observed at all deposition pressures. The primary effects associated with increasing pressure have been a significant increase in the observed film growth rate for a given gas composition and substrate temperature and a dependence of the growth process upon gas flow dynamics.

At a substrate temperature of 950°C the growth rate of polycrystalline diamond was nominally 0.6 microns/hr at 4 KPa, 3-5 microns/hr at 25 kPa, and 10-20 microns/hr at 100 kPa pressure for reaction mixtures containing a methane to hydrogen ratio of about 0.5%. The increase in growth rate with pressure is associated with the arrival rate of the reactive species forming the diamond particles on the substrate surface, but has not been quantified due to the dependence of the growth process on the flow dynamics.

The effects of reactant composition and temperature on the microstructure of the diamond particles formed in the microwave systems were basically the same at all pressures and permits a phenomenological description of the effects of growth conditions to be postulated. Figure 1 (a-l) is a series of SEM micrographs showing the progression of microstructure types associated with the deposited carbon films as a function of distance from the locus of the plasma ball in the low pressure system, and the feather of the plasma flame in the high pressure system. At greater distances from the most intense plasma region there is a decrease in both the surface temperature of the growing particles and the concentration of the radical and atomic species associated with the growth process. In a steady-state system the progression would coincide with increasing temperature and an increasing hydrogen atom to hydrocarbon radical ratio.

At the greatest distance from the plasma (lowest temperature, lowest hydrogen atom, highest unreactive hydrocarbon content) very high nucleation density produced a continuous amorphous carbon film with hemispherical surface protrusions. Nearer to the plasma the nucleation density drops and the particles become distinct and microcrystalline. Raman spectra of the material in this regime show diamond and some sp2 bonded carbon. The particles have very high defect densities with the dominance of surface energy constraints being obvious from the spherical appearance of the particles.

Moving still nearer to the plasma, the particles remain generally spherical, but {100} faces appear and the Raman spectrum shows a decrease in graphitic carbon. The {100} facets become more pronounced as the concentration of hydrogen atoms and etching species increase in toward the center of the plasma. In this region surface energy is competing with the growth and etch rates of the sp2 and sp3 solid carbon to determine the microstructure. The particles still tend to a spherical shape, but preferential <111> direction growth is favoring the exposure of {100} faces.

In regions of greater plasma density, the surface temperature and hydrogen atom concentrations are higher and nucleation as well as defect generation become lower. The particles are more highly faceted, with cubo-octahedral shapes. In this regime the surface energy anisotropy between the crystalline planes is more significant and the particle microstructure becomes controlled by the relative reaction kinetics of growth and etching. The cubo-octahedral particles have the <110> direction being the long axis of fastest growth. This is consistent with the observation that the {110} plane of diamond has the lowest etching rate in hydrogen and oxygen.[5]

In the center of the plasma region the surface temperature and reactive etching species concentrations are the highest. In this regime, high etch rates discriminate against the less stable nucleation centers, favoring the formation of the characteristic five-fold twinned defect nuclei. This crystallographic defect is a successive multiple twinning on the {111} planes in a <211> direction around the <011> axis. Forming at a very fine scale, this defect continues to grow to produce the end member microstructure seen in Figure 1 which is dominated by the exposed {111} planes.

This phenomenological description is consistent with the observation that at growth temperatures near 650°C many films develop a characteristic global (110) orientation as renucleation on the initial film layer leads to increasing thickness[3]. Anisotropic etching and the apparent faster growth in the <110> direction favor global (110) orientation as does the availability of the low energy (111) slip plane twin defect which provides a low-energy site for preferential bonding of radical species, leading to an enhanced growth rate in the (110) orientation (Figure 2).

4. CONCLUSIONS

The growth rate of diamond films from microwave generated plasmas increases by over 40 fold between 4 and 100 kPa pressure with the same hydrocarbon/hydrogen gas ratio and substrate temperature. The film microstructure in the first fully developed continuous film layer is remarkably similar for films grown at low and high pressures and is consistent with a model based on surface energy effects and anisotropic growth. The model suggests that higher etching conditions favor growth along the <110> direction and that high nucleation-lower etching conditions favor growth in the <111> direction. Such films would have (111) and (100) planes exposed respectively.

5. ACKNOWLEDGEMENTS

Portions of this research were sponsored by the Office of Naval Research, Department of the Navy, Arlington, Virginia.

6. REFERENCES

1. K. Kobashi, K. Nishimura, Y. Kawate, and T. Horiuchi, Phys. Rev. B 38 4067 (1988).

2. K.V. Ravi, C.A. Koch, H.S. Hu, and A. Joshi, J. Mater. Res. vol 5, 2356 (1990).

3. J.F. DeNatale, A. B. Harker, and J.F. Flintoff, J. Appl. Phys 69(9), 6456-6460 (1991).

4. K. Kobashi, K. Nishimura, K. Miyata, K. Kumagai, and A. Nakue, J. Mater. Res. vol 5, 2469 (1990).

5. A. Zheng, H. Kanda, T. Ohsawa, and S. Yamaoka, J. Mat. Sci. Lett. 9, 331 (1990).

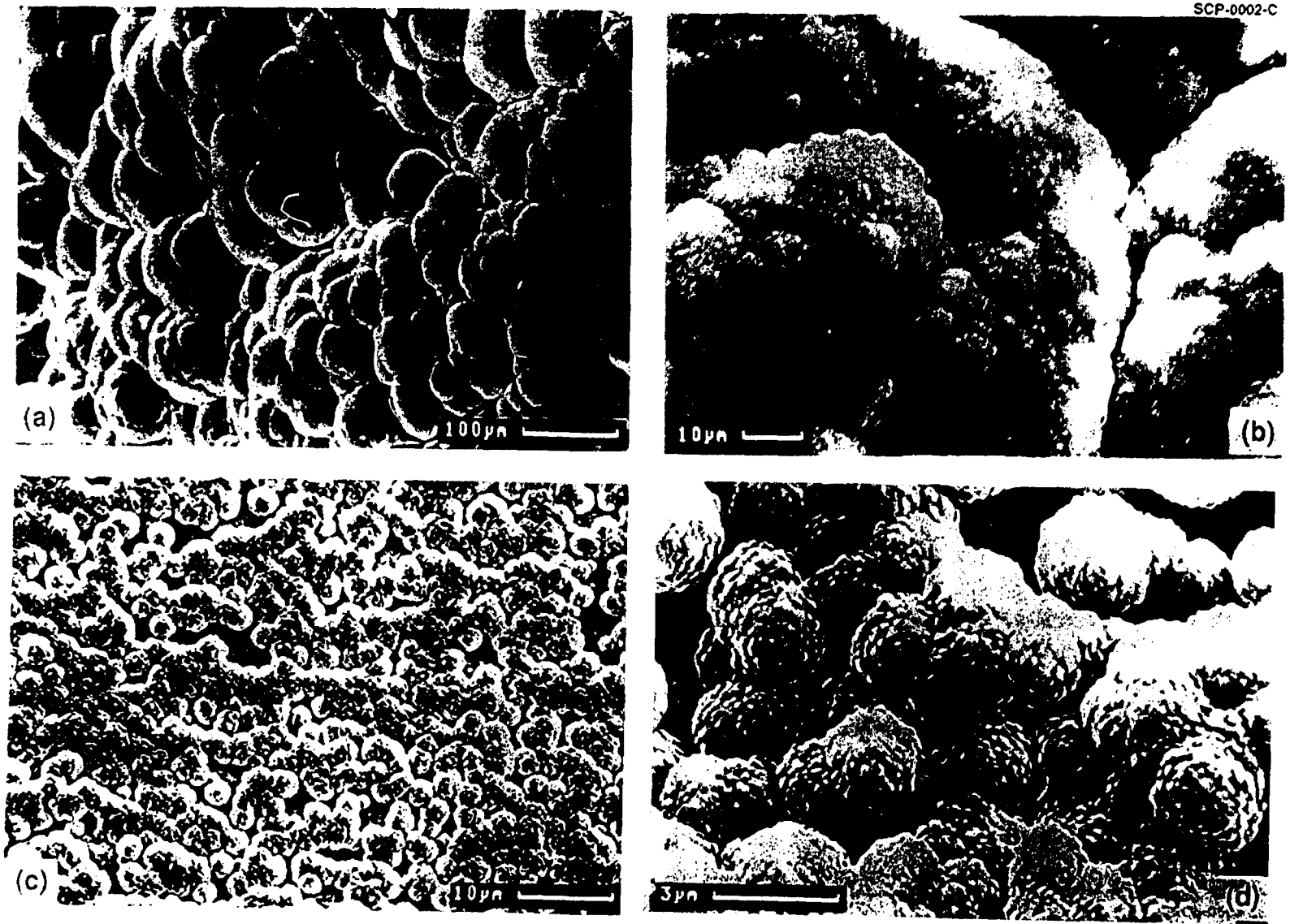

Figure 1 (a-d) SEM micrographs showing the change in polycrystalline diamond microstructure as a function of distance from the center of the growth plasma.

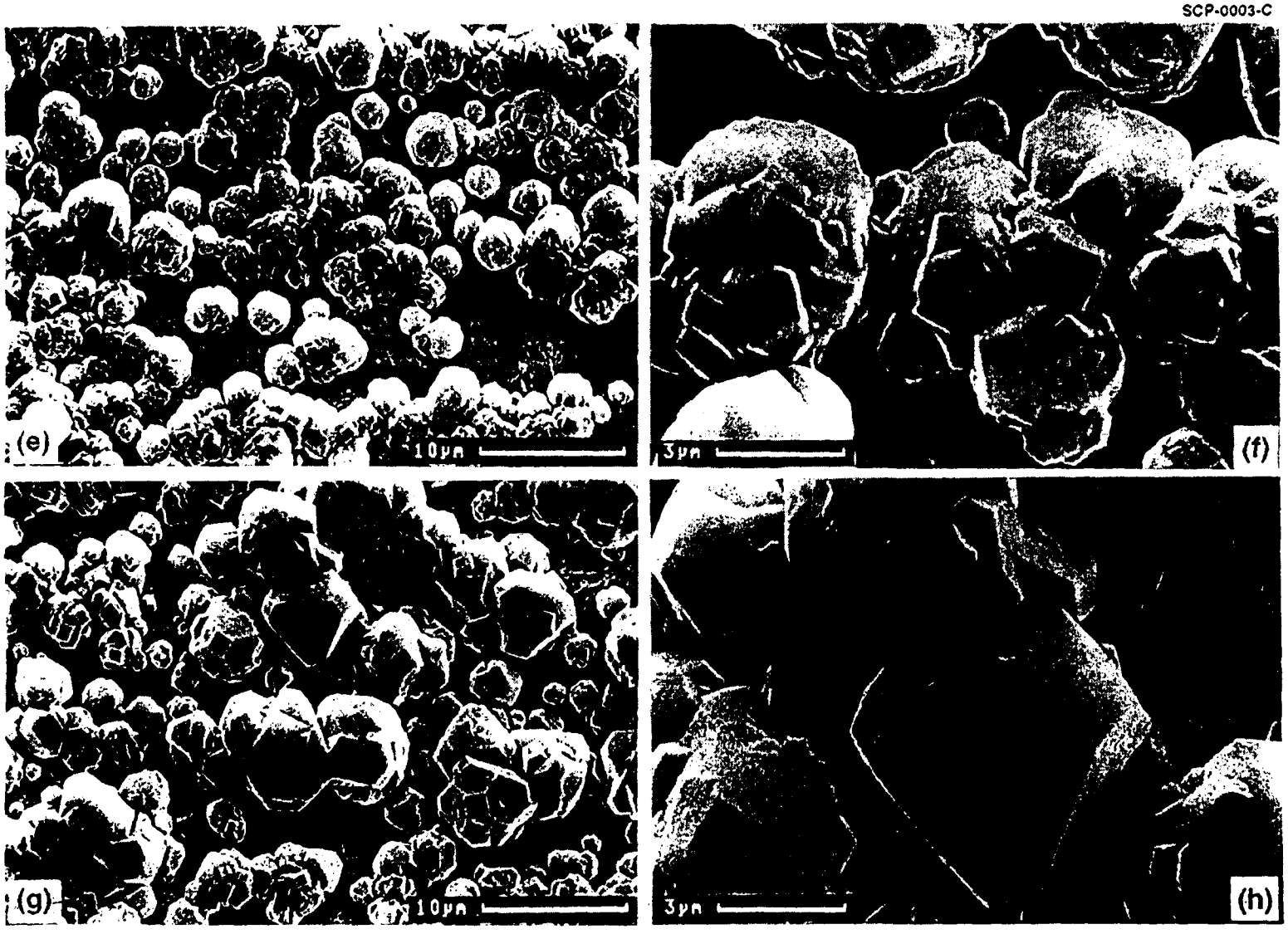

Figure 1 (e-h) SEM micrographs showing the change in polycrystalline diamond microstructure as a function of distance from the center of the growth plasma.

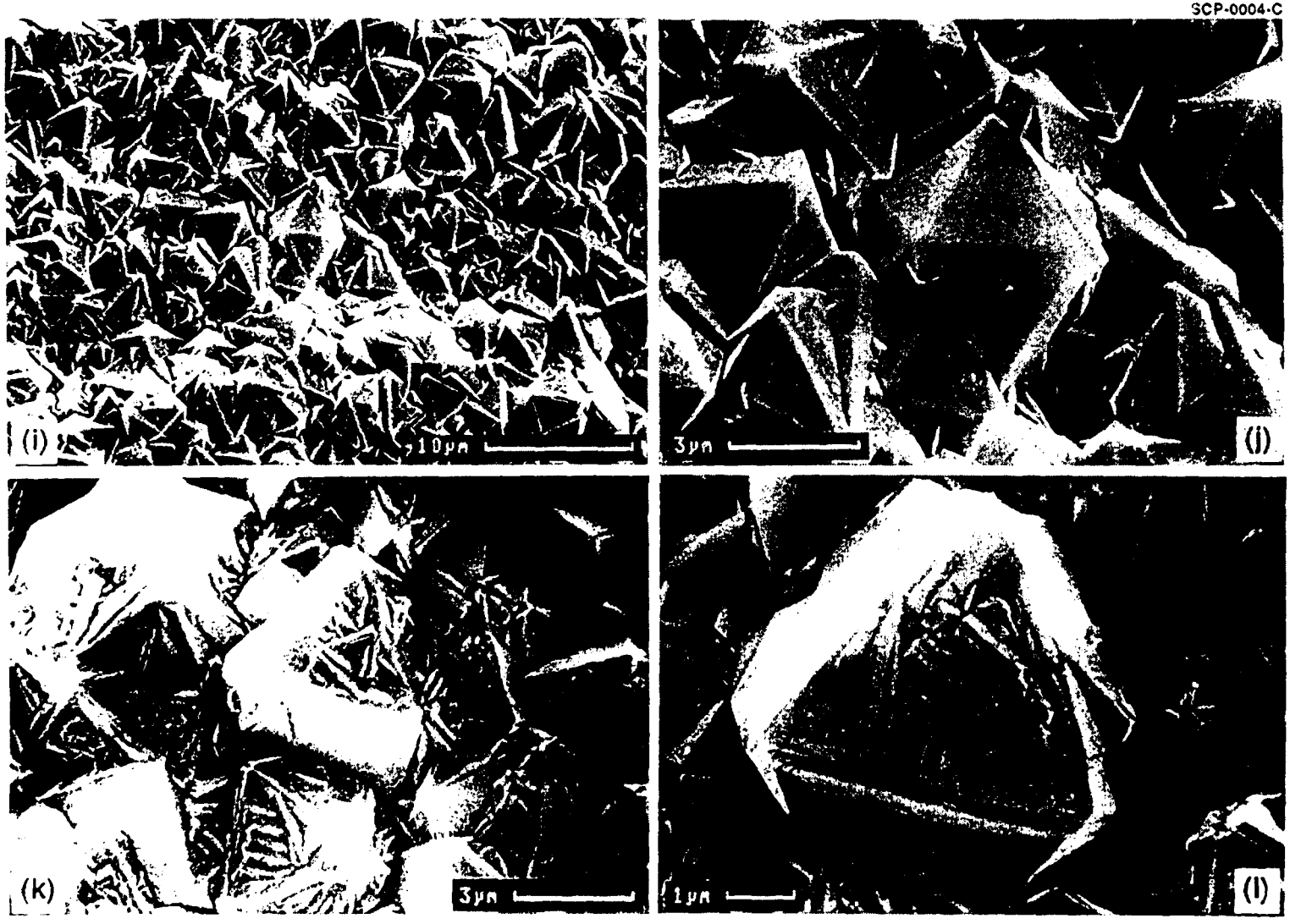

Figure 1 (i-l) SEM micrographs showing the change in polycrystalline diamond microstructure as a function of distance from the center of the growth plasma.

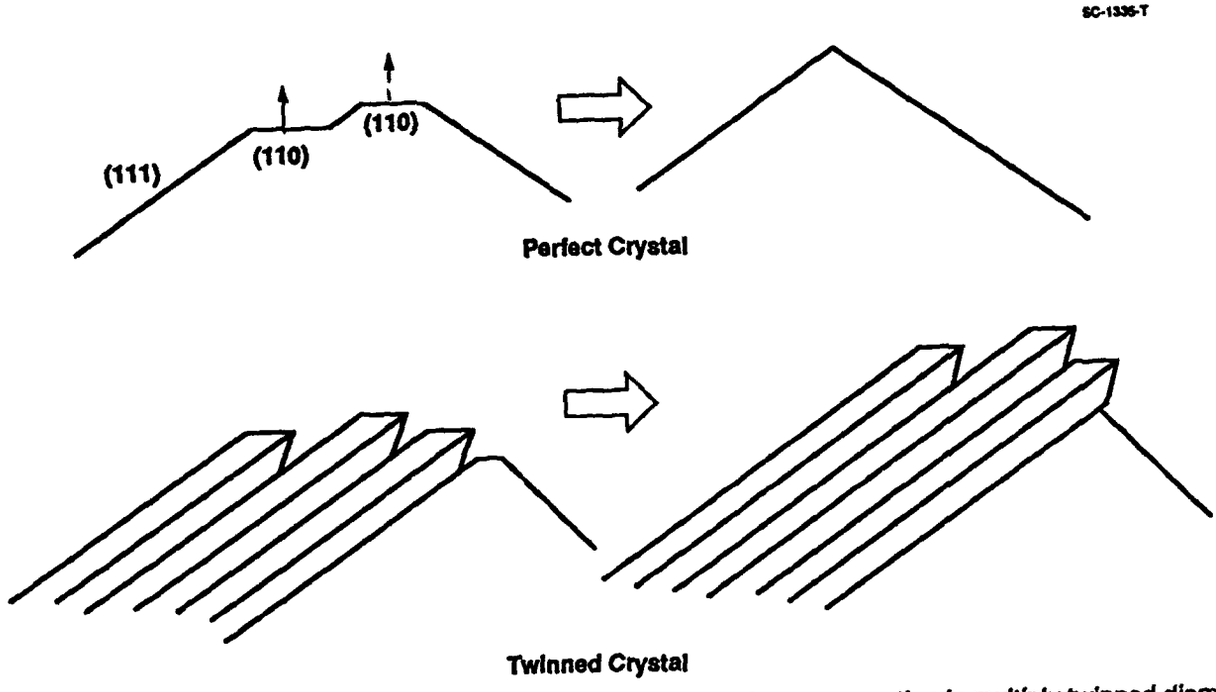

Figure 2. Schematic of a process favoring a (110) oriented growth surface propagation in multiply twinned diamond particles.

Appendix 7

The Polishing of Polycrystalline Diamond Films

PROCEEDINGS REPRINT

SPIE—The International Society for Optical Engineering

Reprinted from

Diamond Optics III

9–11 July 1990
San Diego, California

Volume 1325

The polishing of polycrystalline diamond films

Alan B. Harker, John Flintoff, and J.F. DeNatale

Rockwell International Science Center
P.O. Box 1085
1049 Camino Dos Rios
Thousand Oaks, CA 91360

ABSTRACT

Optically smooth surfaces can be produced on initially rough polycrystalline diamond films through the combined use of reactive ion etching and high temperature lapping on Fe metal. Protective thin film barriers are first applied to the diamond surface to restrict the reactive oxygen or hydrogen ion etching process to regions of greatest roughness. When the overall surface roughness has been reduced sufficiently by etching, mechanical lapping of the surface on an Fe plate at temperatures of 730°C-900°C in the presence of hydrogen can be used to produce surface roughnesses of less than 10 nm as measured by profilimetry. The two techniques are complementary for flat surfaces, while the reactive etching process alone can be used with shaped substrates to produce a surface finish suitable for LWIR optical applications.

1. INTRODUCTION

The fundamental processes involved in the growth of polycrystalline diamond film surfaces leads to a high degree of roughness in thicker films. The general roughness is produced by the protrusion of individual faceted particles as shown in the scanning electron micrograph in Fig. 1. This roughness is often overshadowed, however, by the localized preferential growth of large particulates (Fig. 2). This surface roughness greatly limits the use of such thick diamond films for coating friction-wear surfaces and in optical components.

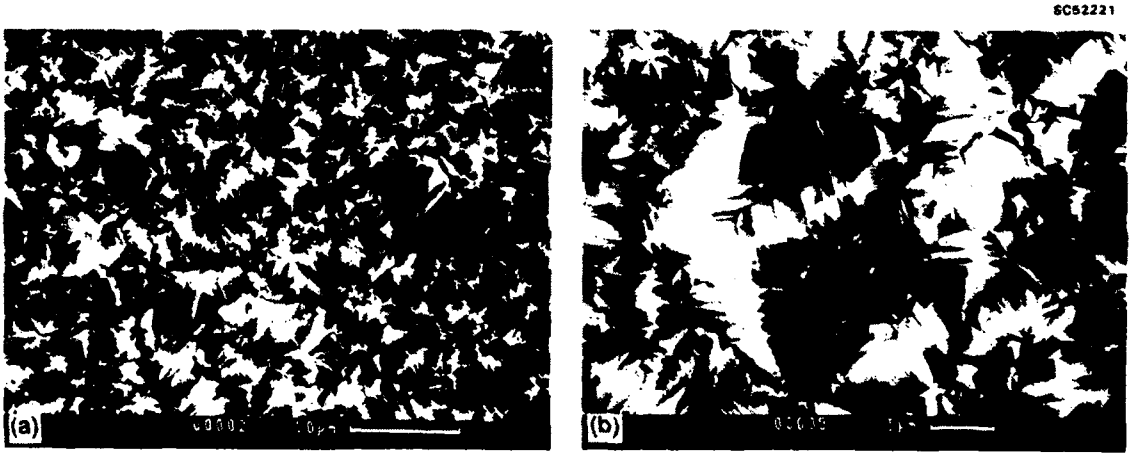

Fig. 1. Electron micrographs of highly faceted polycrystalline diamond surface.

Techniques for limiting such roughness in the deposition process are being explored, but it is reasonable to assume that some degree of postdeposition surface finishing will be required for most thick film applications. Simple room temperature polishing procedures are very difficult

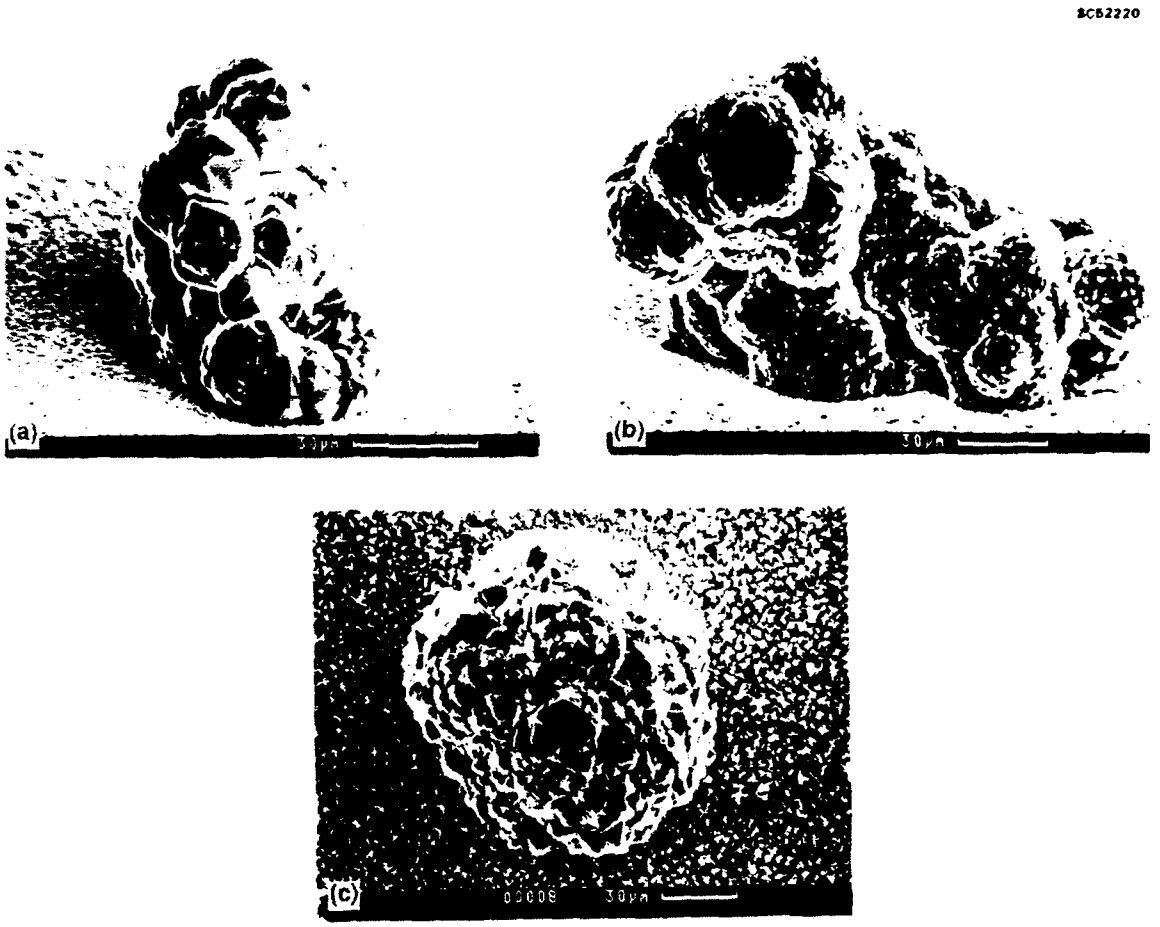

Fig. 2. Electron micrographs of supermicron scale particulates formed during the microwave PACVD growth of polycrystalline diamond.

and time consuming, due both to the mechanical properties of the material and the highly local nature of the roughness. Since the material properties of the diamond greatly limit abrasive polishing, a chemical approach would be preferred.

The polishing of polycrystalline diamond surfaces by contact with iron in a hydrogen atmosphere at elevated temperatures was initially reported in the Japanese literature in 1988.[1] This technique, while quite useful, has severe limitations in terms of scaling to large sample sizes and for use on shaped surfaces. The high temperatures involved (> 730°C) also produce mechanical failures and thermal shocking of the film and substrate. The presence of supermicron particulates on the films limits contact of the polishing plate with the general film surface as does any curvature imparted to the substrate by stress from the growth of the diamond films.

To alleviate some of the problems associated with the high temperature polishing process, a means of using ion etching has been pursued to reduce surface roughness to the degree that the diamond films are suitable for use as IR optical components.

2. EXPERIMENTAL

The diamond films used in these experiments were prepared on 2.5 cm diameter circular (100) single crystal silicon substrates by microwave plasma assisted CVD (PACVD) in a UHV

chamber equipped with an Astex 1500 W magnetron. Typical conditions were 0.7% methane and 0.3% oxygen in hydrogen at temperatures of 450-750°C. Film thicknesses ranged from 30 to 200 μm. As shown in Fig. 1, the films were polycrystalline with local supermicron particulates and generally exhibited a concave surface curvature of near 5 μm depth from edge to center.

Contact polishing experiments were carried out on a rotating 9 cm diameter iron metal plate in a stainless steel UHV chamber at 600-800°C in a hydrogen atmosphere at pressures of 4 to 80 torr. A tungsten filament was operated in the polisher at 1950°C. Chemical etching experiments were carried out in a stainless steel vacuum chamber in mixtures of oxygen in argon and hydrogen in argon, using an AC discharge.

Scanning electron microscopy (SEM), transmission electron microscopy (TEM), Raman microprobe, x-ray photoelectron spectroscopy (XPS), and profilimetry were used to characterize the diamond film samples and iron plate surfaces.

3. RESULTS

3.1 Fe-Plate polishing

The use of the Feplate polishing technique was studied as a function of plate temperature and hydrogen pressure. The progress of the polishing process was observed by SEM and is shown in the series of micrographs in Fig. 3. The major observation is that the primary reactive polishing process occurs only at points of direct contact between the lapping plate and the high points of the faceted film. In areas out of direct contact with the Fe plate, only minor surface roughening was observable by SEM in highly faceted areas, presumably from surface reactions with gaseous species such as residual oxygen, hydrogen atoms and organic radicals produced in the chamber by the hot tungsten filament.

As the lapping process removes the crystalline facets, broader areas of the film contact the plate and eventually a smooth surface is obtained. Profilimetry shows a local surface roughness of ± 100 nm to 5000 nm before polishing and less than ± 10 nm after lapping on the Fe plate.

For the current system under study at 750°C in 80 torr of hydrogen, with a tungsten filament operating at 1950°C, local polishing rates of > 5 μm per hour have been observed. Molybdenum and stainless steel lapping surfaces were also examined. Though limited polishing was observed on the stainless plate, the highest rates of material removal were obtained with elemental iron on which polishing has been observed at temperatures up to 900°C.

The mechanism of the polishing process near 750°C has been studied by Raman scattering spectroscopy and Xray photoelectron spectroscopy (XPS). The carbon 1s electron XPS peak was used to observe the chemical changes occurring at the diamond surface during polishing. The very smooth substrate side of a freestanding diamond film was used in these measurements after being coated by ion beam sputtering with a metallic iron film thin enough (1 - 1.5 nm) such that the XPS carbon peak was still observable. The carbon 1s electron spectrum was determined before and after heating in vacuum and in hydrogen, with and without the Fe metal thin film coating.

The diamond carbon 1s peak shape and chemical shift showed no change after heating in vacuum to 750°C without the Fe film coating. With the Fe overcoating the C 1s peak exhibited broadening and a shift to lower binding energy when heated in excess of 725°C (285.8±0.2 to 284.4±0.2 eV). No changes in the C 1s spectrum were observed after heating to 650°C-700°C in

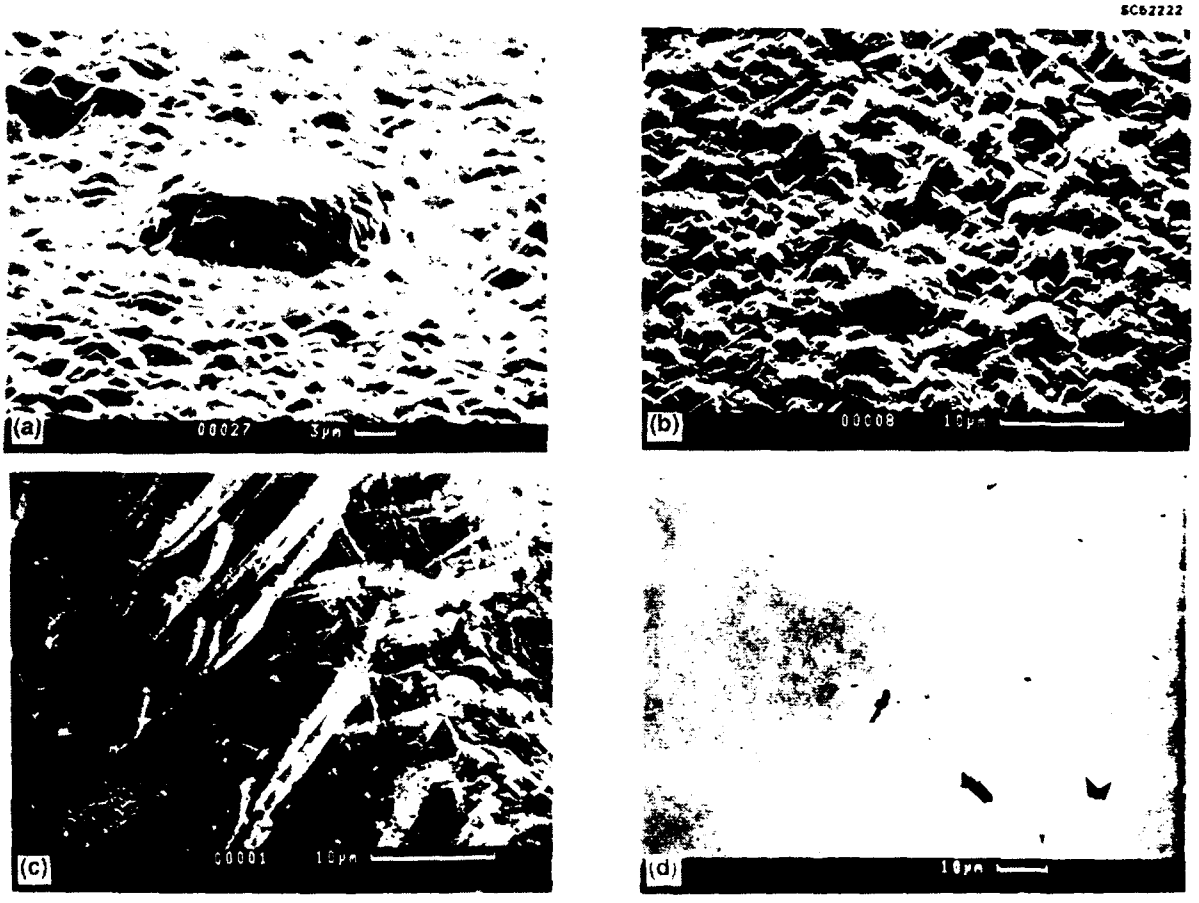

Fig. 3. Electron micrographs showing the progressive polish being developed on a polycrystalline diamond surface during Fe plate lapping at 750°C.

vacuum with the Fe overcoat. This is consistent with the occurrence of the alpha to gamma phase transition occurring in Fe at 723°C. This transition increases the solubility of carbon in the Fe by a factor of 40 to 0.8 wt%.[2]

The broadened C 1s peak observed at 284.4 eV after heating the diamond to 750°C in the presence of Fe is consistent with the diamond surface losing its crystalline properties, but does not indicate the formation of a carbide. However, due to the thinness of the Fe film, any carbide could readily be removed by reaction with residual oxygen in the chamber and is certainly removed by atomic hydrogen. Evidence of this is the observation that the C 1s peak retained its diamond character after heating the Fe coated sample to 750°C in the presence of hydrogen.

Raman spectra taken on the rough polycrystalline diamond surface before and after polishing show that the Fe plate lapping produces an increase in the broad 1450-1600 cm^{-1} peak associated with sp^2 bonded carbon. However, after mechanical surface polishing at room temperature and vigorous cleaning, the sp^2 bonded spectral feature is greatly reduced, indicating that the nondiamond carbon material is localized at the film surface. SEM analysis suggested that at least some of this sp^2 bonded material might be in the form of polishing debris bound at the surface by electrostatic forces.

The results of the XPS measurements on the smooth diamond surface and the Raman analysis of the rougher growth surface suggest that contact of the Fe plate with the diamond at temperatures above 723°C produces loss of crystalline order, converting the outer surface to a more graphitic sp^2 bonded carbon. This graphitic material is then removed from the diamond by reaction with hydrogen and hydrogen atoms. It is also highly likely that iron carbide forms on the surface of the polishing plate which is also etched away by reaction with hydrogen to form methane.

The observation of graphitic carbon residue on the lapped diamond surface by Raman scattering indicates that not all of the reacted diamond is removed by physical abrasion or hydrogen etching. This residual sp^2 bonded material could possibly exist as polishing debris attached to the surface or as material still chemically bound to the diamond that did not experience sufficient etching by hydrogen to be removed.

3.2 Reactive ion etching of diamond

The major limitation to the rapid broad area polishing of thick diamond films is the presence of large particulates of high defect density diamond carbon on the film surface. These particulates are an artifact of the growth process. They are attributed to very rapid growth occurring in local regions of high plasma density around particulate matter initially blown off surfaces in the chamber and deposited on the substrate or particulates formed in the gas phase. Such particulates can achieve dimensions of 20 to 100 μm and cannot readily be removed from the film by mechanical means. During Fe plate lapping these macroscopic particulates are the only diamond surface initially in contact with the lapping plate, greatly reducing the area of polish. Ion etching provides a means to selectively remove these large particulates from the film before further surface polishing.

General area reactive plasma etching with either hydrogen or oxygen has been reported[3,4] and is known to attack nondiamond carbon preferentially. Since the larger particulates have very high defect densities, they are generally more susceptible to ion etching than the strongly faceted grains in the film and at 400-600°C in an oxygen plasma can be etched at a rate near 1 μm per minute.

To insure that the reactive etching is confined to the regions of the large particulates a nonreactive (Au), high-temperature coating can be applied to the whole film and then selectively removed by physical polishing. The exposed areas then can be preferentially etched. Figure 4 shows a micrograph of a 120 μm particle which has been greatly flattened by oxygen plasma etching, while the surrounding finer grained diamond film is unreacted.

Through repetition of the surface coating, mechanical polish, and etching procedure a surface can be obtained with a roughness below ± 50 nm. Such films are suitable for LWIR applications with no further surface polishing and the approach is suitable for shaped surfaces.

Figure 5 shows an infrared transmission spectrum taken from a 1 cm diameter region of a 35 μm thick diamond film after reactive etching and Fe plate lapping. The film, which was initially totally scattering at wavelengths shorter than 10 μm, shows significant improvement in short wavelength infrared transmission, but does not achieve full optical clarity. The spectrum still shows losses from hydrogen impurities in the film, intrinsic diamond absorption, and retained local scattering centers not fully removed by the polishing process in this sample. The degree of improvement in surface roughness in the diamond films can be seen in the Dektak profiles in Fig. 6. The unpolished film had a roughness exceeding ± 100 nm and achieved a final local roughness of less than ± 10 nm after ion etching and Fe plate lapping.

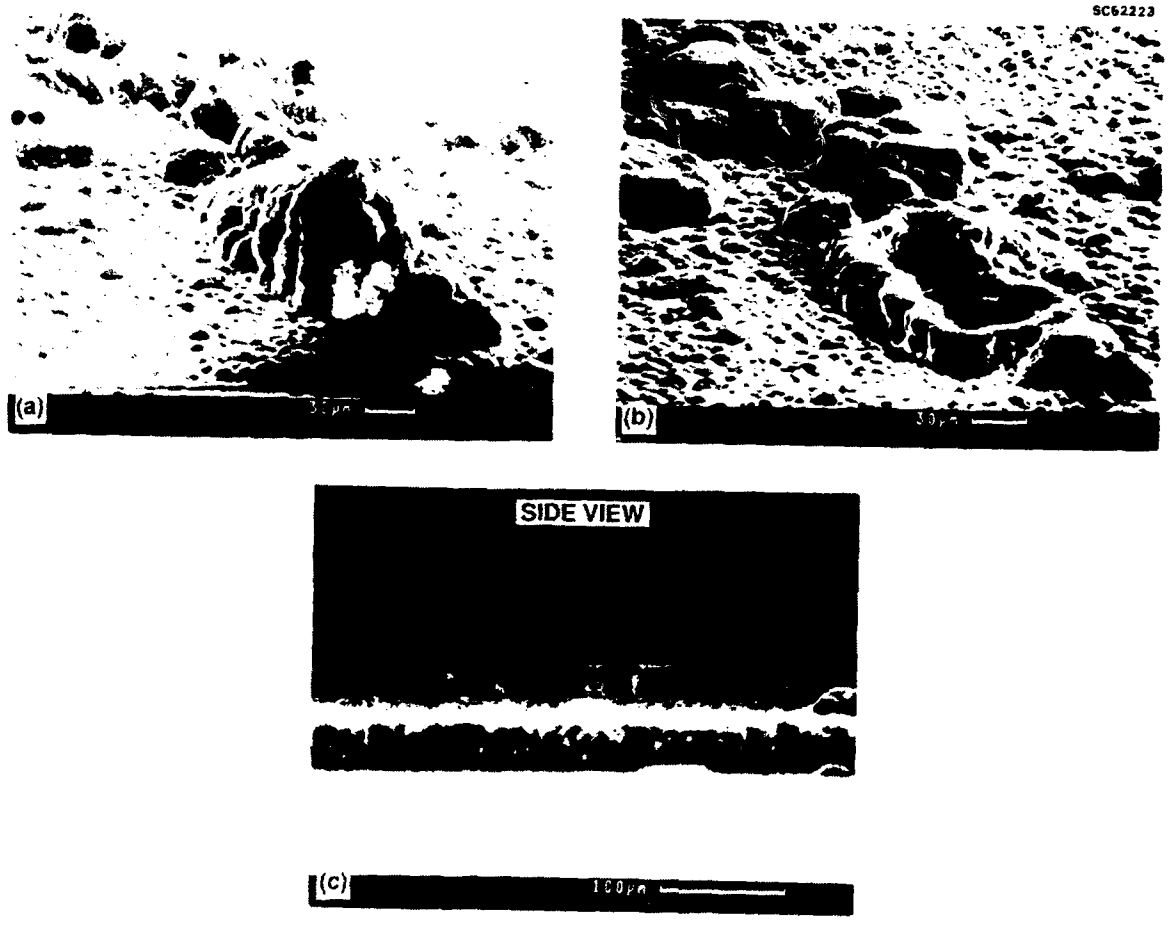

Fig. 4. Electron micrographs showing the progress of local reactive etching of super-micron scale diamond particles.

4. CONCLUSIONS

The combined use of high temperature reactive plasma etching and lapping with an Fe plate in a hydrogen atmosphere can produce a broad area optical polish on the surface of polycrystalline diamond films. The major limitations to the techniques are the stresses and nonuniformities in the initial films themselves. Highly stressed films, poorly adhered to their substrates may not withstand the mechanical and thermal shocks associated with the polishing techniques. However, low stress films deposited on silicon have been shown capable of attaining an optical polish over regions of up to 2 cm in diameter.

5. ACKNOWLEDGEMENT

Portions of this research were sponsored by the Office of Naval Research.

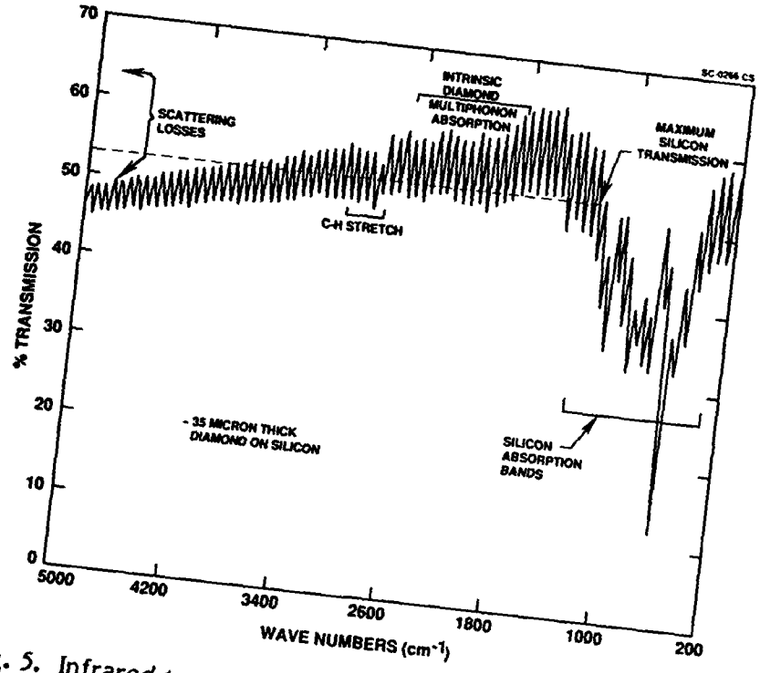

Fig. 5. Infrared transmission spectrum of a partially polished 2.5 cm diameter, 35 μm thick polycrystalline diamond film on silicon.

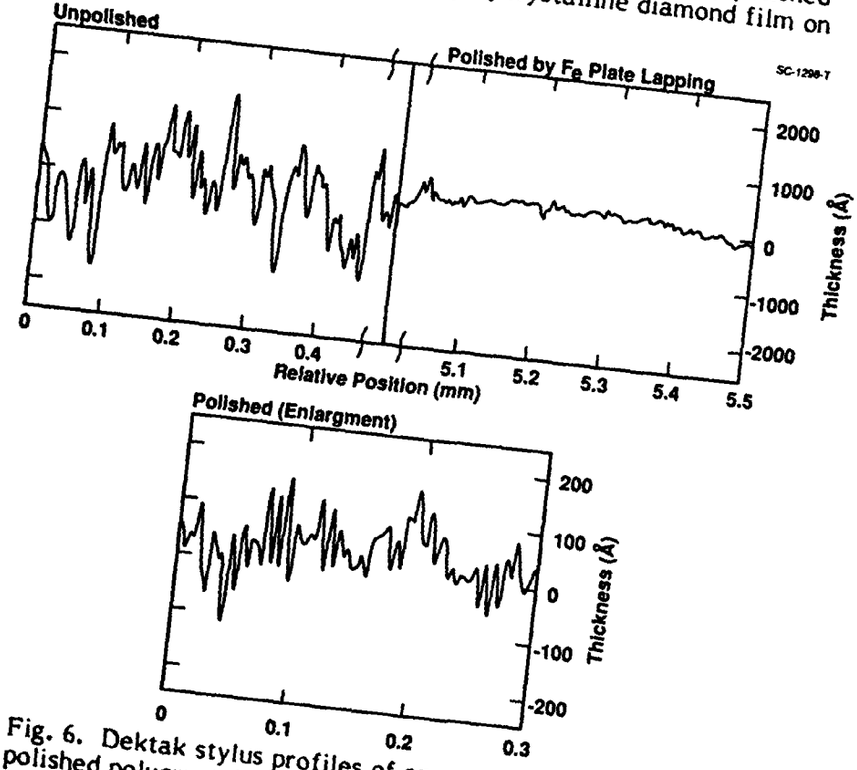

Fig. 6. Dektak stylus profiles of an unpolished and Fe plate final polished polycrystalline diamond film.

6. REFERENCES

1. C. Yang, H. Tokura, a M. Yoshikawa, "Polishing of Diamond Film with Metal," internal report, Tokyo Institute of Technology, Ookayama, Meguroku, Tokyo, Japan, 152 (1988).

2. M. Hansen and K. Anderko, Constitution of Binary Alloys, (McGraw Hill Book Co. Inc., N.Y.) p. 353 (1958).

3. N. Uchida, T. Kurita, K. Uematsu, and K. Saito, "Thermochemical Etching Effect on CVD Diamond in an Oxygen Atmosphere," J. Mat. Sci. Lett. 9, 249-250 (1990).

4. N. Uchida, T. Kurita, K. Uematsu, and K. Saito, "Hydrogen Post-Etching Effect on CVD Diamond Film," J. Mat. Sci. Lett. 9, 251-252 (1990).

Appendix 8

Liquid Jet Impact Measurements in Diamond Coated Ge Substrates

MATERIALS SCIENCE MONOGRAPHS, 73

APPLICATIONS OF DIAMOND FILMS AND RELATED MATERIALS

Y. TZENG
M. YOSHIKAWA
M. MURAKAWA
A. FELDMAN
(Editors)

ELSEVIER

Applications of Diamond Films and Related Materials
Y. Tzeng, M. Yoshikawa, M. Murakawa, A. Feldman (Editors)
Elsevier Science Publishers B.V., 1991

LIQUID JET IMPACT MEASUREMENTS IN DIAMOND COATED Ge SUBSTRATES

M. Thomas[a], D. Price[a], M. Wilson[a], I. Perez[a],
J.B. Boodey[a], W.R. Scott[a], R. Monro[a], A.B. Harker[b]

[a]Naval Air Development Center, Warminster PA 18974-5000

[b]Rockwell International, Thousand Oaks, CA 91360

Abstract

Liquid Jet impact measurements on 1/4" thick Ge flats coated with diamond thin films of different thicknesses will be reported. The threshold velocity (droplet velocity after which fracture starts) will be measured as a function of diamond film thickness. The damage evolution of the films as a function of the droplet velocity will be monitored with light scatterometry.

1. INTRODUCTION

Germanium is a material with optimal infrared (IR) properties but poor mechanical properties. Table I summarizes some of the general physical properties of Ge. There it can be seen that Ge has very small absorption in the 8-12 microns range with very small dispersion, but has a low fracture toughness of .25 MPa $m^{1/2}$ and a fracture threshold velocity (FTV)(velocity such that after 10 impacts fracture initiates) of only 170 m/s for 2 mm spherical water droplets. The purpose of this study is to use a diamond coating to enhance the mechanical properties of Ge domes, in particular the FTV, without deteriorating its IR properties. Hard carbon coatings have been used in the past on ZnS [1] and Ge [2] but with less than optimal results due to debonding problems of the coatings.

Diamond film coatings were chosen for this study because of their extreme mechanical and optical properties. Optical quality diamond coatings are now readily produced through various different plasma-enhanced chemical vapor deposition (PECVD) techniques. As was mentioned above, proper bonding of diamond to germanium is a major problem in the performance of rain erosion resistant (RER) layers. This is a direct result of the high normal and shear stresses produced during the drop impact. This problem can be reduced by using thicker RER layers at the expense of introducing more residual stress in the film. Several multilayer configurations have been produced recently [3] and will be studied in this work. These configurations enhance the bonding of diamond to Ge and

provide adequate antireflecting (AR) capabilities in the 8-12 micron range. A more detailed description will be given in the next section.

Table I.
Physical properties of ZnS, Ge and Diamond

Property	ZnS	Ge	Diamond
Density (gr/cm^3)	4.08	5.32	3.51
K_{IC} (MPa $m^{1/2}$)	.67[a]	.25[b]	>1[c]
Hardness M-Mohs (MPa)	1780[d]	7640[d]	10^7[d]
Youngs Modulus (GPa)	74.1[a]	156[e]	1050[f]
Wave Vel. long.(m/s)	4960[a]	4928[e]	17,047[g]
trans.(m/s)	2600[a]	3546[e]	11,839[g]
Energy gap (eV)	3.54	.67	5.4
Absorption (cm^{-1})	.096[h]	.022[h]	
Dispersion (10^{-2} μm^{-1})	1.35[h]	.088[h]	
Index of refraction	2.2	4.0	2.4

[a] W.F. Adler (1983)[4]
[b] Present work
[c] Paul Klocek [3]
[d] 1989-1990 CRC Handbook
[e] Metal Handbook, V1, ASM 1961
[f] ESNIB 91-01
[g] "Acoustic Fields and Waves in Solids", B. Auld (1973)
[h] @ 10 μm private communication

ZnS was not used in this study because of its larger dispersion (almost two orders of magnitude larger) in the IR region compared to Ge. The requirement for low dispersion in the IR region becomes important in non-axial IR applications encountered in dome configurations.

2. EXPERIMENTAL METHODS

2.1 Materials

Ge flats were obtained from Optical Corporation of America. Ge boules were grown by the Czocharlski method and diamond saw cut to 1/4" flats. Samples were diamond turned producing a polished surface having a roughness of .1 micron. Microstructural analysis revealed a small number of large parallel twins in the samples. The average width of the twins was measured to be 7 mm. This width is much larger than the average impact site and therefore the flats were considered to be single crystal for purposes of data analysis unless specifically stated.

To improve the mechanical properties of Ge, diamond films were deposited onto its surface. Two different processes were followed for diamond thin film deposition. In the first

method a thick chalcogenide glass was deposited over Ge prior to diamond deposition. This chalcogenide layer served as a stress relief boundary layer and improved the bonding properties between diamond and Ge. In the second process a regular array of 5 microns wide by .1 micron deep grooves separated by 25 microns were etched in the Ge surface to enhance diamond growth and improve mechanical bonding. In both processes diamond films were grown by a modified PECVD technique developed at Rockwell Science Center [5]. The diamond film thicknesses used in this study were 6 - 20 microns.

2.2 Liquid Drop Impacts

To simulate high velocity rain drop erosion a liquid jet impact device was purchased from the Cavandish laboratories at Cambridge. It has been demonstrated [6] that this device is adequate for rain drop erosion simulation studies. In this technique a lead slug is fired from a modified .22" caliber air rifle into a momentum exchange steel block that extrudes water from the inside of a stainless steel chamber. The nozzle used in this study has an orifice of 0.8 mm. The equivalent drop diameter varies from 3 - 4 mm in the velocity range of interest to us. Because the drop size is dependent on the liquid jet velocity, it is desirable to express the results in a standard manner. The dynamic fracture criteria has been used in this study for standardizing our results. This criteria correlates the maximum stress and the impact time with a degree of damage in the sample. Our standardized drop diameter used in this study is 2 mm. After careful testing and substantial improvements of the system [7], deviations of less than 5% in the mean velocity of the liquid jet were obtained. The velocities used in this study were in the range of 170 m/s to 350 m/s.

2.3 Sample Characterization

Each sample was impacted up to 30 times in the same area. After each impact a photograph of the impact site was taken, a light scatter measurement was made of the impact site and a infrared transmission measurement was made. All of this data was then correlated to determine the the amount of light scatter after which the window becomes unusable.

Light scatterometer measurements were used as a nondestructive technique to quantify the amount of surface damage. In a typical light scatter experiment, a monochromatic laser beam was rastered across the surface of the sample and the amount of scattered light was recorded. A color plot, with different color codes for different amounts of scattered radiation, was produced. This plot reflects the amount of roughness over the surface of the sample. Regions in this plot with a large amount of scatter radiation can be correlated to regions of increased surface damage.

3. RESULTS

Polymethylmethacrylate (PMMA) target specimens were used in the initial phases of this study to characterize the shape of the liquid jet and establish its velocity reproducibility. For velocities of 280 m/s, the impressions produced by the liquid jet were circular. For velocities of 170 m/s the impressions produced by the liquid jet were not circular, but formed a closed curve. In general the higher the velocity the more circular was the shape of the impression left by the liquid jet.

Our results in uncoated single crystals of Ge showed that damage started after 10 impacts at a liquid jet velocity of 170 m/s. This corresponds to a FTV of 170 m/s in agreement with previous results by [8].

4. ACKNOWLEDGEMENTS

This work was sponsored by grant PMA-24I from NAVAIR under the F-14 IRST program

5. REFERENCES

1 J.V. Hackworth, Annual Report AFML-TR-78-184, Bell Aerospace Textron, Buffalo, NY (1978)
2 S. van der Zwaag and J. E. Field, Phil. Mag. A, 48 (1983) 767-777
3 A.B. Harker, Seventh Annual Program Rev., Research and Development of CVD Diamond, Penn. State University, PA, Oct. 1990
4 R.C.Bradt, A.G. Evans, D.P.H. Hasselman and F.F. Lange (eds.), Fracture Mechanics of Ceramics, pages 27-45, Plenum Press, NY, 1983
5 A.B. Harker, In these proceedings
6 E.D. Case, K.M. Louie and A.G. Evans, J. Mat. Sci. Lett. 3 (1984) 879
7 M. Thomas et al., to be published in Rev. Sci. Inst. (1991)
8 M. Wilson, "Characterization of Hard Carbon Coated and uncoated Germanium Witness Samples", 3rd Workshop on Passive IR Optical Materials, unpublished NATO Forum, 1990

Appendix 9

Reactive Polishing of Polycrystalline Diamond and Measured Spectroscopic Properties

MATERIALS SCIENCE MONOGRAPHS, 73

APPLICATIONS OF DIAMOND FILMS AND RELATED MATERIALS

Y. TZENG
M. YOSHIKAWA
M. MURAKAWA
A. FELDMAN
(Editors)

ELSEVIER

Applications of Diamond Films and Related Materials
Y. Tzeng, M. Yoshikawa, M. Murakawa, A. Feldman (Editors)

Reactive polishing of polycrystalline diamond and measured spectroscopic properties

Alan B. Harker

Science Center, Rockwell International, P.O. Box 1085, Thousand Oaks, CA 91358

Abstract

The use of high temperature reactive etching and high temperature metal plate polishing are being investigated for the preparation of polycrystalline diamond optical surfaces. These techniques have been applied to 5 cm diameter microwave CVD diamond films with thicknesses ranging from 35 to 200 microns. The mechanism of both processes have been established, and physical and chemical parameters limiting scaling are being addressed. Correlations between Raman, microwave, and infrared spectral data indicate that graphitic impurities control the absorption losses in the polycrystalline samples.

1. INTRODUCTION

High surface roughness is a major limiting feature in the adaptation of polycrystalline diamond films for optical and friction reduction applications. Mechanical polishing is made difficult by the numerous facets on the surfaces and the need to remove significant amounts of material (10 to 100 microns thickness) to overcome surface non-uniformities produced during growth. It has been found that surface polishing of diamond films can be achieved by heterogeneous reaction with iron at elevated temperatures (1,2), reaction with oxygen ions (2,3), and laser ablation (4).

Current efforts in this laboratory are focused upon scaling the reactive polishing processes up to samples of reasonable size (2 to 5 cm) for optical applications and the extension of the techniques to shaped surfaces.

2. EXPERIMENTAL

The diamond samples used in this study are grown by microwave CVD using a 1.5kW Applied Science magnetron source and coupler with an ultra-high vacuum all metal sealed chamber. Samples are grown on Si and Si_3N_4 at temperatures of 450-900°C. The gas composition is normally 0.5 vol% CH_4, 0.2 vol% O_2, in H_2.

Two experimental systems are being used. The first is a modified Technics Planar Etch II reactive etching system capable of operating at 650°C. The second is a dual rotation hot plate lapping system in an all metal vacuum chamber. The lapping system uses radiant heating to achieve surface temperatures of up to 900°C on an

11 cm diameter iron, nickel, or cast iron plate in 2-12 kPa of H_2. The plate and sample are driven at speeds of 1 to 60 rpm by a voltage controlled motor and gear system.

In the etching system, the diamond surface is first gold coated, then mechanically lapped to expose the highest facets, followed by etching at 450 to 650°C for periods of 5 to 20 minutes in oxygen. Repeating this process removes exposed features and permits finish polishing on the hot metal plate or by standard mechanical lapping.

3. RESULTS AND DISCUSSION

X-ray photoelectron spectroscopy analysis of the surfaces in the high temperature lapping system show the polishing processes to be one of local graphitization of the diamond, with carbon dissolving into the iron plate. The process becomes effective at temperatures above 725°C (the alpha to gamma phase transition of Fe) at which point the solubility of carbon in Fe increases to 0.8wt%. At higher temperatures, up to 950°C, the process is enhanced with thermal graphitization of the diamond eventually occurring. The polishing process is limited by the stress induced curvature in the polycrystalline samples, which limits plate-diamond contact and the need to achieve polishing pressures of 40-60kPa on the substrates. However, under optimum conditions, polishing rates of 2 to 5 microns/hr have been achieved with final surface roughness of about +/- 10 nm.

The presence of macroscopic features on the polycrystalline diamond surface and the desire to polish curved shapes has led to the development of the ion polishing approach. The gold blocking layer is used in this method to avoid grain boundary etching, which occurs about an order of magnitude faster than etching of the diamond grains themselves. The etching periods are currently quite short (< 20 min at 600°C) to avoid defect pitting and grain boundary etching. Etch rates of 1 micron/min can be achieved for the larger surface particles, however, wide area etching rates are on the order of 3-5 microns/hr. Currently, the limiting features of this process are grain boundary etching and the formation of graphite on the diamond surface which inhibits etching. Alternative gases to oxygen are being explored to overcome the graphite passivation problem. Final surface roughness values of +/- 50 nm are obtained by this process.

The ion etching approach has been found superior for surface smoothing to prepare the samples for hot Fe plate lapping. Since stresses can induce over 100 microns in edge to center curvature in samples grown at higher temperatures, a method of removing significant material is required to obtain an optically flat surface.

Infrared, Raman, and microwave spectroscopic analysis of the samples is being carried out to ascertain the effects of polishing and to derive spectroscopic constants. The Raman analyses indicate that the ion etching process leaves significant residual graphitic carbon on the surfaces that must be mechanically removed. After final lapping, IR spectra have been taken with samples ranging from 12 to 200 microns thickness at wavelengths of 2 to 50 microns. In addition to the fundamental multi-phonon mode, the most readily observable absorption is the C-H impurity stretch at 3.5 microns. The spectra also show an increasing transmission loss extending to shorter wavelengths, consistent with either internal scatter or a very broad SWIR absorption.

The presence of the broad loss in the SWIR transmission spectra correlates with

any observable sp2 bonding in the Raman spectra and the measurement of a high dielectric constant and loss tangent at 67 gHz in the microwave region.

4. CONCLUSIONS

Both high temperature polishing approaches can produce optical quality surface finishes on polycrystalline diamond. The main limitations with the Fe plate lapping approach are the mechanical and thermal problems associated with mechanical operations at high temperatures. The ion etching approach is limited by grain boundary etching and graphite formation.

Spectroscopic analysis of polished samples indicates that losses in the infrared spectrum are associated with both hydrogen impurities and the presence of non-diamond carbon.

5. ACKNOWLEDGEMENTS

Portions of this research were sponsored by the office of Naval Research.

6. REFERENCES

1 M. Yhoshikawa, Diamond Optics III, eds. A. Feldman and S. Holly, SPIE Proceedings Vol. 1325, (1990) 210.
2 A. Harker, J.F. Flintoff, and J.F. DeNatale, Diamond Optics III, eds. A. Feldman and S. Holly, SPIE Proceedings Vol. 1325, (1990) 202.
3 T. Zhao, D.F. Grogan, B.G. Bovard, H.A. Macleod, Diamond Optics III, eds. A. Feldman and S. Holly, SPIE Proceedings Vol. 1325, (1990) 142.
4 S. Tezuka and M. Yhoshikawa, New Diamond (Japanese), Vol. 17, (1990) 36.

Appendix 10

Effects of Interfacial Modification on Diamond Film Adhesion

PROCEEDINGS

SPIE—The International Society for Optical Engineering

Diamond Optics IV

Albert Feldman
Sandor Holly
Chairs/Editors

22–23 July 1991
San Diego, California

SPIE P PROCEEDINGS SERIES

Volume 1534

Effects of interfacial modification on diamond film adhesion

J.F. DeNatale, J.F. Flintoff, and A.B. Harker

Rockwell International Science Center
Thousand Oaks, CA 91360

ABSTRACT

Microlithographic surface patterning has been investigated as a means of improving diamond film adhesion on noncompatible substrates. This technique produces significant improvements in film adhesion beyond identical unpatterned substrates, although sufficient film stresses can develop to induce subsurface substrate fracture. The substrate etching geometry can be chosen to simultaneously produce an antireflective surface relief.

1. INTRODUCTION

Polycrystalline diamond thin films offer a unique combination of physical properties highly desirable for optical device applications: high hardness, wideband transparency, chemical inertness, and high laser damage thresholds. Application of these coatings to optical device structures, however, is often impeded by poor film adherence and surface roughness. While films of substantial thickness can be produced routinely on Si, films grown on numerous other optical materials under equivalent conditions often delaminate at thicknesses of only a few microns due to lack of interfacial chemical bonding, intrinsic growth stresses and thermal expansion mismatch. To fully exploit the potential of the diamond films in optical applications, fabrication on less-compatible substrates must be addressed. Additionally, the highly faceted polycrystalline diamond films cause high levels of scattering and normally must be polished to achieve good optical transmission.

One approach to improving diamond film adhesion is the modification of the original film-substrate interface. In this work, the use of microlithographic patterning of the substrate surface has been investigated as a means of improving diamond film adhesion. Surface patterning has been shown to allow control of film microstructure,[1] and the current work demonstrates that it may also provide significant improvements in film adhesion and infrared transmission.

2. EXPERIMENTAL

For these experiments, fused silica and Ge substrates were used. The substrates were patterned by standard photolithography and dry etching techniques, producing a grid pattern of etched lines approximately 1 μm deep. The line widths were 1-3 μm, with center-to-center separations of 10-15 μm. Diamond films were grown using microwave plasma CVD with a source gas composition of 0.5% CH_4, 0.2% O_2, and the balance H_2. Substrate growth temperatures of 750°C were used for the SiO_2 and 550°C for the Ge as determined by optical pyrometry. Unpatterned substrates were included in the depositions for experimental comparison, with all samples given identical diamond polish pretreatments to enhance film nucleation.

3. RESULTS AND DISCUSSION

Growth of the diamond film on the patterned SiO_2 was continued up to a thickness of approximately 24 μm. By contrast, the film on the bare substrate grown simultaneously began to delaminate after thicknesses of approximately 1-2 μm, demonstrating the adhesion improvement associated with the microlithographic patterning. The patterned film surface continued to

0-8194-0662-7/91/$4.00

exhibit the original substrate topology even after these thicknesses (Fig. 1). Also evident in Fig. 1 is the appearance of surface cracking. Cross sectional examination in the scanning electron microscope (SEM) revealed that these were not due to film delamination, but rather were associated with subsurface substrate fracture (Fig. 2). The interfacial integrity of the film was maintained even at stresses sufficient to induce substrate fracture.

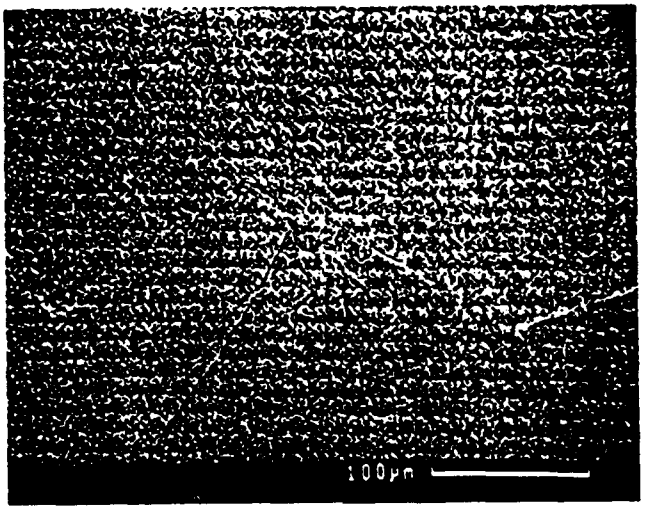

Fig. 1. Surface morphology of diamond film grown on etched SiO_2.

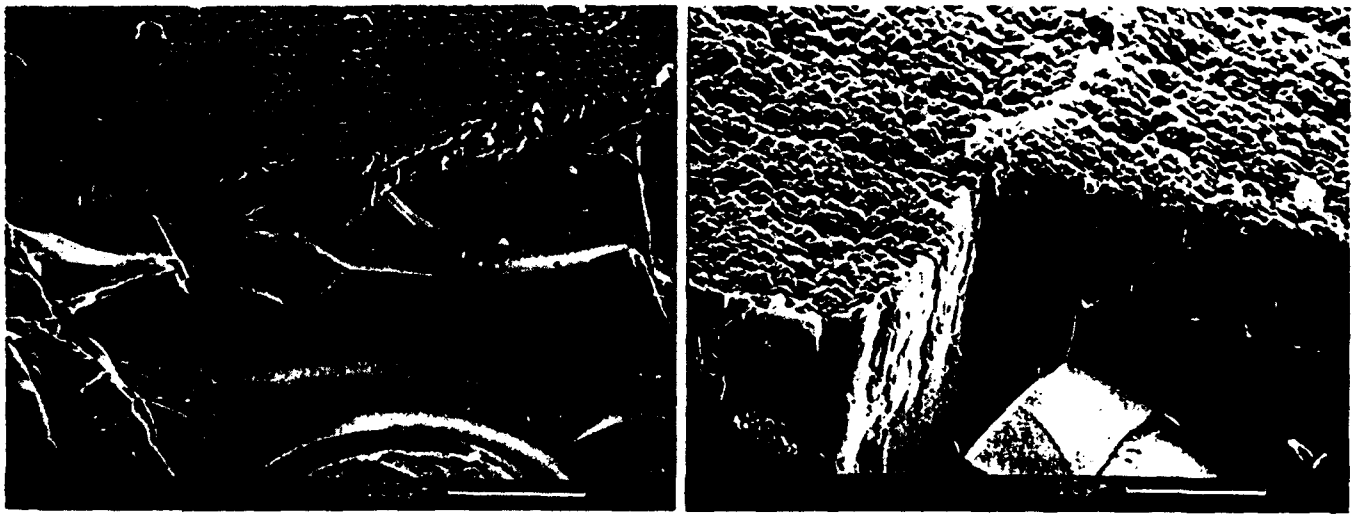

Fig. 2. Cross sectional SEM micrography illustrating subsurface fracture in SiO_2 substrate.

Similar results were obtained for growth on the patterned Ge substrates. Film adherence on the patterned substrate was maintained to thicknesses beyond 30 μm, while on the unpatterned substrate delamination occurred at approximately 1 μm. As observed with the SiO_2, the original surface pattern was maintained in the film even at substantial thicknesses (Fig 3). Ultimately, however, sufficient stresses were generated by the growth process to induce substrate fracture, with the original film-substrate interface still intact after fracture.

Fig. 3. Surface morphology of diamond film grown on etched Ge.

It is well established that the diamond films, with their high modulus and low thermal expansion coefficients, can generate significant stresses.[2] This can induce substantial curvature to bulk substrates, or even lead to substrate fracture as seen here. This type of subsurface fracture by a thin film has been modeled by Drory et al.[3] In their analysis, both shallow and deep cracks will be generated in the substrate parallel to the film interface, with the crack depths related to the film and substrate thicknesses and elastic properties. Using the appropriate values for the diamond film on SiO_2, one arrives at theoretical crack depths consistent with those experimentally observed.

The use of substrate surface patterning, while improving diamond film adhesion, will impact the optical performance of the device by the introduction of interfacial scatter. Modification of the pattern geometry can be made, however, to minimize this effect. Comparison has been made between the original grid pattern and a square array of etched holes of similar spacing. The array of holes reduces the area fraction being etched, significantly reducing the scatter losses in the short wavelength infrared without sacrificing the adhesion enhancement of the grid pattern. An example of the diamond film morphology on Ge produced in this manner is shown in Fig. 4.

An alternate approach may be taken to mitigate the optical scatter losses of the surface etching. Here, the etched geometry can be chosen small enough relative to the design wavelength to prevent diffractive losses. In this manner, a fine-scale etched surface relief which progressively grades the effective index of refraction between that of air and the Ge substrate can be generated. This type of structure, commonly referred to as a "moth eye" surface, can reduce Fresnel reflection losses to provide antireflective properties.[4] Such an antireflective surface relief structure has been fabricated using a polycrystalline diamond film grown on an etched Ge substrate (Fig. 5).[5] By the appropriate choice of the etching geometry and diamond film thickness, transmission levels in excess of 95% can be obtained (Fig. 6).

4. CONCLUSIONS

Microlithographic patterning of substrate surfaces prior to diamond growth provides a means of improving film adhesion beyond that of nonpatterned substrates. This offers a potential method of diamond film growth on incompatible or poorly compatible substrates.

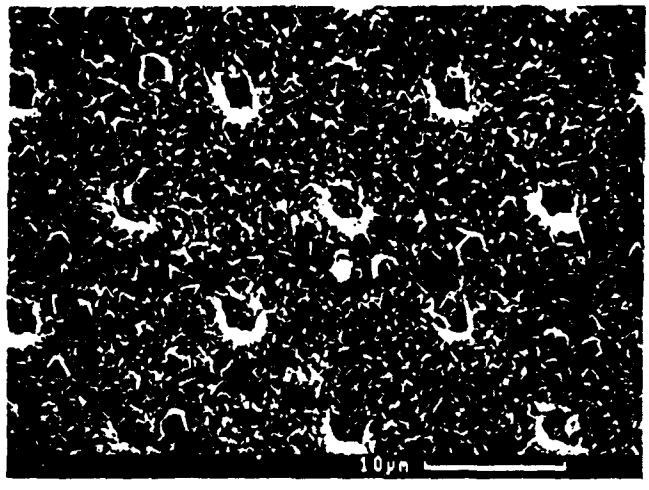

Fig. 4. Diamond film grown on Ge substrate using etched hole array for adhesion enhancement.

Fig. 5. SEM micrograph of diamond film antireflective surface on Ge.

Implementation of this technique for thick diamond films will require considerations of the large stresses that may develop during film growth. For these cases the film stresses may exceed the substrate fracture stress, causing subsurface failure. Certain regimes of temperature and hydrocarbon content which produce reduced stresses in the diamond films have been identified,[2] and growth under these conditions may permit thicker film development on the patterned substrates. By appropriate choice of the etching geometry, this technique can be further extended to the fabrication of diamond antireflective surfaces.

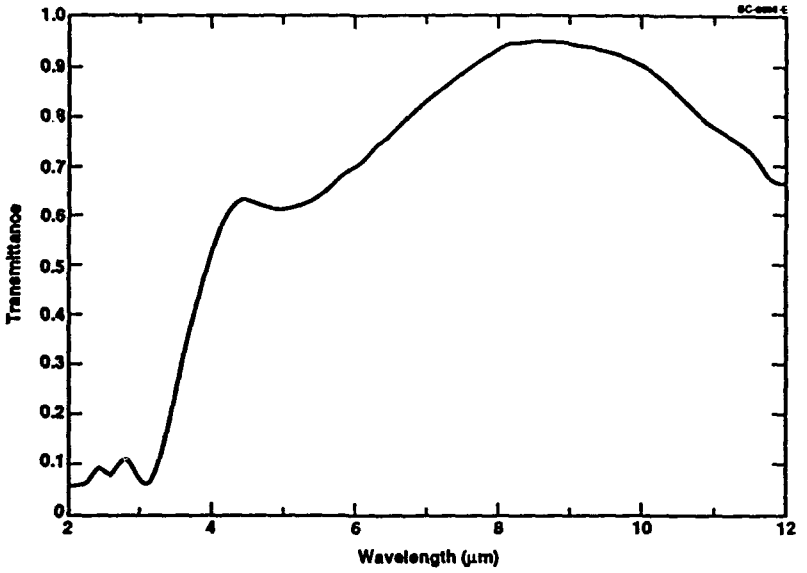

Fig. 6. IR transmission spectra of Ge substrate with diamond antireflective surface. Rear surface coated with dielectric multilayer.

5. ACKNOWLEDGMENT

Portions of this work were sponsored by the Office of Naval Research.

6. REFERENCES

1. J.F. DeNatale, J.F. Flintoff, and A.B. Harker, "Microstructural Control of Diamond Thin Films by Microlithographic Patterning," J. Appl. Phys. 68(8), pp. 4014-4019 (1990).
2. H. Windischmann, G.F. Epps, Y. Cong, and R.W. Collins, "Intrinsic Stress in Diamond Films Prepared by Microwave Plasma CVD," J. Appl. Phys. 69(4), pp. 2231-2237 (1991).
3. M.D. Drory, M.D. Thouless, and A.G. Evans, "On the Decohesion of Residually Stressed Thin Films," Acta Metall. 36(8), pp. 2019-2028 (1988).
4. W.H. Southwell, "Pyramid-Array Surface Relief Structures Producing Antireflection Index Matching on Optical Surfaces," J. Opt. Soc. Am. A 8(3), pp. 549-553 (1991).
5. J.F. DeNatale, P.J. Hood, J.F. Flintoff, and A.B. Harker, "Fabrication and Characterization of Diamond Moth Eye Antireflective Surfaces on Ge," Submitted to J. Appl. Phys. (1991).

Appendix 11

Fabrication and Characterization of Diamond Moth Eye Antireflective Surfaces on Ge

Fabrication and characterization of diamond moth eye antireflective surfaces on Ge

J. F. DeNatale, P. J. Hood, J. F. Flintoff, and A. B. Harker
Rockwell International Science Center, Thousand Oaks, California 91360

(Received 26 July 1991; accepted for publication 20 October 1991)

An antireflective coating on Ge which combines a polycrystalline diamond film with a surface relief (moth eye) structure has been designed and successfully fabricated. This progressive gradation in the effective refractive index between air and the substrate has reduced Fresnel reflection losses to below 1%. This provides a means of overcoming the high refractive index and surface roughness considerations that often limit optical application of polycrystalline diamond thin films.

I. INTRODUCTION

Polycrystalline diamond thin films offer a unique combination of physical properties highly desirable for optical device applications: high hardness, transparency from uv to far infrared (IR), chemical inertness, and high laser damage thresholds. Application of these coatings to optical device structures, however, is often impeded by film adherence, surface roughness, and the relatively high refractive index mismatch between air and the diamond films ($n = 2.4$).

Substrate surface etching has been demonstrated as a means of microstructural control and adhesion improvement in diamond thin films on noncompatible substrates.[1,2] Similarly, use of surface relief structures is effective in reducing Fresnel reflection losses of high-index substrates.[3] These latter structures, commonly referred to as "moth eye" due to their natural analog,[4] use tapered surface patterning (e.g., cones, pyramids) to progressively grade the effective refractive index between that of air and the substrate. Southwell[3] has treated the geometry of these surface relief profiles to optimize their antireflection properties on various substrates.

In this work, substrate surface etching has been investigated as a means of producing a diamond broadband antireflective coating on Ge.

II. EXPERIMENT

The substrates used in these experiments were polished Ge windows, 25 mm diameter by 6 mm thick. Substrates were patterned by standard photolithographic techniques using a contact mask and uv exposure. The pattern used in this work was a square grid with lines 0.5 μm wide and 2.0 μm centerline spacing. The specific spacing, depth, and cross-sectional geometry of the surface relief pattern strongly affect the antireflective (AR) and scatter properties of the coating.[3] This interelement separation was chosen to be small enough relative to the design wavelength to prevent significant diffractive losses, yet to remain within the fabrication limits of the process. After exposure and development, the sample was plasma etched to produce a surface relief.

Prior to growth, the substrates were prepared with a diamond pretreatment to enhance film nucleation. This "seeding" was conducted by sonicating the substrates in a solution of submicron diamond particles dispersed in isopropanol, followed by an isopropanol rinse. This avoided mechanical damage to the patterned substrate from diamond paste abrasion. Diamond films were grown by microwave plasma-assisted chemical vapor deposition (PACVD) using 0.5% methane in hydrogen in a commercial Astex reactor.

Infrared spectral response was characterized using a Perkin–Elmer 983G dispersive spectrophotometer. Microstructural analysis was performed using a Camscan scanning electron microscope (SEM). Laser durability testing was performed by Montana Laser Optics, Inc., using a Lumonics pulsed CO_2 laser.

Total integrated scatter at a wavelength of 10.6 μm was measured using a chopped 10-W cw CO_2 laser, integrating sphere, and pyroelectric detector. Forward and backward scatter were measured with the sample at the entrance and exit apertures of the sphere, respectively. The measured signals were then correlated to an absolute scatter volume using samples with known transmission and reflection characteristics.

III. RESULTS

A. Spectral characteristics

Measurement of the infrared transmission spectra of the patterned substrate was made prior to diamond film growth [Fig. 1(a)]. Significant scattering losses are evident at shorter wavelengths; however, at longer wavelengths substrate transmission increases substantially. Peak transmittance above that of bare, unpatterned Ge indicates some AR properties are present even before deposition of the diamond film. At this intermediate step in the fabrication process, however, the significant Fresnel reflection losses limit the peak transmittance of the device. Examination of the transmittance and specular reflectance data indicates that the scatter losses in the 8- to 10-μm wavelength range are below 3% prior to diamond growth.

Subsequent deposition of the polycrystalline diamond layer produced a substantial increase in the IR transmittance [Fig. 1(a)]. Based on a single surface reflection at an air-Ge interface of 36%, clearly the diamond/moth eye structure provided nearly 100% transmission at its peak.

 0021-8979/92/031388-06$04.00

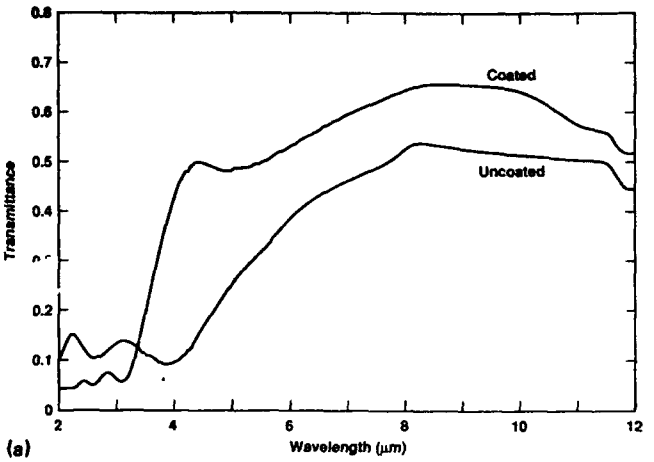

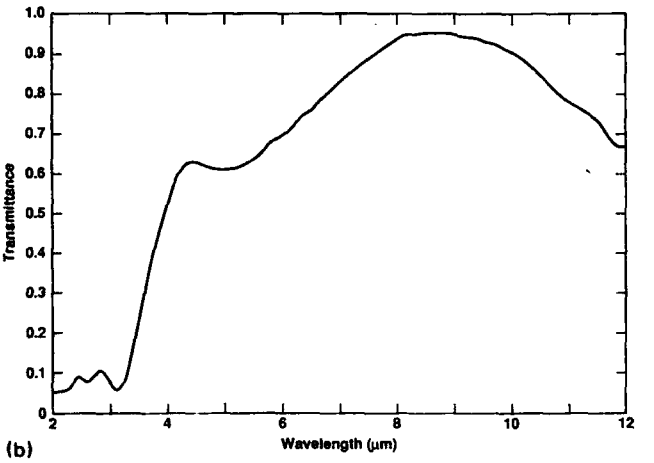

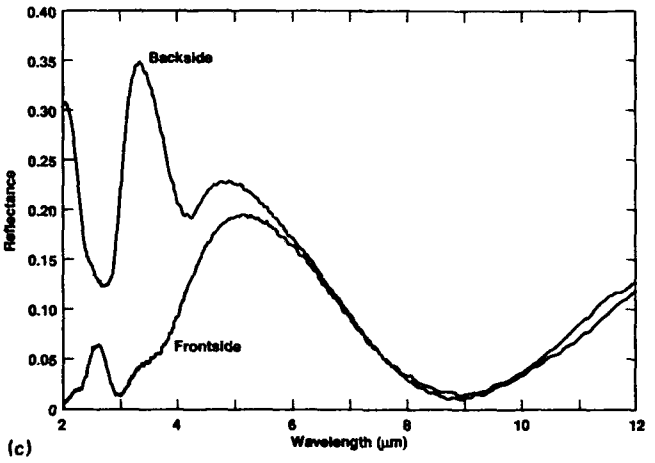

FIG. 1. (a) Infrared transmittance spectra of etched Ge substrate before and after deposition of the diamond film. (b) Infrared transmittance spectra of final device with backside dielectric antireflective coating. (c) Frontside and backside infrared specular reflectance spectra of final device.

To complete the device structure, a conventional thin-film dielectric AR coating was deposited on the backside of the substrate. The IR transmission spectra of the final device structure is shown in Fig. 1(b), with a peak transmission in excess of 95%. Comparison of frontside and backside

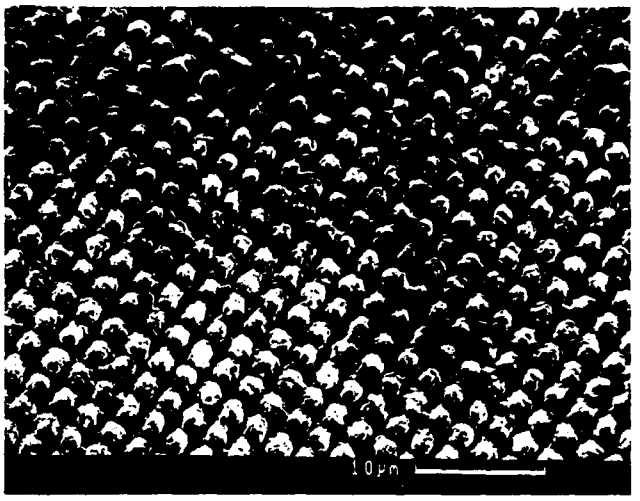

FIG. 2. (a) Microstructure of diamond/surface relief structure. (b) Detail of surface structure.

reflectance spectra from the device illustrates the significant scattering losses present at shorter wavelengths and the minimal losses at the transmission peak [Fig. 1(c)]. The total integrated scatter through 2π steradians was measured to be 0.013 ± 0.001. A portion of this scatter is believed due to degradation of the surface quality of the backside surface during the high-temperature diamond growth process.

B. Microstructure

The microstructure of the composite structure is shown in Figs. 2(a) and 2(b). This illustrates the highly faceted morphology and crystallographic faulting common to the diamond films under the low hydrocarbon growth regime used in these experiments. The absence of substantial amounts of sp^2 bonded carbon is confirmed by the Raman spectra of this sample (Fig. 3). Regions of the diamond film directly above the Ge surface peaks appear to

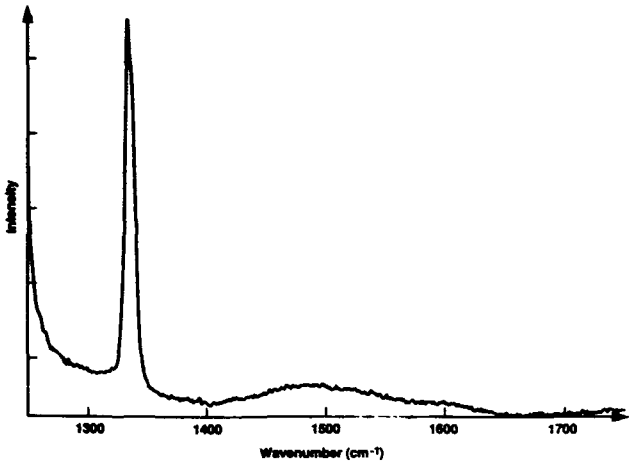

FIG. 3. Raman spectra of diamond film.

have adopted roughly spherical morphologies. This is consistent with the extremely high specific surface energy of diamond.[5]

In local regions of the sample, the diamond film could be removed from the substrate, revealing the underlying surface relief pattern. The pillars were characterized by a tapered pyramidal geometry [Fig. 4(a)]. Examination of the boundary regions of film disbonding revealed uniform film coverage, with the diamond film following the surface contours of the patterned Ge [Fig. 4(b)]. These removed sections of film also allowed examination of the backside of the film, i.e., the surface originally in contact with the patterned Ge substrate. SEM micrographs of this back surface (Fig. 5) demonstrate the high film density and lack of observable porosity at the original substrate interface. These micrographs show the degree to which the diamond film replicates the surface morphology of the Ge substrate.

C. Laser damage testing

Measurements of the laser damage threshold fluences were conducted for both the bare and diamond-coated Ge. For the diamond-coated regions, a threshold fluence of 3.3 J/cm^2 was measured, with a minimal spread of 0.04 J/cm^2. The damage was characterized by local interfacial delamination and substrate melting [Figs. 6(a) and 6(b)]. For comparison, the minimum incident fluence for damage on the uncoated etched Ge surface was 7.6 J/cm^2, with local regions undamaged up to 9.8 J/cm^2. Micrographs of the corresponding damage sites [Figs. 7(a) and 7(b)] reveal that a similar type of damage by substrate melting has occurred in the uncoated regions as well.

IV. DISCUSSION

Modeling of the predicted spectral performance was conducted to compare with the measured data. For this analysis, a thickness profile for the substrate and diamond film were assumed based on the SEM measurements (Fig. 8), assuming a fourfold symmetry about the substrate surface normal. Using this structure, the relative volume frac-

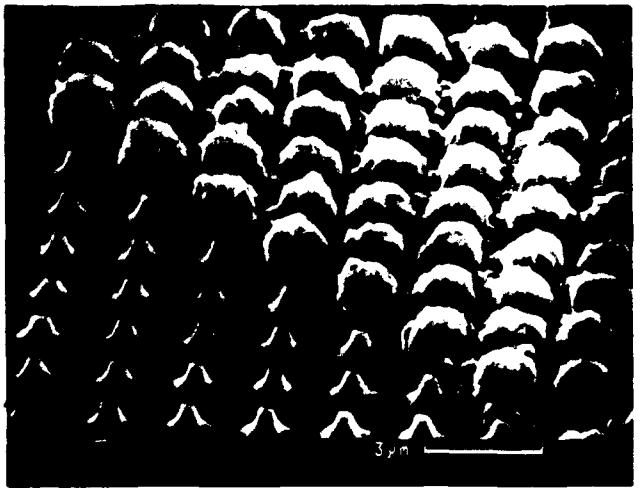

(a)

(b)

FIG. 4. (a) Ge surface relief underlying diamond film (b) Detail of boundary region illustrating film profile

FIG. 5. SEM micrograph of backside surface of diamond film grown on patterned Ge surface.

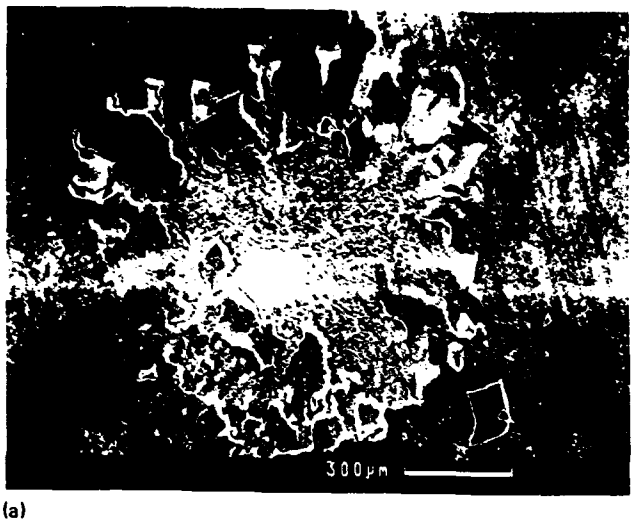

(a)

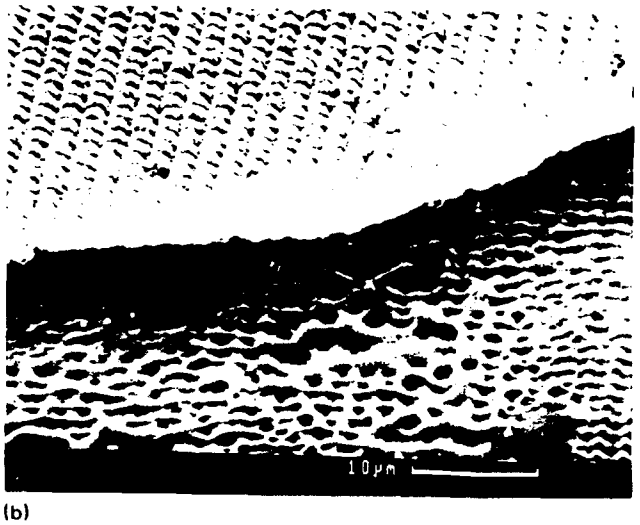

(b)

FIG. 6. (a) SEM micrographs of laser damage site on diamond coated Ge relief surface. (b) Detail of damage site.

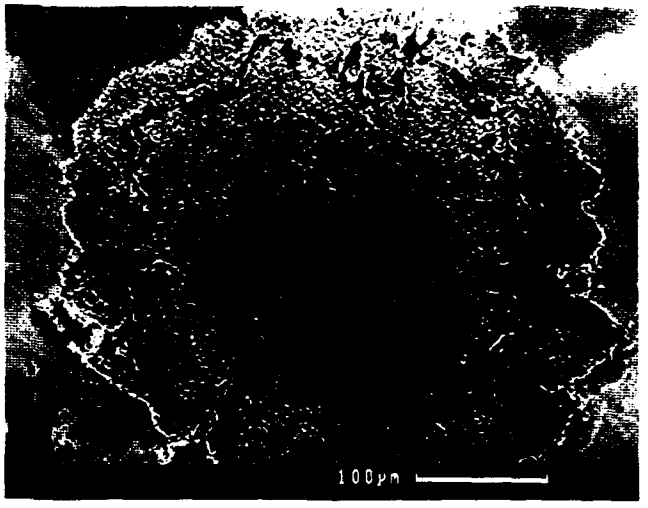

(a)

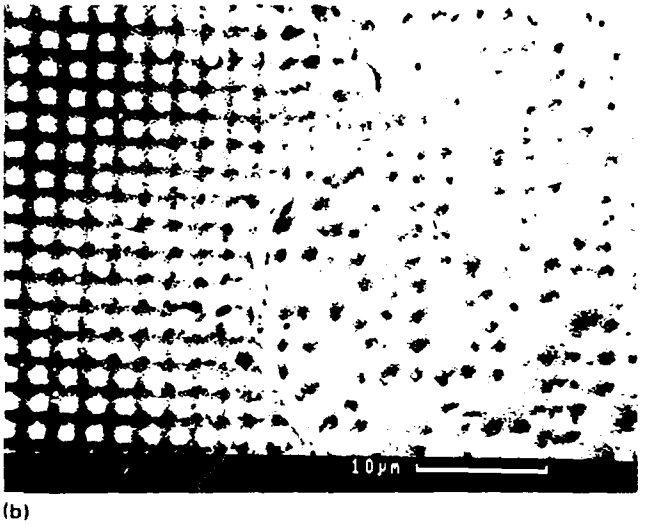

(b)

FIG. 7. (a) SEM micrograph of laser damage site on Ge relief surface without diamond coating. (b) Detail of damage site.

tions of the individual constituents were calculated as a function of thickness. The effective index of refraction profile was calculated based on the effective medium theories for heterogeneous dielectric mixtures. For this analysis, the model of Bruggeman[6,7] was used due to its self-consistency at the high volume fractions and dissimilar host-inclusion dielectric functions appropriate to this work.[8] In the two-dimensional form, the complex dielectric constant of the mixture, $\bar{\epsilon}_m$, can be related to those of the individual components $\bar{\epsilon}_1$, and $\bar{\epsilon}_2$ by the equation

$$(1-\phi)(\epsilon_2-\epsilon_1)/(\bar{\epsilon}_2-\bar{\epsilon}_m)=(\epsilon_1/\bar{\epsilon}_m)^{\frac{1}{2}}, \qquad (1)$$

where ϕ is the volume fraction of ϵ_2. ϵ_m in Eq. (1) can be expressed as

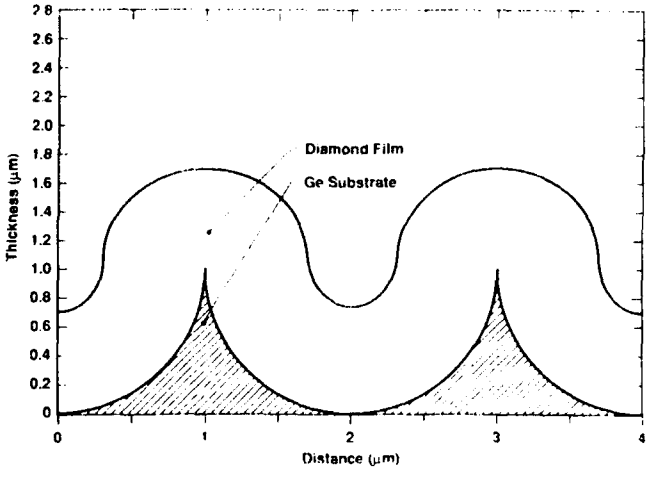

FIG. 8. Thickness profiles of diamond film and Ge relief surface used for theoretical modeling of optical response.

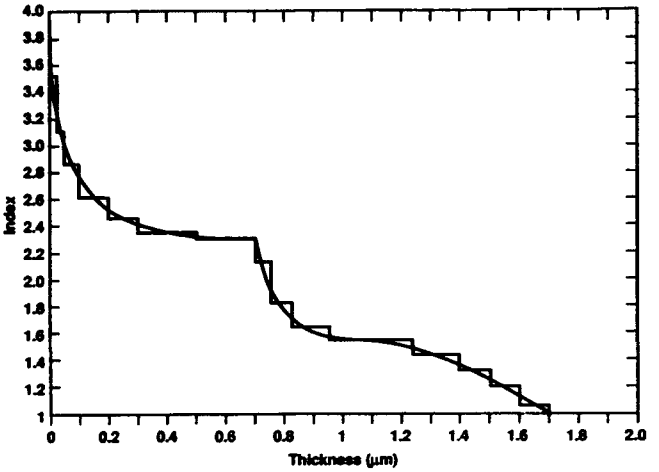

FIG. 9. Calculated effective refractive index profile for the model structure. Also shown is the discrete layer approximation used for the multilayer dielectric equivalent.

$$\bar{\epsilon}_m = \bar{\epsilon}_2 + (1-\phi)^2[(\bar{\epsilon}_2/\bar{\epsilon}_1) - 1]^2\bar{\epsilon}_1/2 - \bar{\epsilon}_1[(\bar{\epsilon}_2/\bar{\epsilon}_1) - 1]\,[(1-\phi)^4[\bar{\epsilon}_2/\bar{\epsilon}_1 - 1]^2/4 + (1-\phi)^2(\bar{\epsilon}_2/\bar{\epsilon}_1)]^{1/2}. \quad (2)$$

The complex index of refraction

$$\bar{n} = n + ik,$$

can be related to the complex dielectric function,

$$\bar{\epsilon} = \epsilon' + i\epsilon'', \quad \text{by}$$

$$\epsilon' = n^2 - k^2$$

$$\epsilon'' = 2nk.$$

Figure 9 shows the resulting effective index profile derived in this manner. The continuous effective index profile was then segmented into discrete layers (Fig. 9), and the layer thicknesses and effective indices were used to calculate the spectral characteristics of an equivalent multilayer dielectric stack. While this neglects the scatter losses at short wavelengths, it does provide an indication of the general transmission levels expected around the design wavelength. The predicted transmittance spectra using this structural approximation is shown in Fig. 10, assuming no backside AR coating on the Ge. This figure also shows the measured device performance prior to application of the backside dielectric AR coating. Comparison of the model with the measured spectra shows it to provide a reasonable prediction of the transmission maximum and peak wavelength range, as well as reproducing some of the wavelength dependence of the measured device transmission. As expected, the dielectric equivalent deviates substantially from the measured response at wavelengths comparable to the interelement separation.

The reduced laser damage threshold of the uncoated motheye surface below that of a standard Ge optic is likely due to a combination of surface damage due to etching, increased surface area, and the thermal transport reduction imposed by the pyramidal feature geometry. This latter

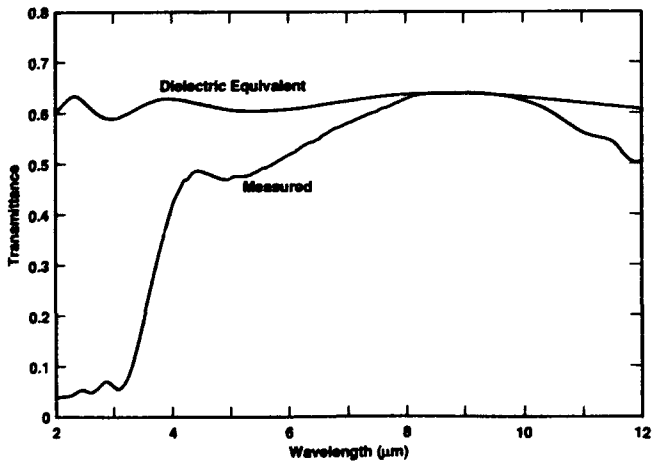

FIG. 10. Predicted IR transmittance spectra for the diamond coating on the Ge relief surface based on an equivalent multilayer dielectric stack. Measured performance shown for comparison.

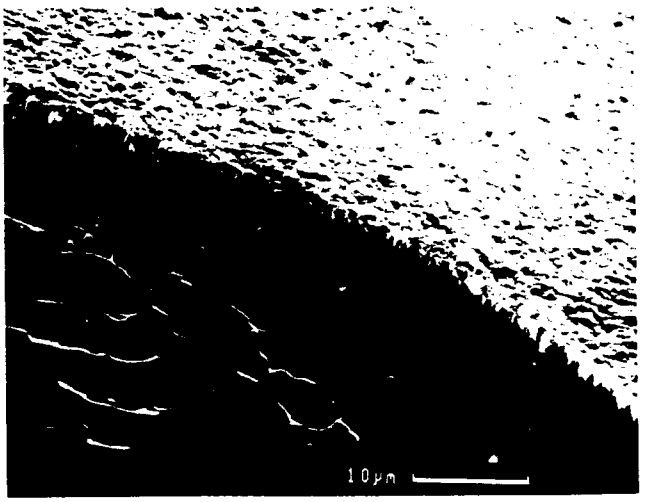

(a)

(b)

FIG. 11. (a) Laser damage morphology for a diamond film on a plane parallel Si substrate (b) Detail of damage site.

effect would be especially important in Ge due to the thermal runaway caused by increased free-carrier absorption with temperature.[9] The contributions from surface damage can be minimized by process refinement, although surface area effects would be constrained by the necessary geometries for antireflective properties. The thermal transport reduction due to the tapered feature profile, however, would be inherent to the use of optimized surface relief structures in Ge, although the consequences may be less significant in other materials such as Si with lower thermal runaway characteristics.

Diamond films on plane parallel Si wafers prepared in this laboratory have also been tested under these laser conditions, and have shown substantially higher laser damage thresholds. For those samples, damage also occurred by substrate melting [Figs. 11(a) and 11(b)] but damage did not occur until incident fluences in excess of 20 J/cm^2. The laser durability testing of the diamond-coated Ge motheye underscores the importance of interfacial quality in the multilayer antireflective relief surfaces. This would include both minimization of interfacial absorption at the substrate surface caused by the etching process and improvement of diamond film adhesion. For substrates such as Ge, for which diamond adherence is difficult, such factors will be significant, and may be addressed by tailored interfacial layers or modification of the etching profile.

V. CONCLUSIONS

The combination of a polycrystalline diamond film and surface relief patterning provides an effective antireflective surface for high index substrates. Such use of a diamond outer surface coating has the potential for increased device mechanical durability beyond simple surface relief structures. These devices are characterized by high transmittance levels and minimal long wavelength scatter, in spite of their coarse-grained morphology. Further refinement of these structures will address substrate and interfacial quality, especially for those materials such as Ge for which diamond films suffer poor adherence.

ACKNOWLEDGMENTS

Portions of this work were sponsored by the Office of Naval Research.

[1] J. F. DeNatale, J. F. Flintoff, and A. B. Harker, J. Materials Sci. (to be published).
[2] J. F. DeNatale, J. F. Flintoff, and A. B. Harker, J. Appl. Phys. **68**, 4014 (1990).
[3] William H. Southwell, J. Opt. Soc. Am. A **8**, 549 (1991).
[4] C. G. Bernhard, Endeavour **26**, 79 (1967).
[5] W. D. Harkins, J. Chem. Phys. **10**, 268 (1942).
[6] L. K. W. van Beek, "Dielectric Behavior of Heterogeneous Systems," *Progress in Dielectrics*, edited by J. B. Birks (Wiley, New York, 1967), Vol. 7, p. 67.
[7] P. J. Hood and J. F. DeNatale, J. Appl. Phys. **70**, 376 (1991).
[8] D. E. Aspnes, J. B. Theeten, and F. Hottier, Phys. Rev. B **20**, 3292 (1979).
[9] P. A. Young, Appl. Opt. **10**, 638 (1971).

Appendix 12

Adhesion Improvement in Diamond Films by Microlithographic Patterning

Journal of Materials Science

CHAPMAN AND HALL

Journal of Materials Science is an international publication reporting recent advances in all the major fields of investigation into the properties of materials. Papers and letters on metallurgy, ceramics, polymers, composites and fibres appear regularly.

Papers for submission to the *Journal of Materials Science* should be sent to Professor W. Bonfield, Dept. of Materials, Queen Mary and Westfield College, Mile End Road, London E1 4NS.

Journal of Materials Science is published monthly by Chapman and Hall Ltd., 2-6 Boundary Row, London SE1 8HN, from whom subscription details are available.

JOURNAL OF MATERIALS SCIENCE 27 (1992) 553–556

Adhesion improvement in diamond films by microlithographic patterning

J. F. DENATALE, J. F. FLINTOFF, A. B. HARKER
Rockwell International Science Center, Thousand Oaks, CA 91360, USA

The use of microlithographic surface patterning has been investigated as a means of modifying the nucleation and adhesion of diamond films on non-compatible substrates. Significant improvements in film adhesion were achieved using this technique, to the point that interfacial integrity was maintained even at stress levels which induced subsurface fracture in the supporting substrate.

1. Introduction

The recent advances in the low-pressure synthesis of diamond thin films have the potential to impact numerous technologies due to diamond's unique combination of optical, mechanical, and electrical properties. Formation of these films from hydrogen–hydrocarbon gas mixtures has been demonstrated by a variety of techniques including hot filaments, microwave plasmas, and high velocity torches [1]. The vast majority of the work described in the literature documents growth and characterization of diamond films on Si and carbide forming metallic substrates due to the relative ease of growth and adherence to these materials. On many substrate materials, however, the diamond films tend to exhibit poor adherence, and typically disbond at thicknesses of the order of a few micrometres due to the development of intrinsic growth and thermal mismatch stresses. To fully exploit the potential of the diamond films, fabrication on less-compatible substrates must be addressed. One approach investigated in this work has been the use of microlithographic patterning of the substrate surface prior to film deposition in order to improve film adhesion. The surface patterning provides an increased surface area for bonding, enhances film uniformity [2] and, if the pattern is undercut, offers a means of physically "locking" the film onto the substrate. This approach has been found to significantly improve film adhesion.

2. Experimental procedure

Fused silica windows were patterned by standard photolithography and dry etching techniques prior to film growth. This produced grid patterns of 1 μm wide etched lines separated by 10 μm square spaces of unetched silica and 3 μm lines separated by 15 μm. The depths of the etched lines were approximately 1 μm in all cases. Processing conditions that gave both sharp sided and rounded etch profiles, respectively, (Fig. 1) were used to determine the effects of profile geometry on film adhesion. Diamond films were deposited using microwave plasma CVD with a source gas composition of 0.5% CH_4, 0.2% O_2, and the balance H_2. Substrate growth temperatures of 750 °C were used as determined by optical pyrometry. Unpatterned substrates were also included in the depositions for experimental comparison. All substrates were prepared using identical diamond polish pretreatments to enhance film nucleation.

3. Results

In the initial experiment, after approximately 16 h of growth local film delamination was observed on the unpatterned substrate, so no further film growth was conducted on this substrate. The patterned substrate with the rounded etch profile exhibited local film adhesion, although much of the film had already disbonded. The films on the substrates patterned with sharp etch profiles, however, maintained their integrity, demonstrating an improvement in adhesion associated with the patterning. The diamond film surfaces were characterized by highly faceted grains approximately 1 to 2 μm in size.

Diamond growth was continued on these substrates, and even after a film thickness of 9 μm, the topology of the initial pattern was still clearly evident in the film (Fig. 2). Subsequent tests showed evidence of the pattern to persist to film thicknesses of over 24 μm. By this thickness, cracks had become apparent in the film (Fig. 2). Cross-sectional SEM revealed, however, that these were not the result of film delamination. Rather, the stresses generated by the growing film and the high temperature processing induced subsurface fracture in the silica substrate itself (Fig. 3). The integrity of the film–substrate interface was still maintained even after the substrate fracture. These micrographs further indicated a strongly columnar grain structure, with the etched lines characterized by slightly inward sloping sides.

A filamentary structure was observed in the regions of the cracks (Fig. 4). This is attributed to H_2 etching of the SiO_2 substrate and the subsequent redeposition

0022–2461/92 $03.00 + .12

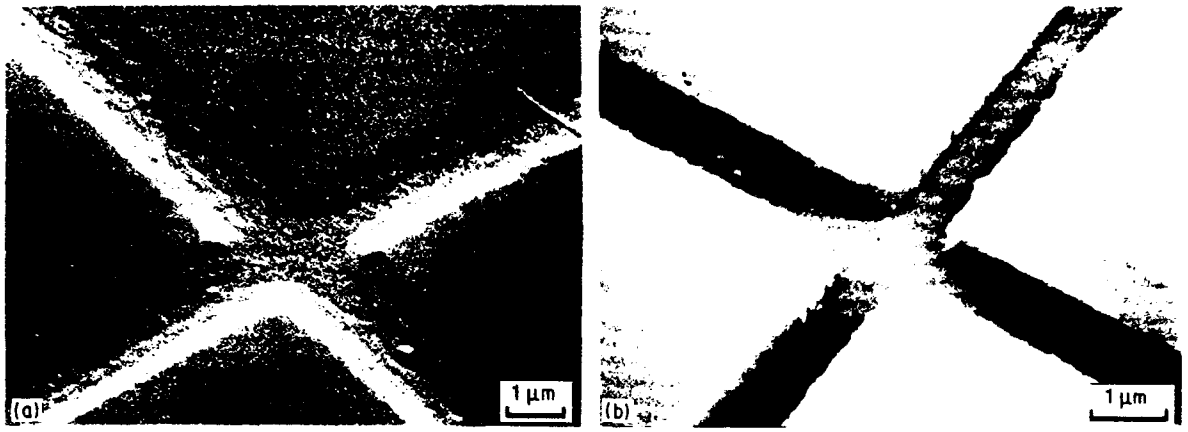

Figure 1 Comparison between SiO_2 substrates with rounded and sharp etch profiles, respectively, prior to diamond growth

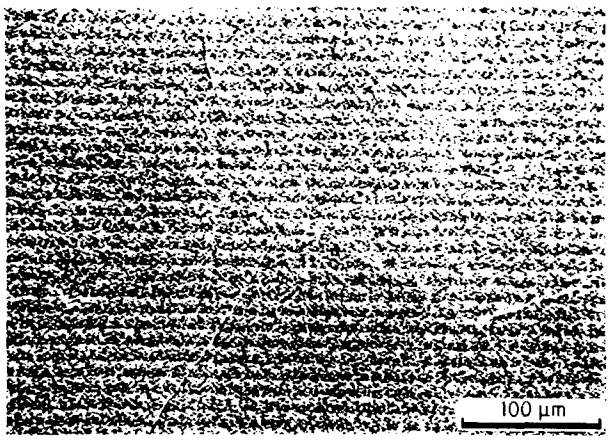

Figure 2 Surface morphology of diamond growth on patterned SiO_2. The film thickness is approximately 9 μm. Note the development of surface cracks

of reduced material. A similar structure was observed to occur on Si substrates with sharp surface discontinuities where the plasma intensity profile is highly non-uniform.

4. Discussion

Microlithographic patterning has been applied to diamond film growth for controlled seeding [2–4] and microstructural control [2]. The current work demonstrates that, in addition to these uses, the technique offers potential improvements in film adhesion.

Even though the profiles of the initial etched lines did not have the desired undercut to physically constrain or "dovetail" the film into the substrate, the process still produced substantial improvement in film adhesion. This is believed to be partially due to increased surface area for film–substrate bonding and enhancement of fine grain nucleation and dense film microstructure. The diamond crystallites are able to grow around the sharp steps of the etched lines, following the contours of the substrate surface pattern (Fig. 5). This provides a means of resisting both planar and normal stresses which could induce film delamination. The minimal improvement in film adhesion provided by the rounded etched lines confirms that the sharp steps are critical to the effect; we anticipate that with refinement of the etching profiles, even further enhancements in film adhesion will be possible.

The cross-sectional microstructure of the diamond film immediately above the patterned regions differed significantly from the non-patterned regions, with the individual columns of the former growing at acute angles to each other and strongly impinging (Fig. 6). The cross-sectional structure far from the unetched regions was similar to that of the unetched control sample, with parallel columnar grains over the entire film thickness. The expanding, columnar structure associated with the etched lines may be instrumental

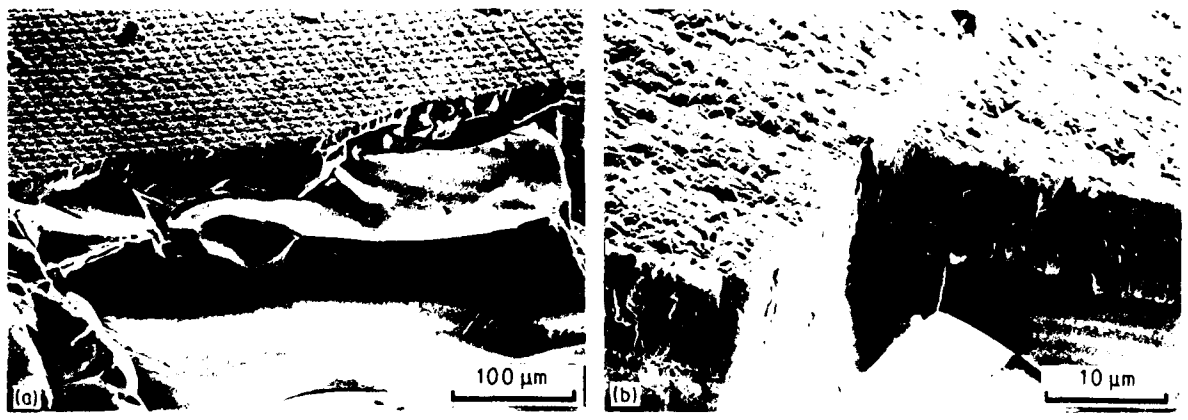

Figure 3 Cross-sectional SEM micrograph illustrating subsurface fracture in SiO_2 substrate after extended diamond growth

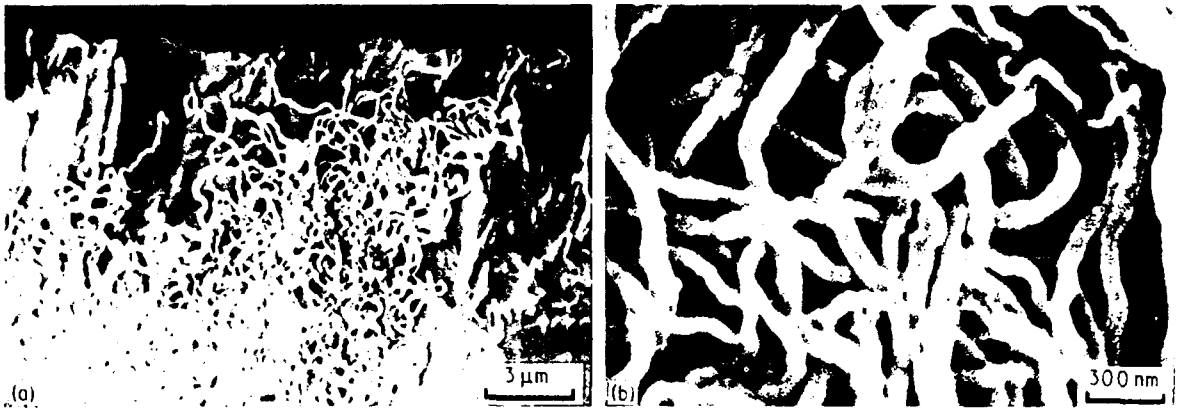

Figure 4 Filamentary microstructure observed in subsurface cracks attributed to redeposition of reduced substrate material

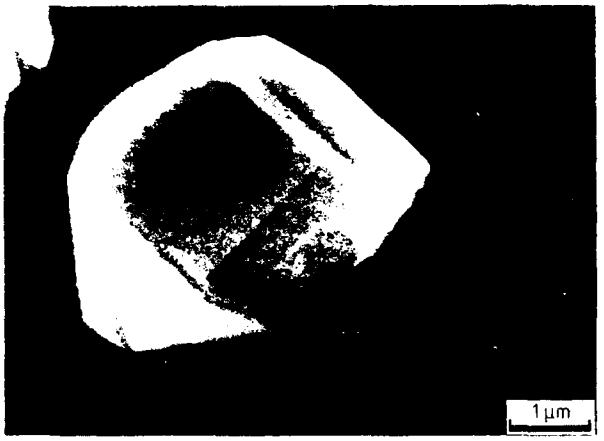

Figure 5 SEM micrograph of diamond crystallite growing around the etched feature on a Si substrate

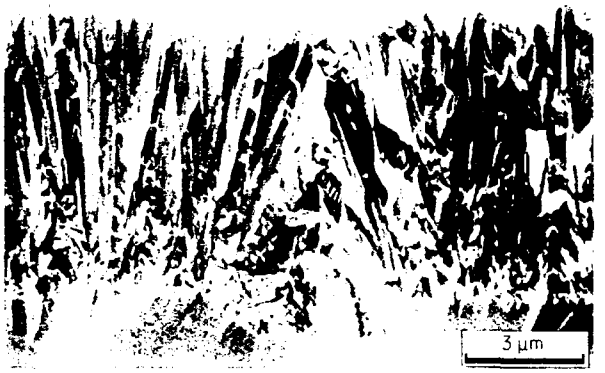

Figure 6 Cross-sectional SEM micrograph illustrating expanding columnar geometry in regions of sharply etched features in SiO_2

in the stress characteristics of the film. An unpatterned diamond film on Si may develop significant stresses of either compressive or tensile nature during growth as evidenced by the degree of substrate curvature. The expanding columnar grain geometries in the patterned films would tend to impose compressive stresses into the films as the columns grow and impinge. These stresses may actually help to balance the net stress in otherwise tensile films. Indeed, if this is the case then by tailoring the periodic spacing of these features, one may be able to independently exercise control over the stress state of a diamond thin film. In films that would otherwise be compressive in nature, the patterning would accentuate the degree of stress. This is most likely the case in the present experiments, with the combined stresses ultimately exceeding the fracture strength of the silica substrate.

The ultimate fracture of the SiO_2 surface is likely to be due to a combination of intrinsic growth stresses and thermal expansion mismatch at the high processing temperatures. Additional reduction of the surface mechanical strength could have resulted from the hydrogen plasma environment, and further studies are required to establish this. The subsurface fracture of a substrate by a tensile thin film has been modelled by Drory and Evans [5] and Drory *et al.* [6] The observed crack geometries in this work are identical to those described above, with both shallow and deep substrate cracks running parallel to the film interface.

Quantitative comparisons of the observed behaviour can be made to the crack depths predicted by the theoretical models and experimental validations of [5] and [6]. A substrate to film thickness ratio of 100 and an elastic modulus ratio of approximately 10 are appropriate for the current experiments. The observed ratio of crack depths to film thickness are 10 and 3.5 for the deep and shallow cracks, respectively. This compares to values of approximately 8 and 2, respectively for the predictions of [6]

5. Conclusions

Microlithographic patterning of a substrate surface prior to diamond growth provides a means of improving film adhesion beyond that of non-patterned substrates. This technique has significant application to the growth of diamond films on non-compatible substrates. The alteration of the growth geometries in the regions of the patterning may be responsible for modification of the film stress, providing a means of control over the mechanical state of the resultant diamond film. Implementation of this technique to thicker film

Appendix 13

Residual Stress Measurements on Polycrystalline Diamond

Proceedings of Window and Dome Technologies and Materials IV, SPIE International Symposium on Optics, Imaging and Instrumentation, San DiegoCA July 24-29, 1994.

RESIDUAL STRESS MEASUREMENTS ON POLYCRYSTALLINE DIAMOND

A.B. Harker, D.G. Howitt*, S.J. Chen*, J.F. Flintoff,
and M.R. James

Rockwell Science Center
Thousand Oaks, CA 91358

*University of California at Davis
Department of Chemical Engineering and Materials Science
Davis, CA 95616

ABSTRACT

The magnitude of the residual stresses in thick samples of polycrystalline diamond were measured by the sine squared, angular resolved x-ray diffraction (XRD) technique and by detailed analysis of electron channeling patterns from individual grains in polished diamond films using a scanning electron microscope. The XRD measurements were made on samples produced by both plasma torch and microwave plasma low pressure growth techniques with a range of microstructures. Results show that residual levels of stress ±0.3 GPa can be generated inside the thinner films on substrates by thermal expansion mismatches, while average residual stress in free standing 0.5 to 2 mm thick diamond plates is negligible. Within the individual grains of the thicker films, localized stress variations on the order of ± 0.5 to 0.8 GPa can be distinguished.

1.0 INTRODUCTION

Both X-ray diffraction (XRD) and electron channeling techniques can be used to directly measure strain. With XRD analysis the measurements are very sensitive because of the precision with which lattice parameters can be determined. The primary drawback is that the measurements provide only an average strain value in any defined direction and cannot resolve the spatially varying strain components. The geometric analysis of electron channeling patterns is not quite as sensitive to lattice strain variations; however, it can be used to determine the individual components of the strain and to map strain at the individual grain level. When the stress is anisotropic, the electron channeling technique can also distinguish angular distortions in the lattice. In both measurements, determining the residual stresses from strains in a diamond lattice is made difficult because of the high modulus (C_{11} = 1076 GPa).

Polycrystalline diamond can currently be grown at low pressures by a number of plasma based techniques, most of which are capable of producing large grained, high purity material after proper system optimization. Along with this, however, has come the observation that growth and thermal expansion stresses in the polycrystalline diamond are a significant factor in determining process yield and film properties. There are several sources of stress in the growing diamond. These include thermal expansion mismatch with the growth substrate, impurity inclusions, crystalline defects, and stresses produced by the evolution of the characteristic columnar grain morphology.[1] To rapidly optimize and scale growth processes for polycrystalline diamond as well as to improve production yields, it is desirable to be able to both measure residual stress in the material and to determine the related processing variables and microstructural features.

2.0 EXPERIMENTAL

Two techniques, angular resolved x-ray diffraction and electron beam channeling, have been investigated for the measurement of strain in samples of polycrystalline diamond. Both techniques provide a measurement of the lattice constants of the crystalline material and can be used to calculate stress levels with the assumption of a value for the elastic modulus.

2.1 Angular Resolved X-Ray diffraction

The XRD technique used in these measurements is based on a determination of the crystal lattice d-spacing associated with a high angle reflection as a function of the angle of incidence of the excitation source.[2] In a randomly oriented polycrystalline diamond with significant lattice strain, a plot of the measured d-spacing versus the sine^2 of the sample tilt angle (from normal to 45° off normal) will produce a straight line. The slope and sign of the straight line can be converted to a measurement of the residual stress when a value for the modulus of the material is available.

In these measurements the hkl {331}, 140.84° 2-theta (d = 0.8182) reflection was observed at 11 separate sample tilt angles varying from 0 to 45° off normal using Cu k alpha radiation. Lattice spacings on both sides of each polycrystalline diamond were measured. The standard deviation was calculated from the scatter in the 11 lattice spacing measurements when plotted against the sine ^{2} value of the sample tilt angle.

2.2 Electron Channeling Contrast

When an electron beam in a scanning electron microscope (SEM) is focused on a highly smooth crystalline surface, those electrons backscattered from the surface have their scattering coefficient weakly affected by the surface potential associated with the crystalline lattice. The backscattering coefficient is maximized at critical beam orientations which satisfy the Bragg condition for the individual crystalline planes and so give rise to a channeling pattern when the angle of incidence of the electron beam is rocked about a fixed location on the sample surface.[3] This two-dimensional pattern actually reflects the three dimensional symmetry of the crystalline lattice through the higher order Laue zone (HOLZ) lines. The separation of the channeling lines is sensitive to the lattice parameter and electron beam voltage.

A channeling pattern recorded from a <001> pole of a single MPACVD diamond grain in a CAMSCAN SEM equipped for electron channeling is shown in Fig. 1, compared to the theoretical pattern. The image is derived from electron scattering from the low index planes in this [001] zone as well as the higher order planes close to it. In the absence of any lattice distortion the pattern reflects the four-fold symmetry of the [001] orientation. The higher order planes produce the lower intensity detail in the central region of the pattern and the lines from these planes are the most sensitive to changes in the lattice strain.

For any given crystal in which the electron beam voltage, crystal symmetry and lattice spacings are known, the channeling pattern can be calculated and compared to the experimental data. However, in the case of diamond and other nonconducting materials, the effects of sample charging must be taken into account. In an uncoated sample at high voltage, this charging can significantly retard the incident beam and accelerate the backscattered electrons (or vice versa at low voltages). The calibration of the beam energy, in the presence of such charging, can be done using the limit of the X-ray continuum emitted by the sample. This can be measured by energy dispersive X-ray spectroscopy to an accuracy of $\pm$ 50 eV.

A computer program was developed to model the channeling patterns in diamond and silicon for comparison with the observed data and for parametric sensitivity analyses of the HOLZ line positions with respect to changes in the lattice spacings and angles. A study of strain in [001] silicon by Kozubowski[4] used the shift in the height of the triangle formed from the intersections of the (660) and two {571} HOLZ lines. Our analyses used the {771} lines of the [001] diamond pattern, which are closer to the center, and are more sensitive to lattice parameter variations because they have a larger value of the diffraction vector,g, and the change of the Bragg angle is proportional to this magnitude.

The shifting of the HOLZ lines in the electron channeling patterns due to strain is derived from both the change in the magnitude of Bragg angle, caused by the change of interplanar spacing and the change in the orientation of the diffracting planes caused by rotation. Thus the former corresponds to a change in the distance of the reciprocal lattice point from the origin while the latter is due to the rotation of a reciprocal lattice point about the origin (i.e. the reorientation of the plane). The total angular change can be written as

$$\Delta\theta=\Delta\theta_B+\Delta\theta_P\approx\frac{\lambda\cdot\Delta g}{2\cos(\theta_B)}+\cos^{-1}\left[\frac{\mathbf{g}\cdot\mathbf{E}\,\mathbf{g}}{|\mathbf{Eg}||g|}\right]$$

where θ_B is the Bragg angle, $\Delta\theta P$ is the rotation of the plane, g is the diffraction vector of length |g|, and Δ g is the change in the diffraction vector. The electron wavelength is represented by λ and |Eg| is the determinant of the matrix **Eg**, which in turn is equal to ε + I, where ε is the strain tensor and I an unit matrix. The equation is inexact due to the use of the small angle approximation where sine ($\Delta\theta_B$)$\approx\Delta\theta_B$ and 1 - $\Delta\theta_B^2\approx$1.

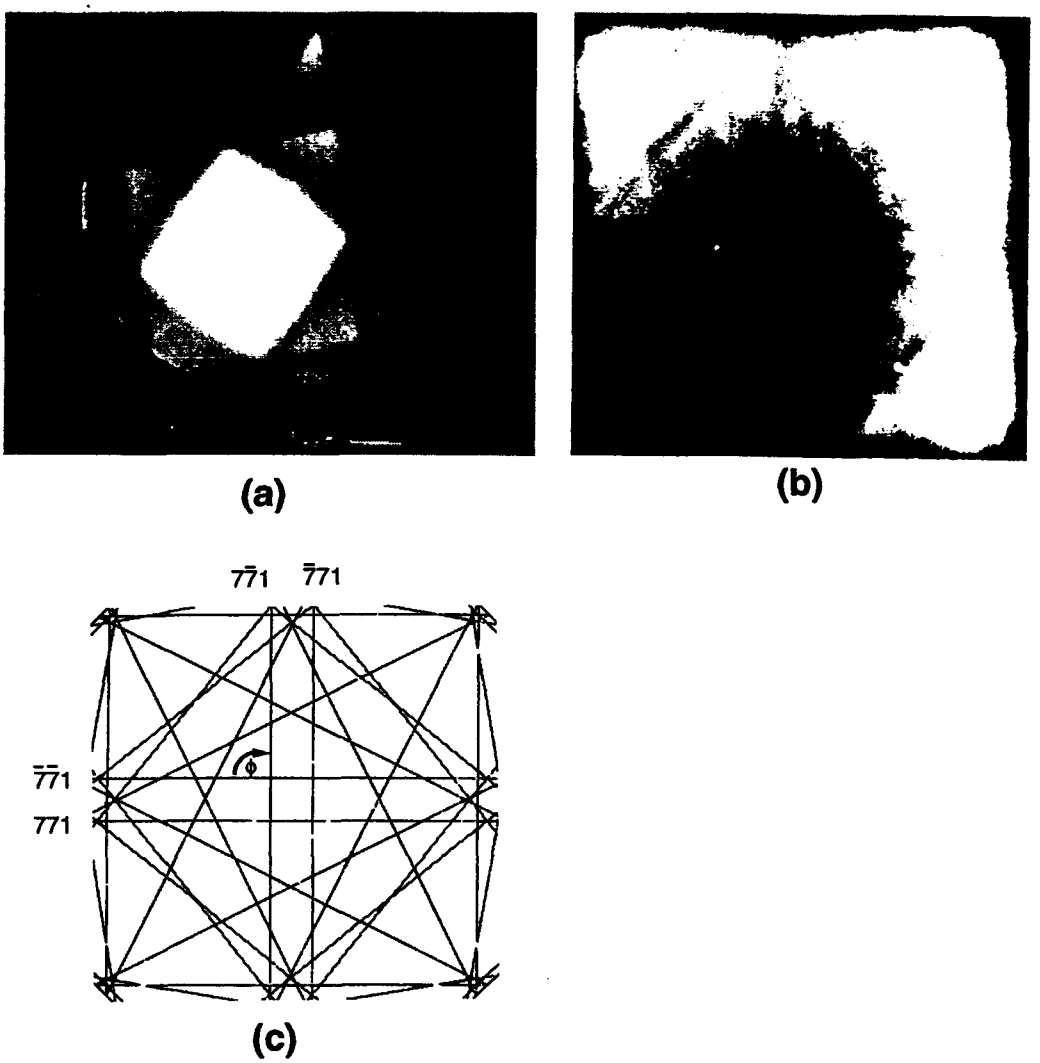

Fig. 1. Experimental and computer simulated [001] channeling patterns from a single MPACVD diamond grain at 29.68 keV. a) Low order lines, b) higher order lines, c) calculated pattern.

When the strain is anisotropic, the sensitivity is also determined by the orientation relationship between the strain ellipsoid and the g vector. Thus the appropriate choice of the g vector can be used to maximize the second term in the equation. The angular separation of the {771} lines in diamond are plotted as a function of the strain along one of the principal axes in Fig.2 along with the corresponding stress value based on the modulus.

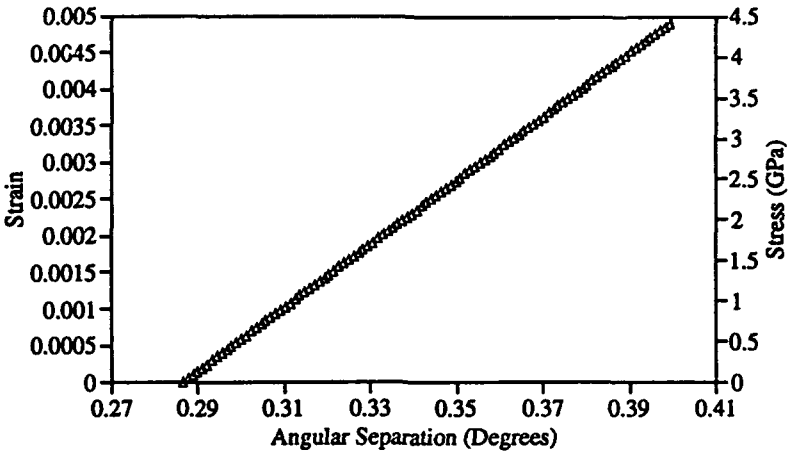

Fig. 2. The magnitude of the one dimensional lattice strain and corresponding residual stress as it varies with the angular separation of the {771} HOLZ lines in the [001] channeling patterns from diamond at 29.68 keV.

3.0 RESULTS

The results of the sine^2 measurements were reproducible, but do not give a clear picture of the residual stresses in thicker polycrystalline diamond films. Table 1 shows the measured residual stress levels for several thick diamond films and a single representative thinner film, both on and off, the silicon substrate. The measurement on the thinner film has good precision and shows a net compressive residual stress. Remeasurement after substrate removal showed the net average stress to be zero with a large scatter in the data. This measurement was typical for thinner films on silicon substrates. The results can be described by a balance between growth stresses and the mismatch in the thermal expansion coefficients of the film and substrate. The measured residual stress can vary in both magnitude and sign, depending on the growth temperature, and is generally relieved when the substrate is removed.

Table 1. Summary of sine^2 XRD measurements of residual stress in polycrystalline diamond disks. All samples were freestanding and polished, unless noted.

Sample: Thickness and Surface Description	Stress (MPa)	StdDev (MPa)	Orientation and Growth Method
Rockwell #1 (growth surface) On Si Substrate, 0.1mm thick (unpolished)	-350	± 62	Moderate (220) MPACVD
Rockwell #1, Removed from Substrate			
(growth surface)	-10	±200	Moderate (220)
(nucleation surface)	-13	±200	MPACVD
Raytheon D383(side 1)	-55	±407	Minor (111)
(0.7mm thick) (side 2)	172	±290	MPACVD
Raytheon H157-01 (side 1)	-179	±290	Minor (111)
0.5mm thick) (side 2)	69	+248	MPACVD
Norton (side 1)	40	±300	Strong (220)
(0.5mm thick)(side 2)	-20	±140	TORCH

For the thicker, free standing diamond plates, the data show the average stress values to be well below the large experimental value of the standard deviation. These measurements are biased by the texture and columnar nature of the samples because the d-spacing values are only derived from those reflections normal to

the incident x-rays. Hence, only those fine grains and renucleation centers which are inclined to the normal growth axis contribute to the measurement. However, the very large standard deviation in the data suggests that the stresses in the sampled grains vary widely in magnitude and sign, and most realistically can be described as microstresses. Hence, the measurements indicate that though the average residual stresses are statistically near zero, the film probably contains significant levels (>250 MPa) of highly local microstresses.

The presence of large microstresses in CVD diamond is supported by the observation of microcracking in growing specimens and by micro-raman scattering studies reported by Vestyck et al.[5] In that work, a strain-induced splitting of the degeneracy in the 1332.5 cm^{-1} Raman fundamental was observed within individual diamond grains. Calibration studies have shown that stress in excess of 1 GPa is required to remove the degeneracy of the Raman fundamental. These Raman measurements also demonstrate that the shape and band center of the micro-Raman fundamental can vary greatly across highly local regions of CVD diamond crystallites. The electron channeling contrast measurements provide another method to directly observe lattice strain at the level of an individual grain.

Figures 3 and 4 show the results of the channeling strain measurements from patterns taken at the same beam voltages rocking about the (001) axis at multiple sites in two different grains in a polished MPACVD diamond plate 0.5 mm thick. The data are displayed in the form of contour lines within the grains, mapping regions of similar lattice strain. The [001] patterns from various points within each grain were digitized, and the angular separation between the individual {771} HOLZ lines and the angle between them were determined directly from the relative line positions. The angular separation can be converted into absolute values of stress (Fig. 2), but in Figs. 3 and 4 the values associated with the contour lines are simply the pixel width of the line separations (± 1 pixel). Contour lines are also shown which correspond to the angle subtending the {771} intersection, which is a direct measure of the distortion of the cubic symmetry along the [100] through the grains.

The contour plots, while far from complete, do show that each grain contains a distribution of strain levels, which can be interpreted as both increasing and decreasing about a "low point." This interpretation is supported by the rotational strain measurement, in which the intersection angle of the HOLZ lines vary around the central value of 90 degrees along the contours within the grains.

The results obtained from the <001> grains in Figs. 3. and 4 both indicate that the principal strains are symmetrical around a grain edge and that the residual stresses differ by about a maximum of 1.5 GPa in the larger elongated grain. In both grains there is also a local loss of cubic symmetry caused by the strains. In the elongated grain, the loss of symmetry follows one of the intermediate contours of the principal strains. Since the strains are anisotropic, quite likely the regions that retain the cubic symmetry are unstressed. Hence, in the equiaxed grain, this assumption suggests a residual stress distribution of about ±0.6 GPa about the grain center. For the elongated grain, the relaxed region follows the middle contour of the variation of the principal strains, suggesting a residual stress distribution of ±0.8 GPa.

The absolute magnitude of these strains could be distinguished unequivocally if the beam electron voltage at the sample surface could be uniquely calibrated. The limit of the maximum energy of the X-ray continuum emitted from the sample provides the most accurate approximation to this voltage. At the microscope setting of 30 KeV this corresponded to 29.68 KeV and was used in the estimation of the magnitude of the residual stress variations in the grains in Figs. 3 and 4 and in the quantative plot in Fig. 2.

These estimated residual stresses are somewhat smaller than those calculated from the micro-Raman peak shift and splitting measurements on similar films reported earlier this year[5]. However, these data are representative of only two grains in the bulk sample and far greater sampling is required for a full description of the stress magnitudes and distributions.

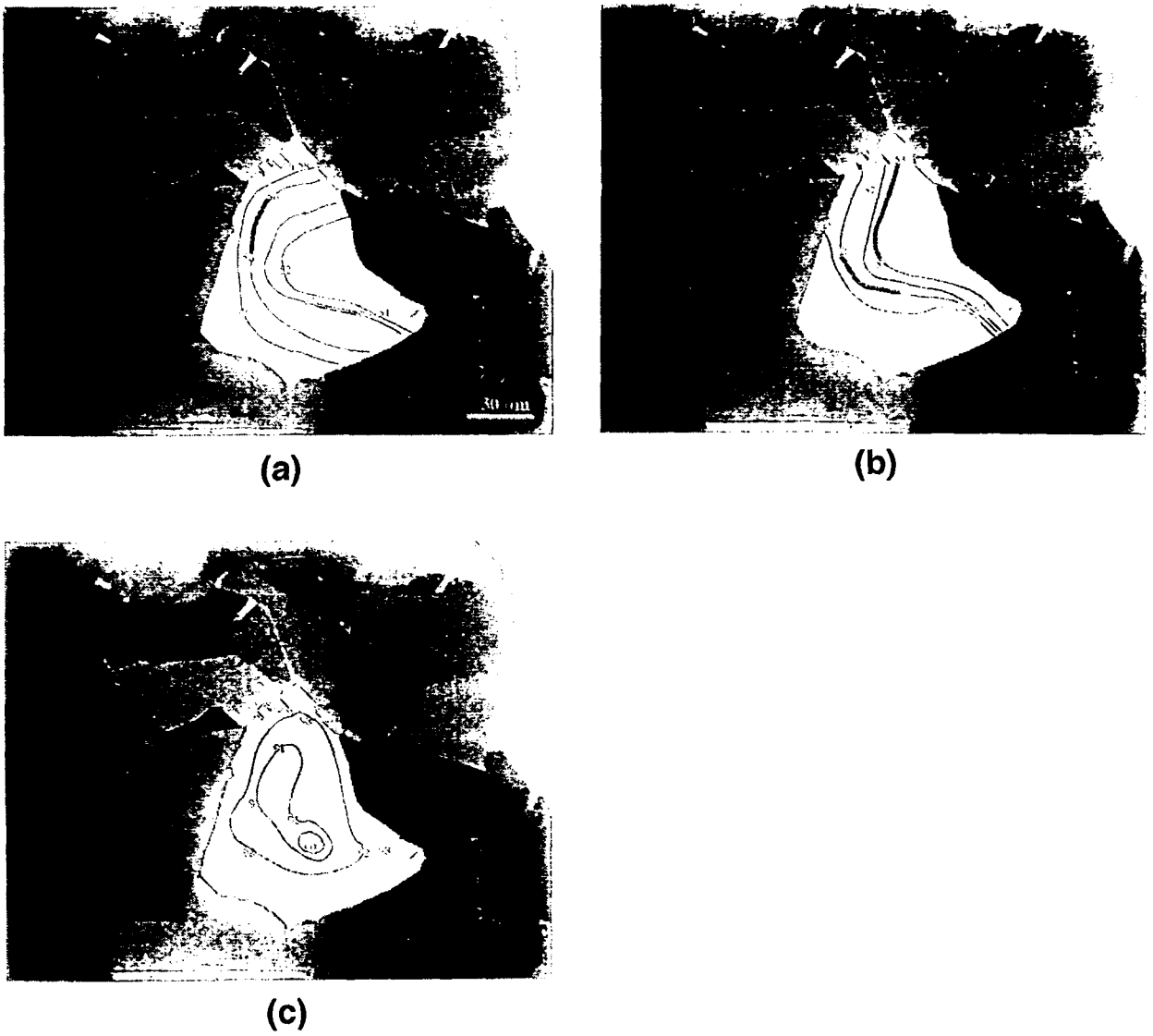

Fig. 3. Backscattered electron image from an [001] oriented equiaxed grain in a diamond film with contour lines showing: a) The absolute magnitude (in digitization pixels) of the angular separation between the (-771) and (7-71), b) The absolute magnitude (in digititization pixels)of the angular separation between the (-7-71) and (771) and c) The angle between (-771) and (771).

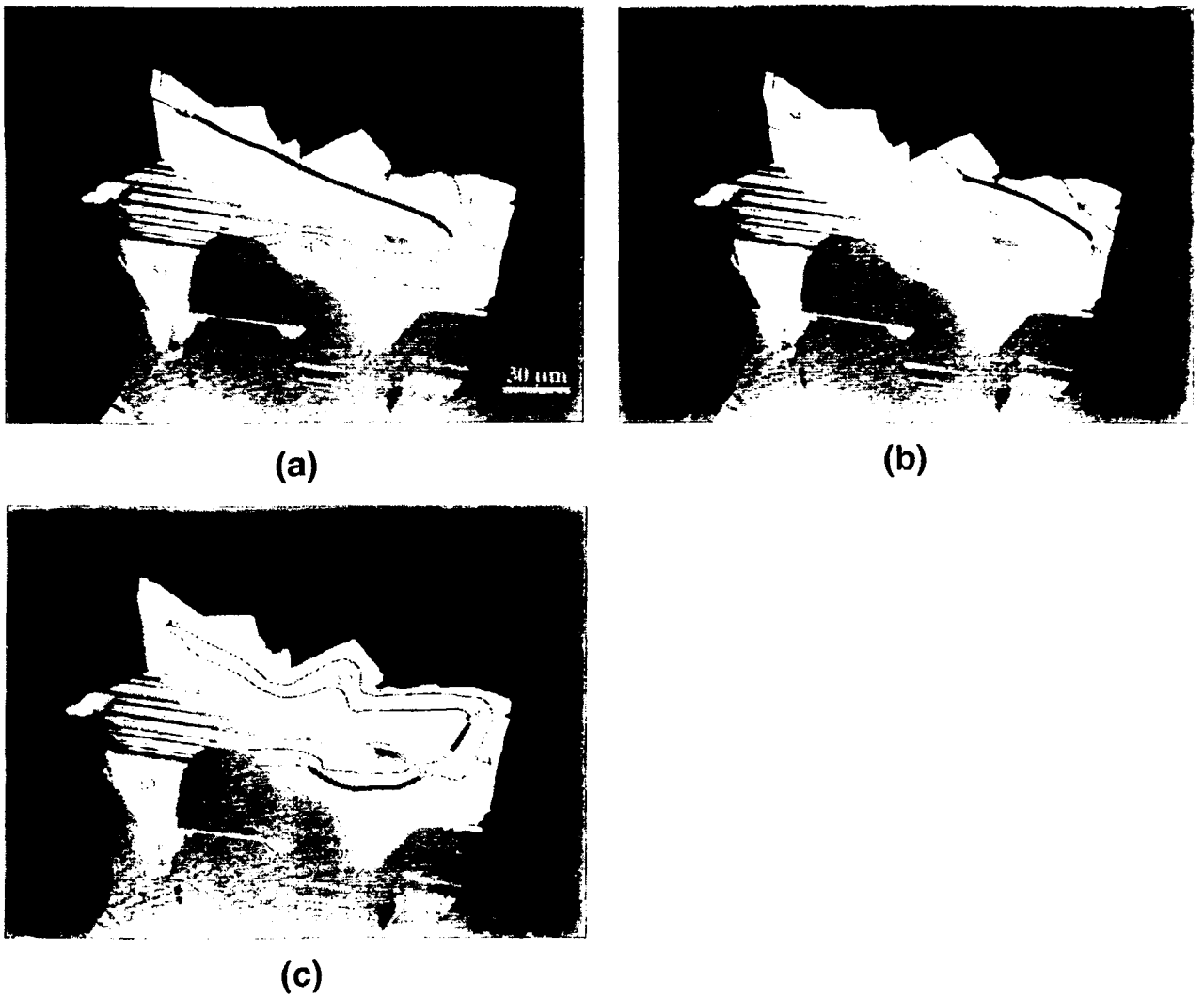

Fig. 4. Backscattered electron image from an [001] elongated grain in a diamond film superimposed with contour lines showing: a) The absolute magnitude of the angular separation (in digitization pixels)between the (-771) and (7-71), b) The absolute magnitude of the angular separation between the (-7-71) and (771) (in digitization pixels), and c) The angle between (-771) and (771).

4.0 DISCUSSION

Diamond is a cubic material and so is completely described by the three stiffness constants[6] c_{11} = 1076.4 GPa, c_{12} = 125.2 GPa and c_{44} = 577.4 GPa
where

$c_{11} = c_{22} = c_{33}$,
$c_{44} = c_{55} = c_{66}$ and
$c_{12} = c_{13} = c_{23} = c_{21} = c_{31} = c_{32}$

The stress is given by

$\sigma_i = c_{ij}\ \varepsilon_j$

and for an isotropic strain, where $\varepsilon_1 = \varepsilon_2 = \varepsilon_3$

$\sigma_1 = (c_{11} + c_{22} + c_{33}) \varepsilon_1$
$\sigma_2 = (c_{11} + c_{22} + c_{33}) \varepsilon_3$
$\sigma_3 = (c_{11} + c_{22} + c_{33}) \varepsilon_3$

where $(c_{11} + c_{22} + c_{33})$ is 1779 GPa. Thus for an average stress of 500 MPa (0.5 GPa) along the principal axes, the isotropic strain is 2.8×10^{-4} (0.028% strain).Since the lattice parameter of diamond is 3.5669, such a strain will change the lattice parameter to 3.5682 Å when it is tensile and to 3.5656 when it is compressive. These lattice parameter changes are more than a factor of 3 smaller than the 0.1% strain, which is considered to be the limit to the resolution that has been achieved using data from electron channeling patterns in silicon. However, in a free standing polished plate the strain will not be isotropic because the strain perpendicular to the film can be relaxed by both macroscopic distortion and material removal. In such a case $c_3=0$ and $\sigma_1 = c_{11}\varepsilon_1 + c_{12}\varepsilon_2$, $\sigma_2 = c_{21}\varepsilon_1 + c_{22}\varepsilon_2$ and $\sigma_3 = c_{31}\varepsilon_1 + c_{32}\varepsilon_2$.

In the event that the strain is symmetrical, i.e. $\varepsilon_1 = \varepsilon 2$, then $\sigma_1 = (c_{11} + c_{12})\varepsilon$, $\sigma_2 = (c_{21} + c_{22})\varepsilon$ and $\sigma_3 = (c_{31} + c_{32})\varepsilon$. Under these circumstances an in–plane stress of 500 MPa would actually produce a strain of 0.04% along the principal axes. Given sufficient resolution in the pattern these principal strains could be determined directly by electron channeling in a <001> oriented film. Under the same circumstances these in-plane strains would correspond to a mean stress (i.e. 1/3 $(\sigma_1 + \sigma_2 + \sigma_3)$), which compares reasonably to the levels of 0.2 to 0.5 GPa observed by X-ray diffraction in thinner films and the scatter level in the XRD data. Very similar levels of sensitivity are predicted if the stress perpendicular to the film is assumed to be zero after substrate removal and polishing.

The $\sin^2$ measurements combined with the electron channeling data suggest that even though bulk CVD diamond plates contain no measurable average residual stress, there are still high levels of microstress within the material. The microstresses appear to be localized in regions of opposite strain within the individual grains and to be distributed in relation to grain shape and defect content.

The electron channeling technique seems to have sufficient sensitivity to map strain within grains of CVD diamond, but improved calibration of the absolute electron beam energy at the surface is required to achieve full quantification of the measurements.

5.0 ACKNOWLEDGMENTS

This work was supported in part by the U.S. Office of Naval Research. Our thanks to John Armstrong at the California Institute of Technology and David Joy at the University of Tennessee for suggesting the measurement of the x-ray continuum as a method for more precisely determining the energy of the channeling patterns.

6.0 REFERENCES

1. P.R. Chalker, A.M. Jones, C. Johnston, and I.M. Buckley-Golder, "Evaluation of Internal Stresses Present in CVD Diamond Films," Surface and Coatings Technology, 47, pp.365-374, 1991.

2. I.C. Noyan and J.B. Cohen, Residual Stress, (Springer-Verlag, N.Y. Inc. 1987).

3. D.E. Newbury, D.C.Joy, P. Echlin, C.E. Fiori, and J.I. Goldstein, Advanced Scanning Electron Microscopy and X-Ray Microanalysis, (Plenum Press, N.Y. 1986) pp.87-145.

4. J.A. Kozubowski, W.W. Gerberich, and T. Stefanski, "Measurement of Small Elastic Strains in Silicon Using Electron Channeling Patterns" J. Mater, Res.3, pp.710-713, 1988.

5. D.J. Vestyck,Jr., D. Shectman, and J.E. Butler, "Characterization of Localized Stress in Polycrystalline Diamond," presented at Workshop on Characterizing Diamond Films III, Feb. 23-24, 1994, Gathersburg, MD, NIST doc. NISTIR 5418, 1994.

6. M.H. Grimsditch and A.K. Ramdas, Phys. Rev. B, 11, 3139,1975.

Appendix 14

Diamond Gradient Index "Moth Eye" Antireflection Surfaces for LWIR Windows

Diamond gradient index "moth-eye" antireflection surfaces for LWIR windows

Alan B. Harker and Jeffrey F. DeNatale

Rockwell International Science Center
Thousand Oaks, CA 91360

1. ABSTRACT

An optical surface can be microscopically textured in a pattern with physical features whose dimensions are below that of the operational wavelength to produce a physical gradient in the effective optical index of refraction. The performance of such "moth-eye" surface features, typically cones or pyramids, can be predicted based on dielectric mixture models by use of the optical properties of the base material and air. The performances of LWIR antireflective moth-eye surfaces formed in silicon, germanium and diamond are consistent with theoretical predictions.

2. INTRODUCTION

The requirement for aircraft infrared (IR) radiation detection and imaging systems to operate in adverse environments has increased the need for highly durable optical windows and antireflection (AR) coatings to avoid impact erosion and damage by water, salt, and sand particles. Current aircraft IR systems typically use zinc sulfide, zinc selenide, or germanium front windows to achieve long wavelength (LWIR) operation with minimal absorption and scattering losses. Zinc sulfide and germanium have the best mechanical properties of current LWIR window materials and can survive water particle impacts at velocities up to about 200 m/sec before suffering erosion damage.[1,2]

Since both zinc sulfide and germanium have a relatively high index of refraction, the erosion resistance of the materials used in front surface dielectric stack AR coatings must be considered. Even diamond, the most erosion resistant LWIR transparent material, has an index of refraction of 2.35 at 10 μm wavelength and requires an AR coating to achieve maximum transmission. Such dielectric coatings are typically prone to erosion and can be damaged by liquid and solid particles at velocities well below that of the bulk window, causing scattering centers on the front surface.

In this paper, the use of surface relief texturing to produce a physical gradient in the index of refraction (n) is explored for achieving LWIR reflection reduction. Such relief feature AR surfaces are known as moth-eye's, due to their similarity in form and function to the conical protuberances on the corneas of the natural analogue. This concept is not new and has been the subject of study by several researchers.[3-5] Recently in this laboratory, Southwell[6] modeled the effect of surface relief feature configurations for the optimum AR properties, and DeNatale et al[7] demonstrated a high performance germanium-diamond moth-eye surface for application in the 8 to 12 μm spectral region. These initial efforts are being extended to examine the effects of fabricated surface shapes and substrate materials on optical and mechanical performance.

3. EXPERIMENTAL

Surface microlithographic patterning and etching of germanium and silicon were used to prepare a range of surface relief textures. These patterned surfaces were characterized for AR performance and were then used as substrates for the subsequent growth of diamond overlayers by microwave plasma assisted chemical vapor deposition. All patterning was achieved by optical photolithography using standard

0-8194-0933-2/92/$4.00

semiconductor resists and etches. Masks were prepared by electron beam microlithography using a Cambridge EBMF 6.5 system, writing into PMMA resist.

IR transmission and reflection measurements were carried out in a dual beam Perkin Elmer spectrophotometer calibrated against gold mirror standards. Scattering measurements were made with a gold coated total integrating sphere using 10.6 μm wavelength CW CO_2 laser source. Physical characterization was accomplished by low voltage imaging in a Camscan scanning electron microscope.

4.0 RESULTS

Southwell's[6] work has shown that a regular pyramidal surface-relief feature does not provide optimum AR performance, and that the feature shapes must be more highly optimized with increasing optical index of refraction in the bulk material. To achieve broadband AR properties in a moth-eye structure the feature shapes must achieve a higher degree of curvature and taper as the index of the base material increases. The primary consideration for the lower index materials is the spacing or period (p) of the microscopic features and their height (h). The ratio of the relief feature height and period defines the aspect ratio of the design (R = h/p). In general, the optical bandwidth of the moth-eye designs is limited by grating effects and scatter at shorter wavelengths. To minimize these effects, the period should be less than the design wavelength (λ) divided by the index (n_S) of the substrate ($p < \lambda/n_S$) and the height must be greater than half the design wavelength ($h > \lambda/2$). These relationships, taken to the limiting case, show that to obtain AR behavior over a wavelength factor of 2, the aspect ratio must approach the optical index of the substrate. Useful AR properties can be achieved at lower aspect ratios, but with reduced bandwidth.

In germanium, which has n = 4, superior broadband AR performance in the LWIR would generally be expected with the individual relief features spaced with a period of less than 2.5 μm and a height of 5 to 10 μm. This packing density and height are quite difficult to achieve in polycrystalline materials, using photolithography and etching. However, this problem can be circumvented, to a degree, through the use of a two-layer moth-eye structure, combining Ge and diamond. The use of a surface layer of lower index increases the degree of index gradation that can be accomplished in physical features of lesser aspect ratio. Such a structure should also benefit mechanically from the high hardness and toughness of the diamond outer layer.

To accomplish a two-layer moth-eye surface, the germanium was first patterned and plasma etched to produce highly tapered features 2.25 μm on center, with a height of 1.25 μm. These features were then covered with a 1.0 μm thick layer of polycrystalline diamond. The initial and final surface morphologies are shown in the electron micrograph (Fig. 1) along with the observed IR transmission of the part. The back surface of the germanium substrate was given a simple two-layer AR coating to reduce the back surface reflection. The peak transmission of the window was in excess of 95% at 9 μm wavelength with minimal LWIR scattering. Total integrating scattering measurements on the two-layered relief surface were made at 10.6 μm wavelength and showed scattering of less than 1.3% which included back surface losses.

Lower optical index substrate materials have less stringent physical requirements for the moth-eye feature aspect ratio; hence, relief features of varying heights and shapes were investigated in silicon and diamond. Silicon undergoes highly anisotropic etching which permits a range of regular surface features to be fabricated, the most simple of which are arrays of tetrahedral pits crated by KOH etching of the <100> crystalline surface. Figure 2 shows an electron micrograph of an array of such inverted pyramidal features with an on-center spacing of 3 μm. Figure 2 also shows the "positive" replicate image of these etch pits formed by filling them with CVD diamond and then acid etching away the silicon. Such a pyramidal feature shape, though not ideal, is suitable for moth-eye application if sufficient depth can be achieved. Figure 3. shows a calculation of the effect of the feature height on its AR performance in the IR using a substrate index of 2.35 at 10 μm and ignoring both scatter and dispersion in the index. At feature

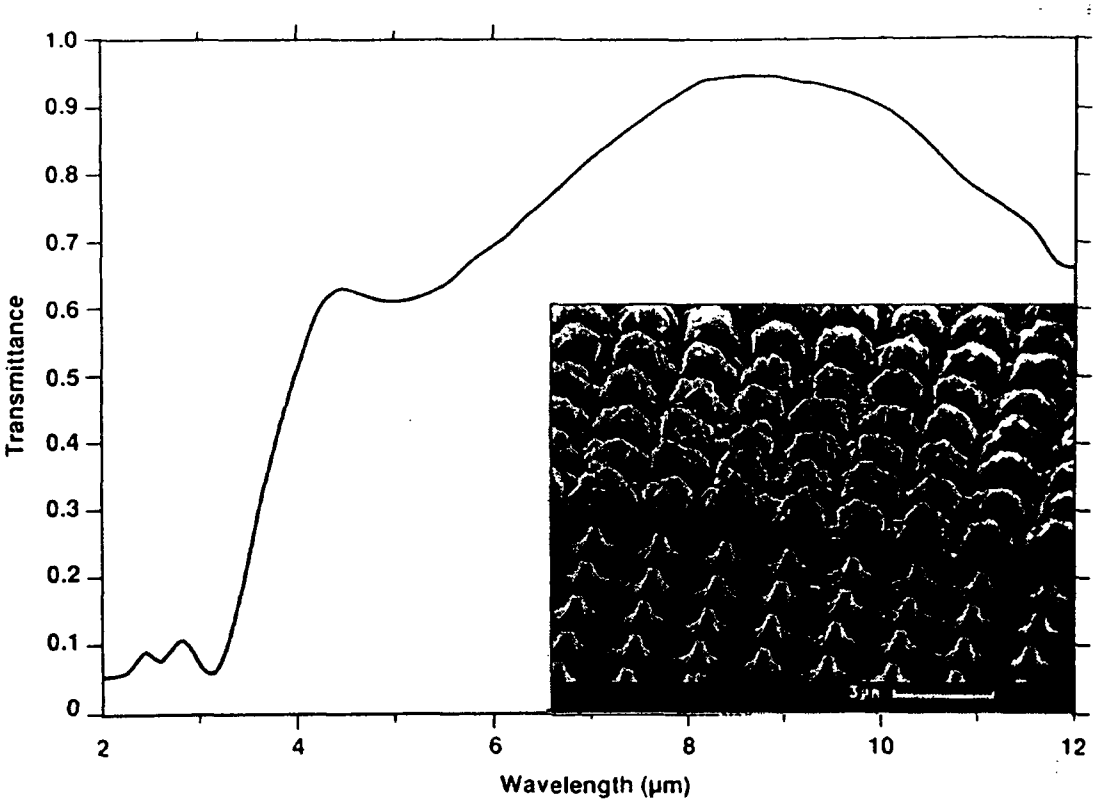

Fig. 1. Scanning electron micrograph of the surface morphology of a diamond-germanium moth-eye AR surface and the observed IR transmission of the optical component.

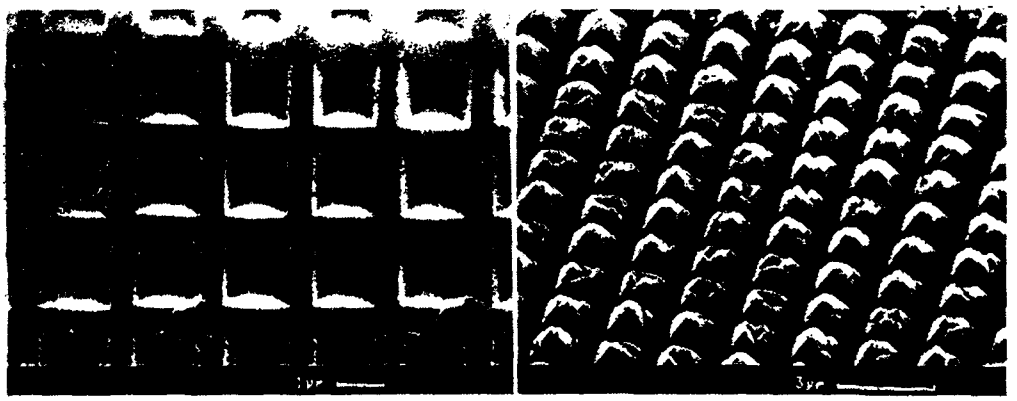

Fig. 2. Scanning electron micrographs of etched <100> silicon and a polycrystalline diamond replicate of the etched surface.

depths greater than about 5 μm, for the selected period of 2 μm, the calculated performance achieves that of a two-layer, high-low dielectric coating.

Silicon's cubic structure limits the aspect ratio that can be achieved in pyramidal etch pits through anisotropic etching. Isotropic etching of silicon can, however, be used with advanced resists to achieve pit depths of over 4.5 μm with center-to-center spacing of 2 μm. These features are more columnar than conical and their optical performance can be approximated by the use of a pyramid-on-a-column, obelisk type, geometry. Figure 4 shows the predicted performance of such columnar features produced in diamond as a function of the column height. Again, short wavelength scatter and dispersion in the

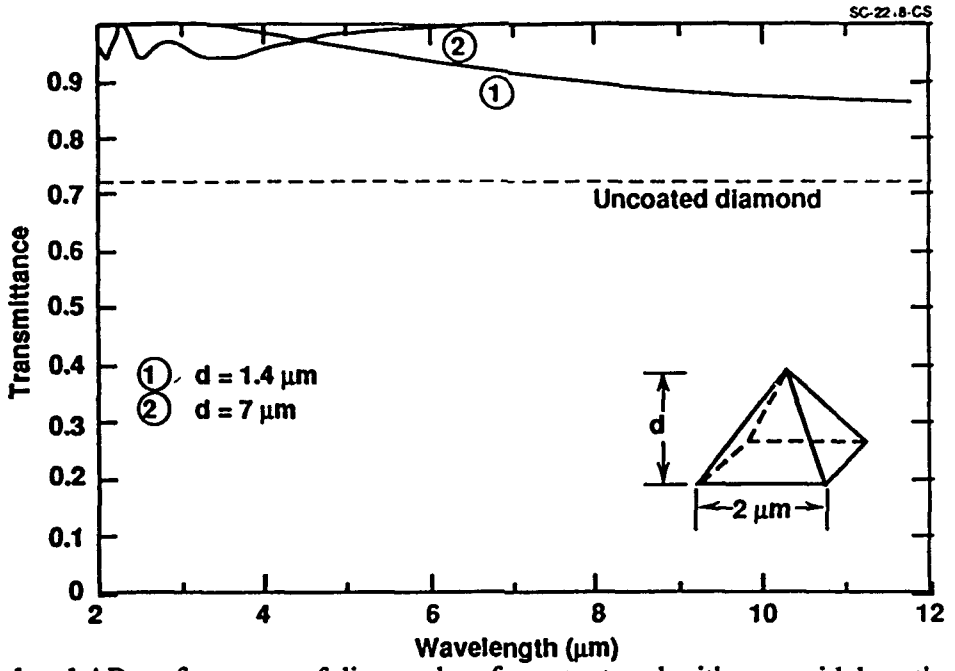

Fig. 3. Calculated AR performance of diamond surfaces textured with pyramidal moth-eye features.

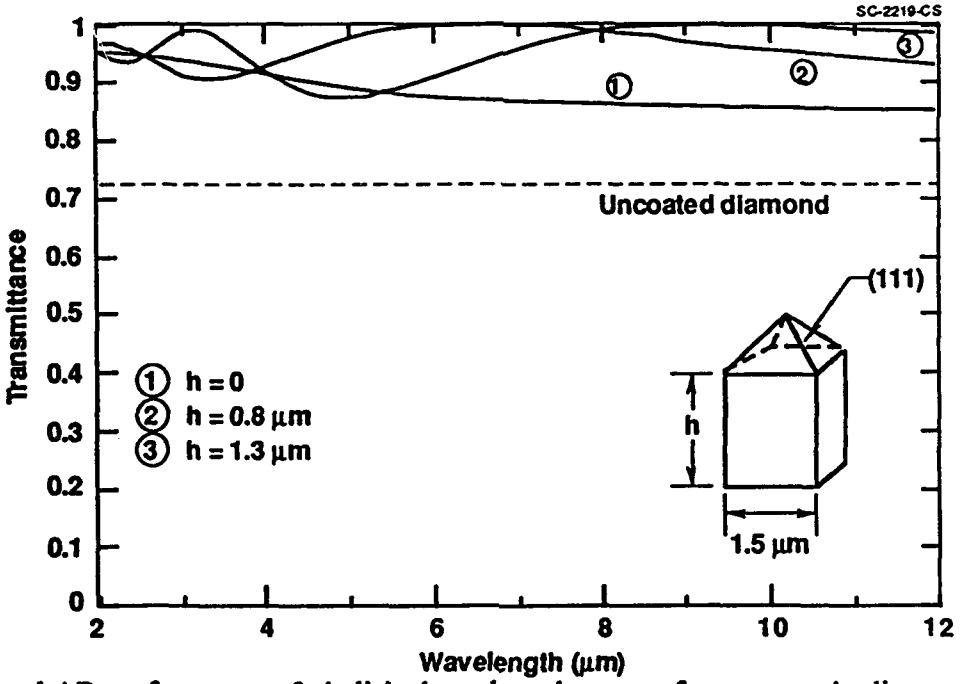

Fig. 4. Calculated AR performance of obelisk shaped moth-eye surface texture in diamond as a function of feature height.

adiamond have been neglected. The calculations do show that for a column spacing of 2 μm and a height of bout 1.3 μm with a 1.4 μm pyramidal tip, transmission greater than 99% can be achieved at the design wavelength of 10 μm.

To test these predictions such columnar shapes were etched in silicon on both sides of a <100> wafer. The reflection spectrum of the double-sided moth-eye window, Fig. 5a, shows the useful

bandwidth of the AR surfaces to be roughly 8 to 12 μm in wavelength. The peak transmission of about 95% occurs at 7.5 μm as shown in Fig. 5b. The absorption features of the silicon substrate as well as the long wavelength role-off of the antireflection texture limit the LWIR transmission.

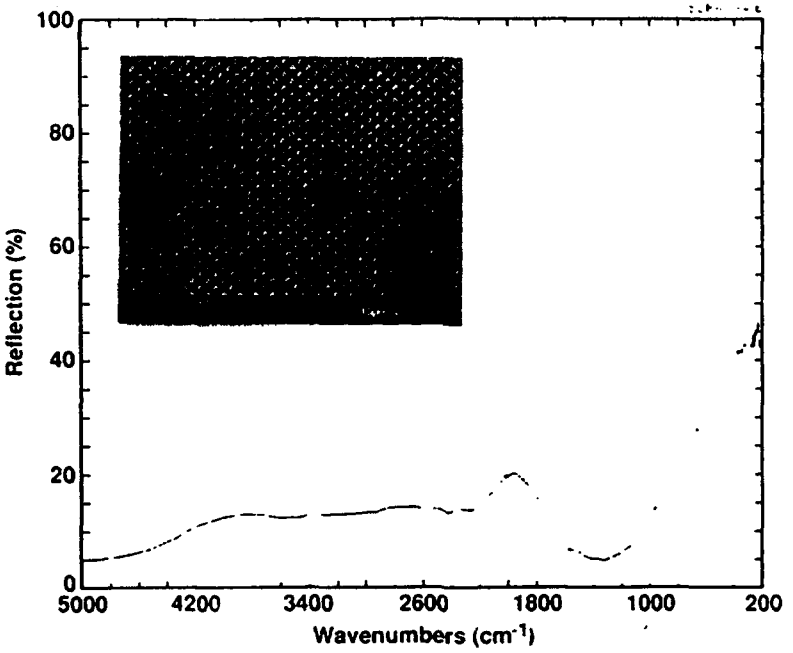

(a)

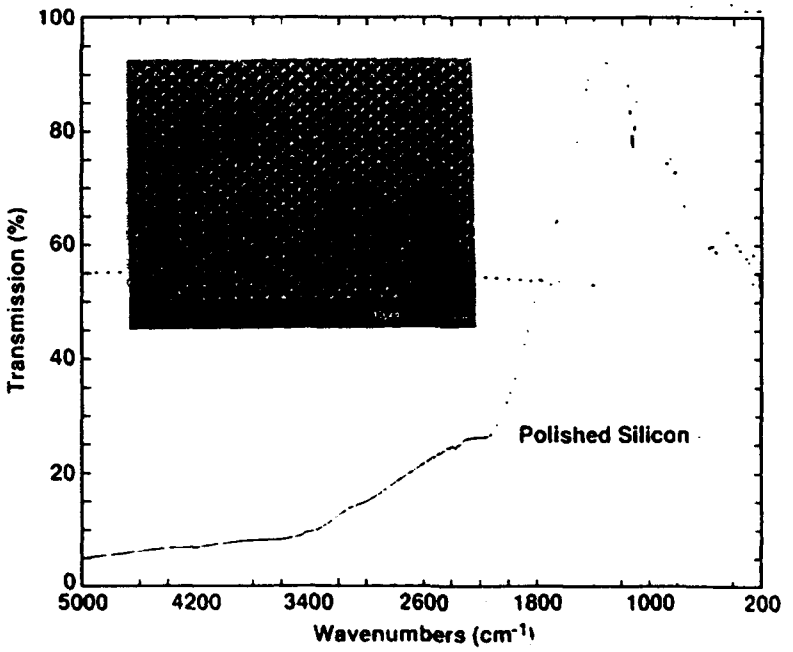

(b)

Fig. 5. (a) IR reflection spectrum of a silicon wafer with a obelisk type moth-eye AR texture on both surfaces. (b) IR transmission and surface morphology of the two-sided moth-eye silicon wafer.

The obelisk texture moth-eye in silicon was fabricated to serve as a growth surface for diamond to replicate the negative image of the texture and to shift the AR band center to longer wavelengths. The resulting diamond surface structure is shown in the electron micrograph (Fig. 6). The diamond moth-eye surface was produced in a 50 μm thick film which was adhered to a germanium substrate for characterization by an IR transparent adhesive, using index matching coatings at the interfaces to minimize internal reflection losses in the stack. The resulting IR reflectance spectra of diamond adhered to germanium with and without a moth-eye front surface are shown in Fig. 7. The diamond-on-germanium without the moth-eye has its spectrum dominated by the front surface diamond reflectance, 0.15, and the Fresnel reflections from the interfaces of the composite stack, producing an average reflectance near 0.18 at 10 μm wavelength. With the moth-eye surface present, the Fresnel reflections are greatly suppressed and the average reflectance is reduced to about 0.07 at 10 μm. With a greater aspect ratio in the moth-eye texture, this value should drop to less than 0.05

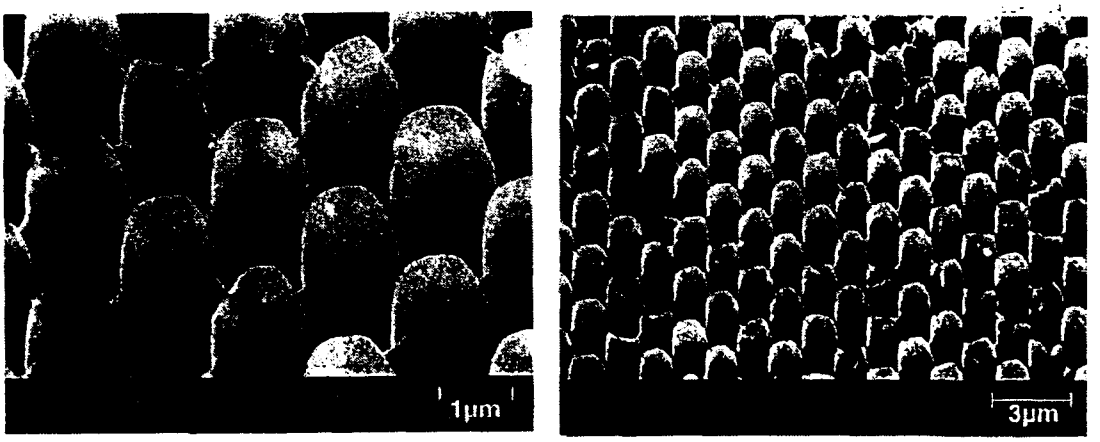

Fig. 6. Scanning electron micrograph of a diamond moth-eye surface with columnar features.

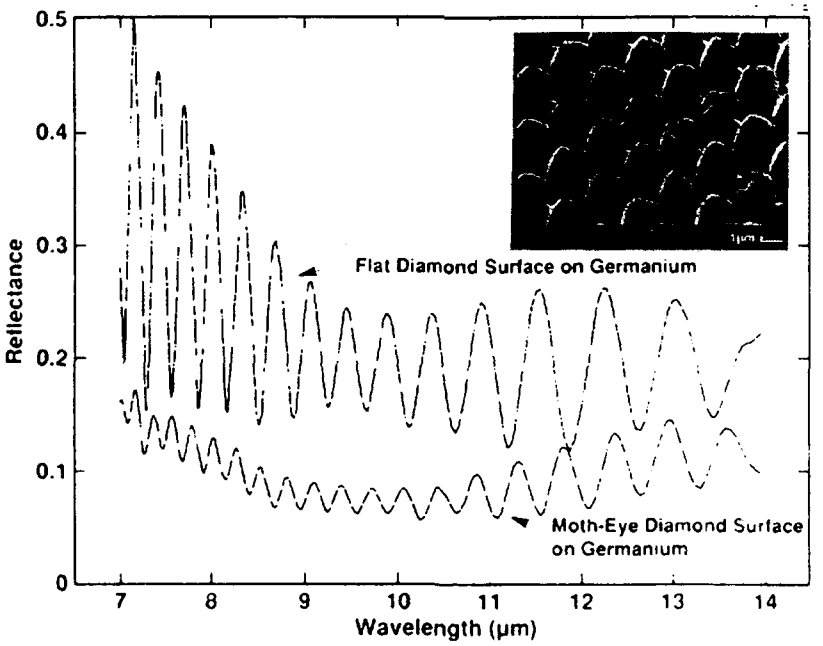

Fig. 7. Surface IR reflectance spectra of a 50 μm thick diamond layer adhered to germanium with and without a moth-eye textured front surface.

5.0 CONCLUSIONS

Moth-eye surface texturing can produce effective reflection reduction in LWIR transparent materials if the ratio of feature height to spacing can be made sufficiently great. The observed reflectance behavior of the textured surfaces agrees with predictions of dielectric mixture models, but is dominated at shorter wavelengths by scattering phenomena. Significant improvement in moth-eye bandwidth and peak reflectance reduction can be achieved in high index materials if a bi-layer index matched structure such as diamond on germanium is used.

The replication of surface features etched in silicon with polycrystalline diamond appears to be an effective method of achieving a moth-eye AR surface for diamond front surface optics. Further research into the effects of feature shape is required to optimize the optical and mechanical performance of such AR surfaces.

6.0 ACKNOWLEDGMENT

This research was sponsored by the Office of Naval Research and Rockwell International.

7.0 REFERENCES

1. M. Wilson I. Perez, M. Thomas, J.B. Boodey, W.R. Scott, and A.B. Harker., "Liquid Jet Impact Measurements in Diamond Coated Ge Substrates," Materials Science Monographs, 73, Y. Tzeng, M. Yoshikawa, M. Murakawa, and A. Feldman eds.(Elsevier Science Pub. B.V., Amsterdam),pp. 217-220 (1991).

2. J.V. Hackworth, L.H. Kocher, and I.C. Snell, "Response of Infrared Transmitting Materials to High-Velocity Impact by Water Drops," in Erosion: Prevention and Useful Applications, editor W.F. Adler, ASTM Special Technical Publication 664 (ASTM, Philadelphia, PA, 1977), p. 255-278.

3. C.G. Bernhard, "Adaptations in a Visual System," Endeavour 26, 79-84 (1967).

4. B.S. Thorton, "Limit of the Moth's Eye Principle and Other Impedance-Matching Corrugations For Solar Absorber Design," J. Opt. Soc. Am. 65, 2670270 (1975).

5. S.J. Wilson and M.C. Hutley, "The Optical Properties of "Moth-Eye" Antireflection Surfaces," Opt. Acta 29, 993-1009 (1982).

6. W.H. Southwell, "Pyramidal-Array Surface-Relief Structures Producing Antireflection Index Matching on Optical Surfaces," J. Opt. Soc. Am., 8(3), 549-553 (1991).

7. J.F. DeNatale, P.J. Hood, J.F. Flintoff, and A.B. Harker, "Fabrication and Characterization of Diamond Moth Eye Antireflective Surfaces on Ge," J. Appl. Phys. 71(3), 1388 (1992).

Appendix 15

Direct Observation of the Defect Structure of Polycrystalline Diamond by Scanning Electron Microscopy

Direct observation of the defect structure of polycrystalline diamond by scanning electron microscopy

A. B. Harker, J. F. DeNatale, and J. F. Flintoff
Rockwell International Science Center, Thousand Oaks, California 91362

J. J. Breen
Indiana University-Purdue University at Indianapolis, Department of Chemistry, Indianapolis, Indiana 46205-2810

(Received 21 September 1992; accepted for publication 25 March 1993)

A method has been demonstrated to directly observe the surface crystallography and defect structures in diamond films by scanning electron microscopy. Individual diamond crystals in the polycrystalline films are polished to a rms smoothness of less than 2 nm using iron metal at temperatures in excess of 725 °C. In the absence of topography, the detailed microstructure of the films can be characterized by secondary electron imaging in a scanning electron microscope by charge-induced electron contrast which shows strong beam voltage dependence. It is hypothesized that defects and grain boundaries form a connected pathway in the film which has greater conductivity than the generally insulating diamond and creates the charge-induced contrast.

Extensive characterization has been conducted on low pressure plasma torch and plasma assisted chemical vapor deposited (CVD) polycrystalline diamond films to relate the growth morphology to the properties of the substrate, the reaction kinetics, and the deposition conditions.[1-3] The observation of the development and growth relationships of defect structures in diamond, however, has been limited to transmission electron microscopy studies of thin foils,[4-6] electron- and photon-induced fluorescence of electronic defects,[7,8] and interpretations based upon the relationships between the general morphology and the crystal structure.[9,10] However, to directly follow the generation of crystalline defects as a function of growth conditions and film thickness, it is necessary to have a microscope characterization technique which can observe the detailed microstructure of the growing surface.

Standard scanning electron microscopy (SEM) generally only produces images of topographic detail, not fine scale crystallographic microstructure, and transmission electron microscopy is applicable only to submicron-thickness films and foils. In this work, an approach has been demonstrated to observe defect microstructures in the near-surface regions of polycrystalline diamond films in a standard scanning electron microscope. The approach is based upon removing all surface topology by reactive iron polishing of the diamond surface, and observing detailed microstructure by charge-induced electron contrast imaging.

Polycrystalline diamond films were grown on (100) silicon by low pressure microwave plasma assisted CVD in an Applied Sciences reactor. A deposition pressure of 28 Torr was used with a reaction mixture of 99.5% hydrogen and 0.5% methane at 700 °C. Characterization was carried out in a CAMSCAN scanning electron microscope. Optical microscopy showed the films to have grain size that increased with film thickness and local surface roughness on the order of ± 0.5–2 μm. Raman scattering spectroscopy showed the films to have primarily $sp3$ bonding and x-ray diffraction indicated a preferential ⟨110⟩ axis normal growth. SEM revealed the surfaces to have the morphology typically associated with polycrystalline diamond films, but the crystallographic defects that could be distinguished were limited to those which affect the general crystal shape.[12]

Both mechanical and reactive polishing were applied to samples of the low pressure CVD grown polycrystalline diamond films. Using successively finer levels of diamond abrasive grit on a rotating wheel with oil, a final surface roughness of ± 30 nm was obtained by mechanical polishing. The secondary electron images of the unpolished and mechanically polished surfaces in Fig. 1 show no microstructural detail beyond the surface topology, with some indication of grain boundaries and porosity in the polished surface.

High temperature iron metal polishing was also applied to the surface of several polycrystalline diamond films, by contacting the diamond surface with iron metal at a temperature of 725–750 °C in 20–80 Torr of hydrogen for 1 h. The hot iron contacting the diamond surface isotropically removes carbon as iron carbide, which is subsequently vaporized by the hydrogen atmosphere as methane. The details of the polishing approach are described elsewhere.[11,12] Following the reactive polish, the samples were cleaned by immersion in concentrated HF at 40 °C in a sonic bath. After cleaning, no residual iron was observable on the surface by energy dispersive x-ray fluorescence or x-ray photoelectron spectroscopy. Raman analysis of the reactively polished and HF washed surfaces showed no observable increase in $sp2$ bonded carbon from the procedures.

The areas of the diamond film brought into contact with the iron achieved a high level of smoothness as shown by the secondary electron micrographs in Fig. 2 taken at an incidence angle of 60° to the uncoated specimen. The micrograph provides topographic detail, but is incapable

 0003-6951/93/243105-03$06.00

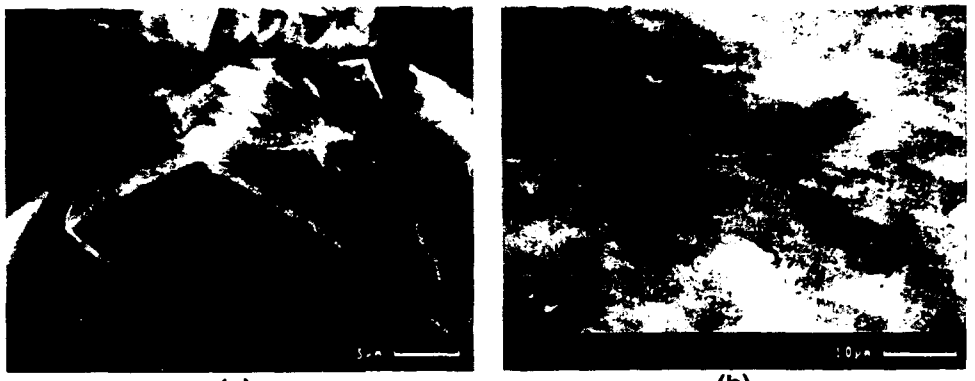

FIG. 1. Secondary electron micrographs of a polycrystalline diamond film (a) before and (b) after mechanical polishing.

of resolving the surface roughness or fine scale microstructure.

Normal incidence secondary electron imaging of the reactively polished regions of the uncoated diamond revealed a time and beam voltage dependent electron contrast. At voltages above 3 keV, well-resolved regions of dark contrast develop within a few seconds to clearly define the defect microstructure in the near-surface regions of the film. Figures 3 and 4 show two separate regions on the same diamond film with significantly different microstructures. Figure 3 shows a 35-μm-wide region of the film with a random polycrystalline microstructure. Densely joined individual 3–5 μm sized grains are visible with parallel dark lines defining the presence of twin structures in the more lathlike grains (far right center). In Fig. 4, however, the characteristic low pressure diamond, fivefold defect[6] is clearly defined in a 15–20-μm-wide crystalline grain, which also shows extensive twinning. This defect is formed by the successive generation of multiple twins on the {111} planes in the ⟨211⟩ direction around the ⟨011⟩ axis. Twinning is also visible in the other polished regions of the sample as is the gross morphology of the unpolished areas.

Regions up to 12 by 12 μm^2 of the reactively polished surface were imaged by atomic force microscopy (AFM) to obtain a quantitative measure of the surface roughness and atomic scale topography.[13] AFM imaging revealed that the reactive polishing technique had removed the "tops" of exposed diamond facets, leaving flattened surfaces with roughness of 1–2 nm rms. The AFM images did not resolve any of the fine scale defect or grain boundary microstructure in the polished regions.

The direct observation of the defect microstructure of grains in a polycrystalline diamond film by secondary electron imaging in a scanning electron microscope has been demonstrated. The beam voltage and time dependence associated with the appearance of the images clearly shows them to be produced by a charge-induced electron contrast in the generally insulating uncoated films. It is hypothesized that the ability to form the images results from the high degree of smoothness produced in the samples by reactive iron polishing and the extreme nonconductive nature of diamond. To the authors' knowledge, the observation of this level of microstructural detail by SEM has not been achieved with other materials and may be unique to diamond.

Normal mechanical polishing [Figs. 1(a) and 1(b)] leaves sufficient surface roughness that the electron-beam-induced charging in the uncoated samples is distributed over the surface and the electron contrast image is dominated by

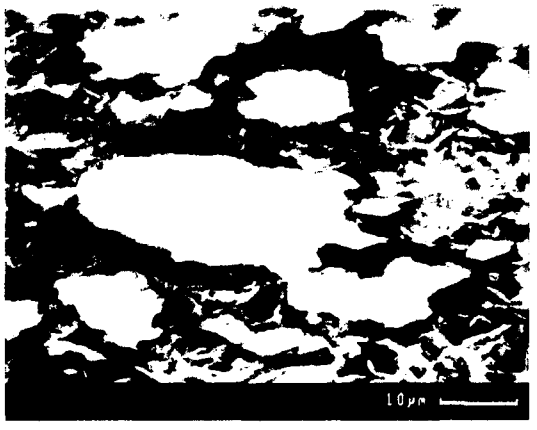

FIG. 2. Secondary electron image taken at an incident angle of 60° to the diamond sample polished by hot-iron metal

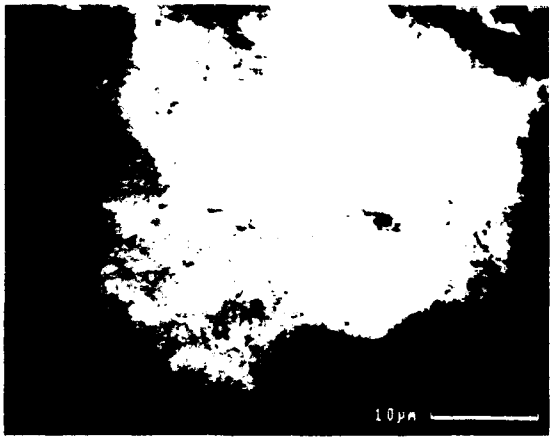

FIG. 3. Secondary electron micrograph taken at normal incidence to a iron metal polished region of the diamond sample.

FIG. 4. Secondary electron micrograph of the defects in a single crystalline grain of a polycrystalline diamond film.

the surface topology. When the reactive iron polishing process has been applied, the variations in conductivity associated with the defect structures and grain boundaries become clearly apparent. The beam voltage and time dependence of the image demonstrates that charge development is required, and indicates a high degree of connectivity between the regions of charge dissipation.

The level of differential charge accumulation in the polished diamond surface is sufficient to provide defect contrast only in the low energy secondary electron image. Under backscatter electron imaging, the higher energy electrons are far less susceptible to the charge distribution and the defect contrast is not apparent.

It is apparent that the crystallographic defects, grain boundaries, and regions of impurities or sp^2 bonding act as connected charge dissipation paths for the highly insulating diamond surface and produce the high resolution detail of the crystalline microstructure. This imaging is possible because of the extremely low conductivity of diamond, but may generalize to other nonconductive materials if appropriate polishing techniques are available to achieve the required surface smoothness.

Developing growth process control over the crystalline microstructure of synthetic diamond is critical to its eventual application as an electronic and optical material. To accomplish this, microscopic characterization of the crystallography and defect structure is required. The SEM microstructural characterization of diamond after hot-iron reactive polishing can be applied to both thin and thick samples and is nondestructive to the sample. The characterization technique should provide valuable insights in process optimization studies and in establishing the relationships between synthetic diamond properties and microstructures.

This work was sponsored by the Office of Naval Research.

[1] K. V. Ravi, J. Mater. Res. 7, 384 (1992).
[2] K. Okada, S. Komatsu, S. Matsumoto, and Y. Moriyoshi, J. Mater. Sci. 26, 3081 (1991).
[3] A. B. Harker and J. F. DeNatale, J. Mater. Res. 5, 818 (1990).
[4] W. Zhu, A. R. Badzian, and R. Messier, J. Mater. Res. 4, 659 (1989).
[5] D. Shechtman, E. N. Farabaugh, L. H. Robbins, and A. Feldman, Proc. SPIE 1325, 26 (1990).
[6] J. Narayan, A. R. Srivatsa, M. Peters, S. Yokota, and K. V. Ravi, Appl. Phys. Lett. 53, 1823 (1988).
[7] A. R. Lang and M. Moore, *New Diamond Science and Technology*, edited by R. Messier, J. T. Glass, J. E. Butler, and R. Roy (Materials Research Society, Pittsburgh, PA, 1991), pp. 683–694.
[8] K. Nishimura, J. S. Ma, Y. Yokota, Y. Mori, H. Kotsuka, T. Hirao, M. Kitabatake, M. Deguchi, K. Ogawa, G. Ning, H. Tomimori, and A. Hiraki, Proc. SPIE 1534, 199 (1990).
[9] I. Sunagawa, J. Cryst. Growth 99, 1156 (1990).
[10] A. B. Harker and J. F. DeNatale, Proc. SPIE 1534, 2 (1990).
[11] M. Yoshikawa, Proc. SPIE 1325, 210 (1990).
[12] J. F. DeNatale, A. B. Harker, and J. F. Flintoff, J. Appl. Phys. 69, 6456 (1991).
[13] D. A. Chernoff and H. Windischmann, J. Vac. Sci. Technol. A 10, 2126 (1992).

Appendix 16

Charge-Sensitive Secondary Electron Imaging of Diamond Microstructures

SCANNING Vol. 16, 87–90 (1994)

Received October 1, 1993

Charge-Sensitive Secondary Electron Imaging of Diamond Microstructures

A.B. HARKER, D.G. HOWITT,* J.F. DENATALE, J.F. FLINTOFF

Rockwell International Science Center, Thousand Oaks, *Department of Chemical Engineering and Materials Science, University of California at Davis, Davis, California, USA

Summary: The surface orientation and detailed defect microstructure of polycrystalline diamond can be observed in a scanning electron microscope through local changes in the surface conductivity. The electron contrast in uncoated samples is straightforward to distinguish when the rms surface roughness is less than about 2 nm. This degree of smoothness occurs on some of the faceted surfaces of individual diamond grains but can also be achieved by polishing. The contrast, observable only in the secondary electron imaging mode, shows a strong dependence on both beam voltage and current. It is postulated that the contrast is produced solely by the differential rate at which the electron beam-induced charge can be locally dissipated through crystalline defects and grain boundaries in the otherwise highly nonconductive diamond matrix. The appearance of the charge-related contrast requires that highly connected pathways exist between the crystalline defects and the high-angle grain boundaries.

Key words: diamond, microstructure, defects, imaging, charging

Extensive characterization has been carried out on the growth morphology and crystalline defects that occur in polycrystalline diamond films formed by low-pressure plasma-assisted chemical vapor deposition (PACVD) (DeNatale *et al.* 1991, Hetherington *et al.* 1990, Zhu *et al.* 1989). Observation of the diamond film microstructure has been critical in establishing the relationships between growth parameters and the resulting electrical, optical, mechanical, and thermal properties of the material. These studies have been limited primarily to transmission electron microscopy (TEM) of thin foils (Zhu *et al.* 1989), electron- and photon-induced fluorescence of electronic defects (Collins 1991, Yacobi *et al.* 1991) and interpretations based on the relationships between general morphology and the crystal structure (Ravi 1992). Recently we reported a charge-induced contrast imaging technique for observing the detailed microstructure of the diamond growth surface (Harker *et al.* 1993).

Scanning electron microscopy (SEM) investigations of diamond and other nonconducting materials are usually either conducted at low voltage or the sample surfaces are coated with a very thin conductive layer of carbon or gold for sample grounding. These techniques are employed because, when an insulating specimen such as diamond is exposed to an electron beam, a surface charge imbalance occurs which can inhibit secondary electron imaging of surface detail. The surface charging occurs because of the difference between the rate at which electrons are deposited into the specimen interior from inelastic scattering processes and the rate at which secondary electrons escape from the surface. The detailed nature and beam voltage and the current density dependence of the charging processes are related to both the intrinsic secondary electron yield of the material being examined and the microscopic homogeneity of the particular specimen.

When an uncoated, relatively rough, polycrystalline diamond sample is examined at electron beam voltages below the point at which strong surface charging occurs, the secondary electron image is dominated by the sample topography. This can be seen in the SEM image in Figure 1 taken at 3 keV. In the micrograph the (111) faces of individual crystallites are well resolved, and local regions of twinning can be distin-

This work was sponsored by the Office of Naval Research.

Address for reprints:

Alan B. Harker
Science Center
Rockwell International Corporation
1049 Camino Dos Rios
P.O. Box 1085
Thousand Oaks, CA 91358, USA

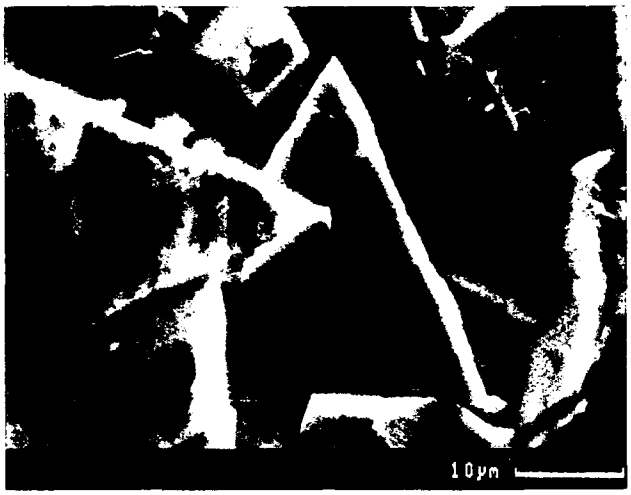

FIG. 1 Secondary electron micrograph recorded at 3 keV from individual (111) faces of grains in an uncoated polycrystalline diamond surface with no surface preparation

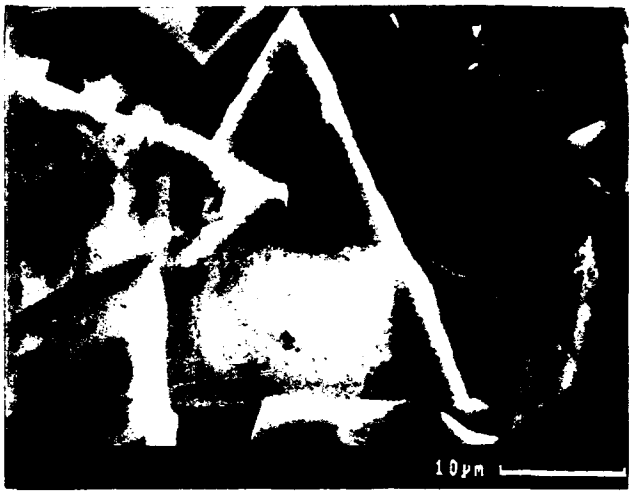

FIG. 2 Secondary electron micrograph of the uncoated polycrystalline diamond shown in Figure 1, recorded at 3 keV after exposure of the central diamond crystallite to the electron beam at 12 keV

guished by the surface contours (characteristic dark parallel lines) on the exposed facets.

Greater detail of the twin generated defect microstructure of the (111) face in the central diamond crystallite is shown in the micrograph in Figure 2, taken by using the charge-induced contrast method. In this micrograph, the beam voltage was first increased to 12 keV and the beam was rastered over the rectangular region of the grain until the enhanced contrast appeared. Before excess charge buildup could occur to obscure the image, the beam voltage was reduced to 3 keV and the micrograph was recorded. Exposure to the 12-keV beam produced a negative charge throughout the specimen which consequently increased the low-energy electron signal to the secondary electron detector from those regions where charge dissipation pathways did not exist. Hence, the regions which maintained this charge appeared brighter and continued to do so until the charge that had been introduced was dissipated. The darker contrast regions, which provide the fine scale detail, are uniquely associated with crystalline defects and the crystallite grain boundaries and must have a higher rate of charge dissipation.

Because of the extreme nonconductive nature of the diamond matrix, once the charge-induced contrast from the surface microstructure had been created, the electron beam voltage could be reduced without immediate loss of detailed contrast. This permitted a high-resolution micrograph to be recorded at 3 keV and avoided excessive charging and loss of contrast.

The charge induced contrast image remains visible at the lower beam voltage for periods of 1–5 min once different surface charges have been established. This ability to sustain the electron image can be attributed to the superior insulating properties of the regions around the defects where the band gap is close to the ideal value of 5.45 eV (Spear 1989). By varying the magnitude of the local charge on the individual faces of a single diamond grain, the details of the near surface microstructure can be brought into sharp contrast as shown in the higher magnification image in Figure 3. The fine-scale twins which intersect the (111) crystal face are clearly resolved, and these time-dependent images can be reversibly generated or eliminated by increasing or decreasing the beam voltage or current.

The charge induced contrast is apparent, in as-grown polycrystalline diamond films, only for those grains which exhibit highly smooth faceted surfaces. Hence, it was postulated that in order to distinguish the microstructure of a broad region of the film it

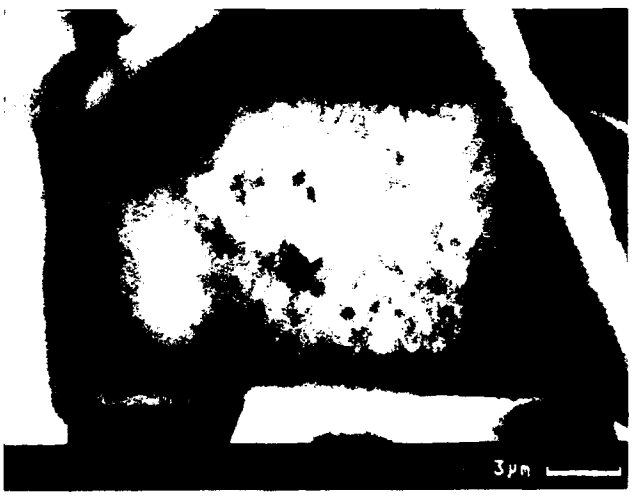

FIG. 3 Higher magnification secondary electron image of the twin defects in the (111) face in a diamond grain exhibiting the charge enhanced electron contrast.

would be necessary to remove the general topography by fine-scale polishing. However, secondary electron images recorded from a mechanically polished polycrystalline diamond surface did not exhibit the charge-enhanced contrast effect. The samples had obtained a 30–40 nm roughness after extensive polishing with successive size ranges of diamond abrasive with an oil lubricant. The secondary electron contrast of the uncoated polished samples was dominated by the topography from the general polishing damage and the grain boundaries.

Polycrystalline diamond films were also polished by contacting their surfaces with a hot iron plate at temperatures above 725°C in 80 torr of hydrogen. The reaction of the iron with the diamond in the hydrogen atmosphere converts the solid carbon to gaseous methane and acts to polish the surface to a very fine scale (Harker 1991, Yoshikawa 1990). Atomic force microscopy shows the polishing technique to be capable of producing a subnanometer surface rms roughness (Harker 1993). Figure 4 shows a secondary electron micrograph of such a polished surface taken at a 60° angle of incidence. The polished regions appear as mesas in the generally faceted diamond topography and have an rms roughness below 2 nm, as determined by atomic force microscopy.

Imaging the mesa regions with a normal incidence beam, after increasing and decreasing the beam voltage from 3 to 12 keV and then back to 3 keV, produces the more detailed charge-enhanced contrast. The micrograph in Figure 5a, recorded at normal incidence at 3 keV after exposure to the electron beam at 12 keV, shows a 20 micron wide polished region with fine-scale grain structure and low defect density.

Figure 5b is a micrograph of another polished region of the same sample. In this region an individual 10 micron crystallite has its microstructure dominated

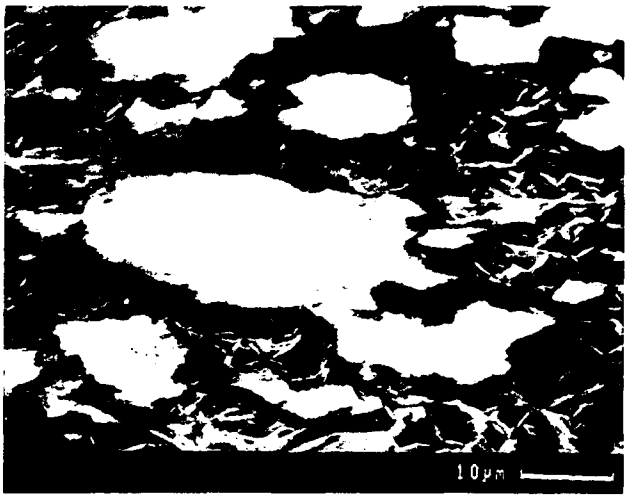

FIG. 4 Micrograph of highly polished "mesa" regions in a polycrystalline diamond film produced by contact with iron in a hydrogen atmosphere at T > 725°C.

by the characteristic fivefold reentrant twin characteristic of low pressure CVD diamond films (Ravi 1992). This defect is formed by the successive generation of multiple twins on {111} planes in the ⟨211⟩ direction around an ⟨011⟩ axis. Twinning is also visible in the other polished regions of the sample and contributes as well to the morphology of the unpolished areas. For comparison, a high-magnification TEM micrograph of a more clearly defined fivefold twin configuration is shown in Figure 6, taken from a free-standing 200 nm thick diamond film.

The differential charge accumulation that occurs in the polished diamond surface produces detectable defect contrast only in the low-energy secondary electron imaging mode. The differential surface charging has little effect on the more energetic electrons ob-

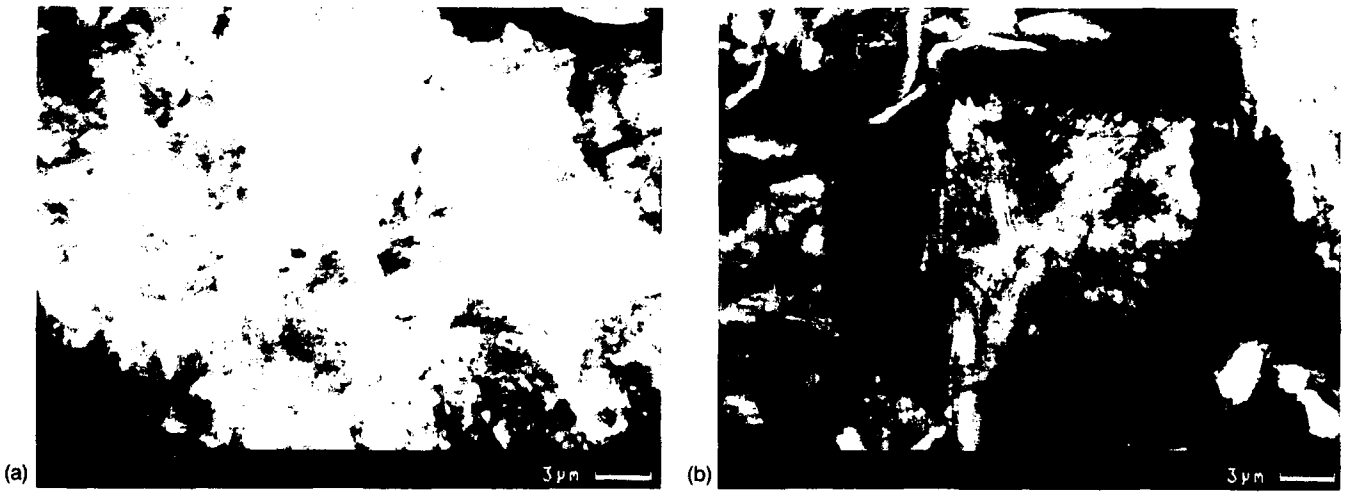

FIG. 5 (a) Secondary electron micrograph taken at 3 keV, showing the fine grain structure of a polished CVD diamond surface after exposure to a 12 keV electron beam. (b) Secondary electron micrograph taken at 3 keV after 12 keV exposure, showing the fivefold twin defect characteristic of CVD diamond.

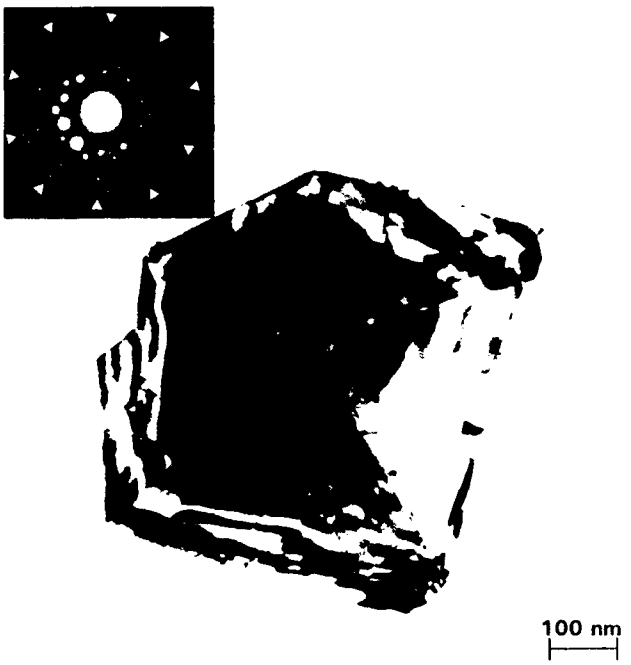

FIG. 6 TEM micrograph showing the detailed microstructure of the fivefold reentrant twin defect in a 200 nm thick CVD diamond.

served in the backscattered imaging mode. In addition, there is very little channeling contrast from the different crystallographic orientations of the grains in the backscatter mode, which provides far less resolution of the surface microstructure than is provided by the charge-induced contrast.

The observation of the charge-induced contrast over general areas of the diamond films argues that the grain boundaries and defects act not only to accelerate the rate of charge dissipation locally but also combine to provide an interconnected pathway to ground the specimen. Thus many of the {111} twins either are interconnected or pass fully through the individual crystallites to intersect with the high-angle grain boundaries.

Although the charge-induced contrast technique has been explored only with polycrystalline diamond film samples, it is probably not unique to this material. It is quite likely that defects present in any insulator can be revealed by this technique if sufficient flatness can be achieved on the surface. In this application, however, we have been able to use the technique to observe nondestructively the changes in the defect microstructure in diamond films as a function of growth conditions and film thickness. Individual grains with highly smooth facets can be characterized with no sample preparation, and regions up to several square mm can be imaged with less than an hour of polishing by the reactive iron contact approach. The characterization technique should provide valuable insights into the continuing development of polycrystalline diamond films for optical and electronic applications.

References

Collins AT: Optical centers in synthetic diamond—a review. In *New Diamond Science and Technology* (Eds. Messier R, Glass JT, Butler JE, Roy R). Materials Research Society, Pittsburgh, Penna. (1991) 659–670

DeNatale JF, Harker AB, Flintoff JF: Microstructure and orientation effects in diamond thin films. *J Appl Phys* 69 (9), 6456–6460 (1991)

Harker AB: Reactive polishing of polycrystalline diamond and measured spectroscopic properties. In *Applications of Diamond Films and Related Materials* (Eds. Tzeng Y, Yoshikawa M, Murakawa M, Feldman A). Elsevier Science Publishing B.V., Amsterdam (1991) 223–226

Harker AB, DeNatale JF, Flintoff JF, Breen JJ: Direct observation of the defect structure of polycrystalline diamond by scanning electron microscopy. *Appl Phys Lett* 62 (24), 3105–3107 (1993)

Hetherington AV, Wort CJH, Southworth P: Crystalline perfection of chemical vapor deposited diamond films. *J Mater Res* 5 (8), 1591–1594 (1990)

Ravi K: Morphological instabilities in the low pressure synthesis of diamond. *J Mater Res* 7 (2), 384–393 (1992)

Spear KE: Diamond—ceramic coating of the future. *J Am Ceram Soc* 72 (2), 171–191 (1989)

Yacobi BG, Badzian AR, Badzian T: Cathodoluminescence, raman spectroscopy and infrared absorption of diamond films. In *New Diamond Science and Technology* (Eds. Messier R, Glass JT, Butler JE, Roy R). Materials Research Society, Pittsburgh, Penna. (1991) 695–701

Yoshikawa M: Development and performance of a diamond film polishing apparatus with hot metals. *Proc SPIE* 1325, 210–221 (1990)

Zhu W, Badzian AR, Messier R: Structural imperfections in CVD diamond films. *J Mater Res* 4 (3) 659–663 (1989)

Appendix 17

Temperature Dependence of Absorption in CVD Diamond

Temperature dependence of absorption in CVD diamond

Michael E. Thomas

The Johns Hopkins University Applied Physics Laboratory
Laurel, Maryland 20723

Alan B. Harker

Rockwell International Science Center
Thousand Oaks, California 91360

ABSTRACT

The infrared transmittance of a high-optical-quality chemical vapor deposition (CVD) diamond sample was independently measured by The Johns Hopkins University Applied Physics Laboratory, Rockwell International, and Texas Instruments, Inc., from room temperature to 780 K. At 0.745 mm thick, the sample is one of the thickest high-optical-quality CVD diamond samples produced so far. Measurements were taken with both dual-beam grating spectrometers and a Fourier transform spectrometer so that experimental artifacts of a particular instrument could be identified and reduced. The data sets were in good agreement from room temperature to 780 K. This work definitively establishes the high-temperature optical properties of CVD diamond.

Keywords: CVD diamond, temperature, absorption coefficient

1. INTRODUCTION

Transmission measurements on thin samples of diamond in their transparency range are difficult to make accurately. Temperature-dependent measurements are problematic because the furnace used to heat the sample is a source of stray radiation. In single-beam spectrometers, the sample can move, and the characteristic time interval between sample and reference runs leads to degradation of baseline stability. Dual-beam spectrometers, which are typically grating spectrometers, have good absolute baseline stability, but are limited in throughput for even moderate-resolution runs. The Fourier transform spectrometer (FTS) has good throughput and high signal-to-noise performance, but it is a single-beam system and sensitive to baseline drift. Thus, for complete, accurate characterization, each sample should be measured by multiple spectrometers.

In the study reported here, The Johns Hopkins University Applied Physics Laboratory (JHU/APL), Rockwell International Science Center, and Texas Instruments, Inc. (TI), carried out temperature-dependent measurements on a single chemical vapor deposition (CVD) diamond sample using different spectrometers. The sample was manufactured by Raytheon. The study objective was to experimentally establish the high-temperature optical properties of CVD diamond on the basis of multiple data sets. The sample was 0.745 mm thick and displayed good optical quality (low scatter). The JHU/APL measurements were made on an FTS. Rockwell and TI used dual-beam grating instruments. Measurements were taken from room temperature to 500°C.

2. EXPERIMENTAL PROCEDURE

2.1 Dual-beam spectrophotometric measurements

The transmission experiments at Rockwell were carried out in a commercial Perkin Elmer Model 983 dual-beam multi-grating spectrophotometer, equipped with reflectance and high-temperature transmission accessories. The PE-983 system uses four gratings and order-sorting filters to provide a scanning bandwidth from 5000 to 280 cm^{-1}. The instrument maintains a uniform signal-to-noise ratio across this spectral region by automatically adjusting the input slits to the monochromator section. This feature reproducibly changes the resolution of the instrument in different spectral regions. Under the operating conditions used with our sample, the approximate resolution in each spectral region was:

Wave number (cm^{-1})	Slit (mm)	Resolution (cm^{-1})
4000	0.652	24.7
3000	0.652	13.3
2000	0.469	12.0
1000	1.310	7.8
800	2.294	8.0

The sample was mounted for heating in the center of a 10-cm commercial SPECAC high-temperature transmission vacuum cell with water-cooled walls and ZnSe windows. The observation field of view was restricted so that transmitted light was collected from the central portion of the sample through a 0.5-cm aperture placed 6 cm from the sample. The temperature of the cell could be ramped to 475°C and maintained within ±1°C.

The measurement procedure was subject to error because the high-temperature cell had to be demounted and remounted for sample insertion. To eliminate any non-reproducibility in the cell alignment, a dual-beam spectrum of the sample was collected in the standard transmission mode and again at room temperature after the sample and vacuum cell were mounted. The ratio of these two spectra provided a normalization function for correcting the background spectrum of the elevated-temperature runs. To verify the validity of this normalization procedure, backgrounds measured with an empty vacuum cell at each temperature were compared with those collected with no cell. The spectra showed no systematic deviations from the "no-cell" background other than a constant multiplier over the spectral range of 4000 to 700 cm^{-1}. At longer wavelengths, there were systematic errors due to emitted radiation from the empty vacuum furnace.

Individual infrared spectra were collected at 22, 300, 400, and 475°C and recorded at five wave number intervals. No digital averaging was applied to the individual points and no attempt was made to improve the statistics through spectrum averaging. Three replicate measurements of the transmission spectrum of the diamond at 475°C showed the measurements to be reproducible within the signal-to-noise ratios of the individual measurements.

Transmission measurements at Texas Instruments were performed with a Perkin Elmer Model 883 infrared spectrophotometer in double-beam mode. The instrument uses pre- and post-sample choppers and a phase-lock detection scheme to detect only the transmission of the source light and not the sample emission. Room-temperature transmission was measured using matching 11-mm-diameter circular apertures at the sample and reference mounts. For the elevated-temperature measurements, the sample was mounted within an evacuated cell with CsI windows that housed a helical cable heater. The transmission of the empty cell varied less than 2% with temperature. Custom-fitted 1-mm-thick copper rings around the sample ensured precision mechanical contact between sample and heater. Temperature was measured via a thermocouple attached to one of the rings. The sample temperature as a function of ring temperature was measured separately and the relationship was used to determine the sample temperature during the transmission measurement to within 20°C.

The monochromator program was set to maximize the signal-to-noise ratio for a 146-s scan from 4000 to 200 cm^{-1}. The resulting slit program yielded a resolution similar to that obtained with the PE 983 used by Rockwell. Each measurement was an average of four scans at temperature. The high-temperature transmission measurements were normalized by the transmission of the empty cell at the same temperature to eliminate cell-induced transmission features. The resulting error in transmission or wave number above 400 cm^{-1} was approximately ±0.5%, corresponding to an extinction coefficient error for this sample of ±0.1 cm^{-1}. A few artifact absorption bands introduced by the monochromator were as strong as 0.3 cm^{-1} but were narrow and well separated from the two- and three-phonon features. Errors in determining the real average thickness of the wedged sample contributed to an error in the magnitude of the absorption coefficient of about 2%.

2.2 Fourier transform spectrometric measurements

The transmission measurements at JHU/APL were made with a BOMEM DA3.02 Fourier transform spectrometer configured with a globar source, a Ge on KBr beamsplitter, and a MCT detector. The spectral range obtainable with this configuration is 500 to

5000 cm^{-1} (2-20 μm). A quartz–halogen lamp, quartz beamsplitter, and Si detector are used for near-infrared/visible measurements. The entire optical path of the spectrometer can be purged or evacuated. Room-temperature measurements are taken in the purge mode, which minimizes the time between reference and sample spectra. System drift, which affects baseline stability, is also minimized when the time between measurements is small.

Heated samples are measured in the vacuum mode, which improves the performance of the furnace and prevents oxidation of the diamond samples. The furnace is a commercially available cell from SPECAC capable of operating from room temperature to 800 K. The sample temperature is monitored via a chromel/alumel (type K) thermocouple directly inserted into the stainless steel cell. Water lines supply cooling water to a jacket between the furnace and the outer body of the cell, which is designed to suppress heating of the outer body and reduce cell movement. The cell holds samples up to 1 in. in diameter and up to 0.25 in. thick. Typical vacuum levels in the sample compartment are 0.8 to 0.5 torr. Since sample heating is slow (about 1.5 h to heat the sample from room temperature to the highest temperature), the transmittance baseline can drift significantly (on the order of a few percent), reducing the accuracy of the heated sample measurements. A post-data-collection baseline correction is required in these cases. The resolution for these experiments is typically 4 cm^{-1} (0.04 μm at 10 μm).

The two main difficulties to be overcome with this single-beam system are (1) the effect of backward radiation from the furnace towards the interferometer and (2) cell motion. Front and back cold shields on the furnace prevent furnace radiation from illuminating the detector and the interferometer, and a wire screen attenuator between the furnace and the interferometer further restricts backward radiation from the furnace that could lead to detector saturation. Backward radiation from the furnace towards the interferometer returns modulated in the opposite sense of the main interferogram from the globar source. The resulting signal reduction becomes significant at approximately 7 μm and increases at longer wavelengths. This effect has been reported in other experiments,[1] including those employing grating spectrometers, but is not often appreciated as an experimental artifact.

We used two measurement approaches to attempt to compensate for these anomalies. First, we inserted small- and medium-aperture cold shields between the cell and interferometer. The small-aperture cold shield effectively blocked the cell radiation, but cell motion became a factor, leading to a uniformly depressed baseline as a function of temperature (Fig. 1a). We could eliminate cell motion distortions by using a larger aperture, but cell radiation then affected the measurements (Fig. 1b). The figures show the magnitude of the baseline reduction with temperature for the two apertures. In each case, the system ratioed a reference room-temperature transmission measurement with no sample present to a transmission measurement with the empty cell at the temperature listed in the figure. We used these curves to correct our transmittance measurements at temperatures above 500 K in the 8- to 20-μm region.

For the JHU/APL study, the diamond samples were contained in a nickel holder with a clear aperture of 7 mm. We first collected a reference spectrum with no sample present, and then measured transmittance with the sample at the focus of a 3.5-mm-diameter f/4 beam.

3. DATA ANALYSIS

Transmittance measurements can used to obtain the extinction coefficient β_{ext}, which is the sum of the absorption coefficient β_{abs} and the scatter coefficient β_{sca} when single scatter occurs. A straightforward procedure can be applied in the case of diamond because it has low dispersion in the infrared.

The specular transmittance τ through a medium of refractive index n, is given by

$$\tau[n(\nu),\theta_i] = \frac{\{1 - R[n(\nu),\theta_i]\}^2 e^{-\beta_{ext}(\nu)d(\theta_i)}}{1 - R^2[n(\nu),\theta_i]e^{-2\beta_{ext}(\nu)d(\theta_i)}} \tag{1}$$

where ν is the wave number, d is the thickness of the medium, θ_i is the angle of incidence, R is the single-surface power reflection coefficient, and

$$d(\theta_i) = d/\cos\left[\sin^{-1}\left(\frac{1}{n}\sin\theta_i\right)\right] \tag{2}$$

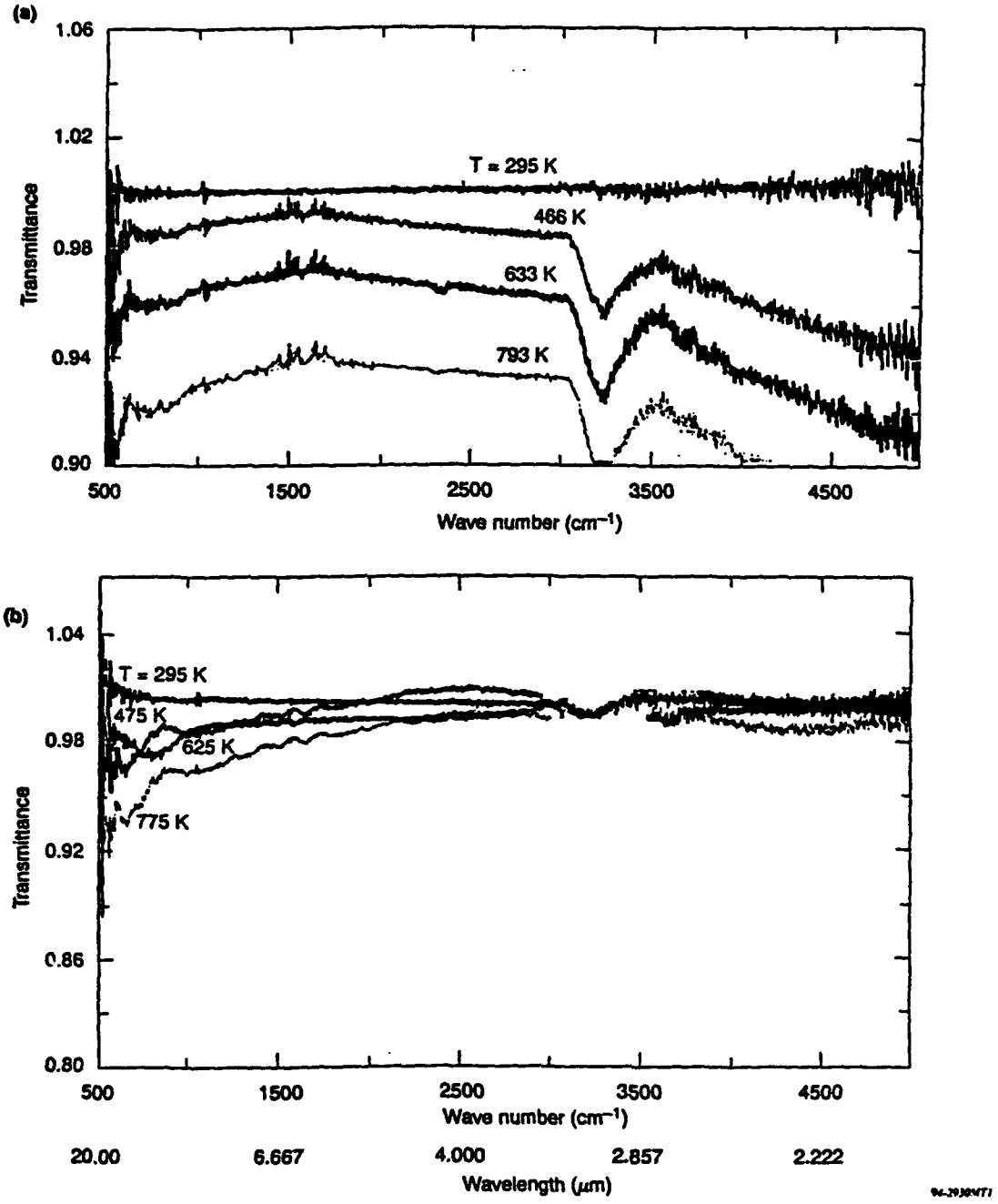

Figure 1. Transmittance baseline measurements on a Fourier transform spectrometer as a function of cell temperature for (a) a small aperture and (b) a large aperture between the cell and interferometer.

All measurements are made near the normal so that $\theta_i = 0$ and the distance traveled in the medium essentially is the sample thickness. If we assume that R^2 is small and $\exp(-\beta_{ext} d)$ is close to 1, then the transmittance can be expanded to become

$$\tau = \frac{1-R}{1+R} e^{\beta_{ext} d} - \frac{R^2 (1 - e^{-2\beta_{ext} d}) e^{-\beta_{ext} d}}{(1+R)^2} + \ldots \qquad (3)$$

Because R is basically constant with frequency over the experimental range (500 to 5000 cm^{-1}), this formula can be used to directly reduce the transmittance to the extinction coefficient. For diamond, the ratio $(1 - R)/(R + 1)$ (the lossless transmittance) is 0.714. The last term of the expansion is small, typically less than 1% unless the absorption is strong, which is never true for measurements on thin samples.

4. RESULTS

Figure 2 displays the spectrometer measurements on a CVD sample at room temperature, including laser calorimetry measurements obtained at 10.6 μm.[2] It is interesting to note that the calorimetry data range over the same values as the transmittance data. All measurements agree closely in the two-phonon region (the TI data are slightly lower). In the three-phonon region, the JHU/APL measurements are slightly higher. (The Rockwell and TI data end at 4000 cm^{-1}.) The four-phonon band is observed in one of the APL measurements. However, scattering generally masks the weak four-phonon band in CVD diamond, and a second scan of a region of the sample with higher scatter does not show the band structure. Figure 2 establishes the consistency of the different room-temperature measurement techniques used by JHU/APL and Rockwell for obtaining the absolute extinction coefficient.

Figures 3 and 4 compare extinction coefficients collected at intermediate temperatures. Agreement is reasonably good, although the APL data are consistently lower than Rockwell's because they were measured at a lower temperature.

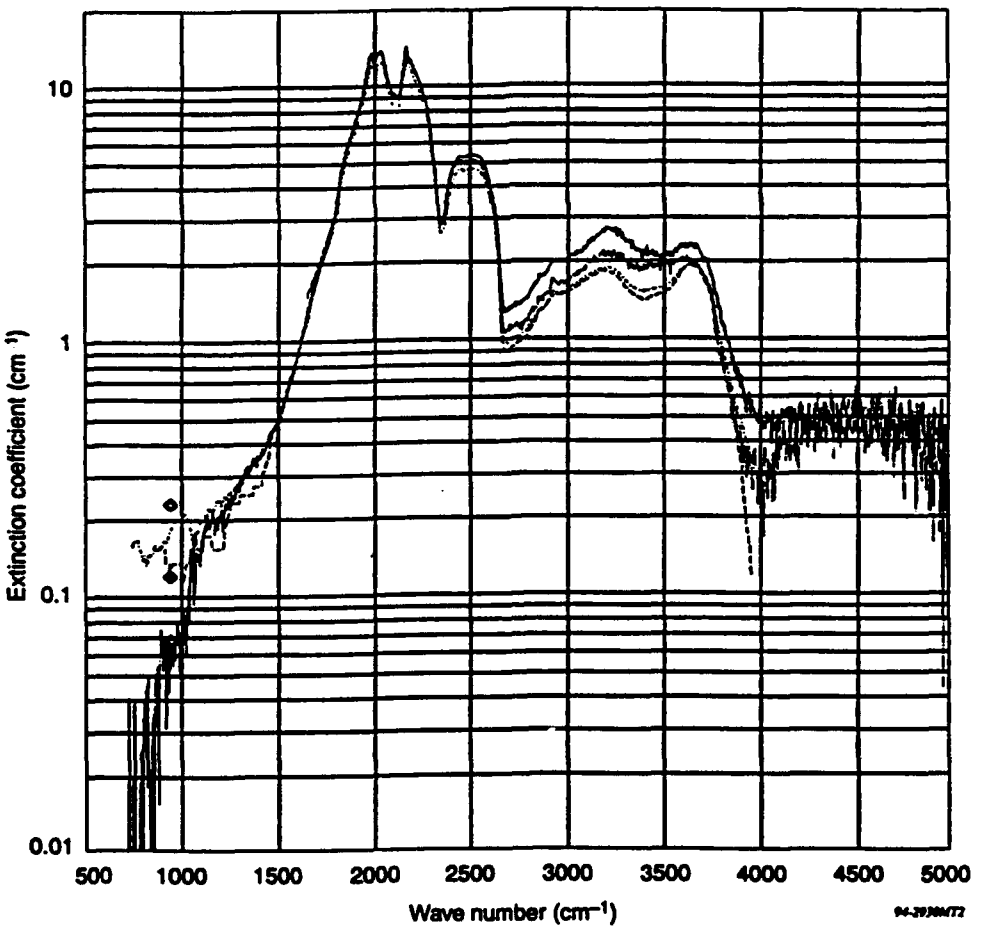

Figure 2. Comparison of spectrometer measurements by JHU/APL (solid and dotted lines), Rockwell (dashed line), and Texas Instruments (dash-dot line), and laser calorimetry measurements at 944 cm^{-1} (◊) of the extinction coefficient of a common CVD diamond sample at room temperature.

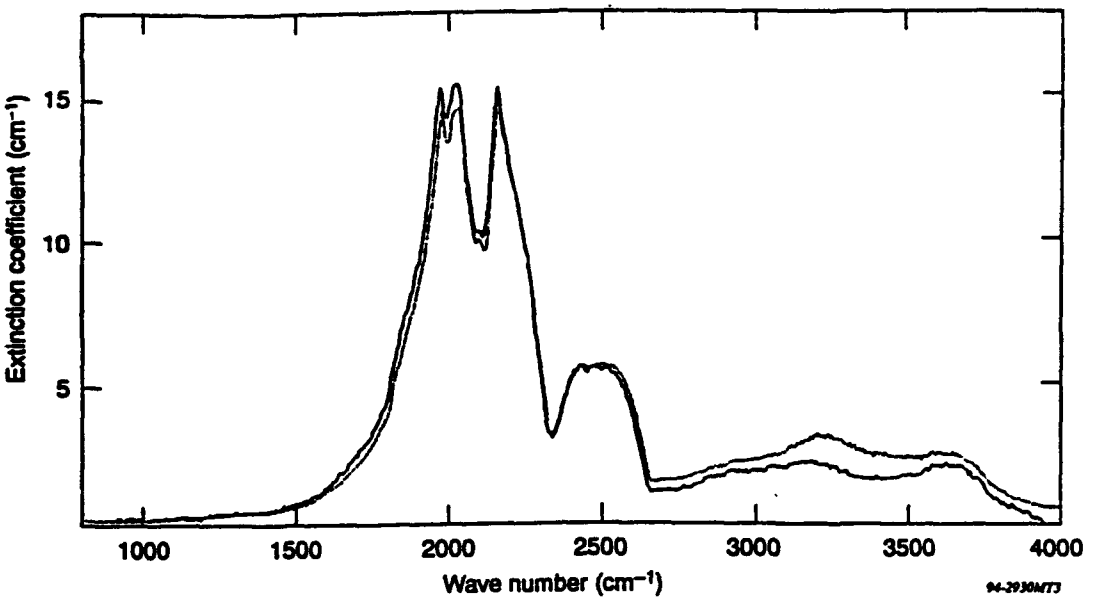

Figure 3. Temperature-dependent extinction coefficient of a common CVD diamond sample versus wave number at 573 K and 476 K (Rockwell–solid line, JHU/APL–dotted line).

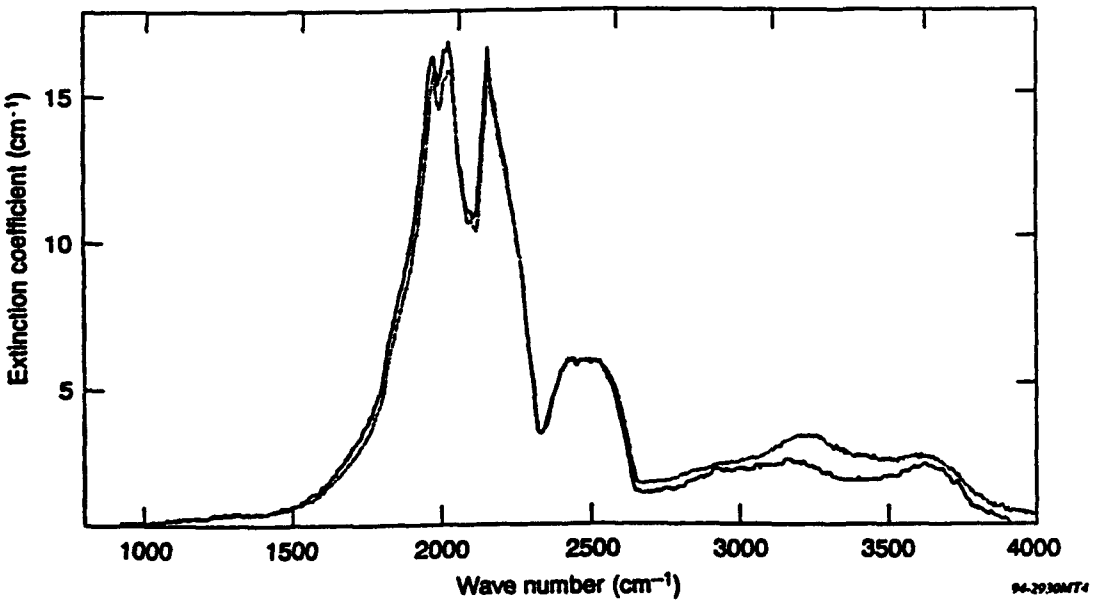

Figure 4. Temperature-dependent extinction coefficient of a common CVD diamond sample versus wave number at 673 K and 629 K (Rockwell–solid line, JHU/APL–dotted line).

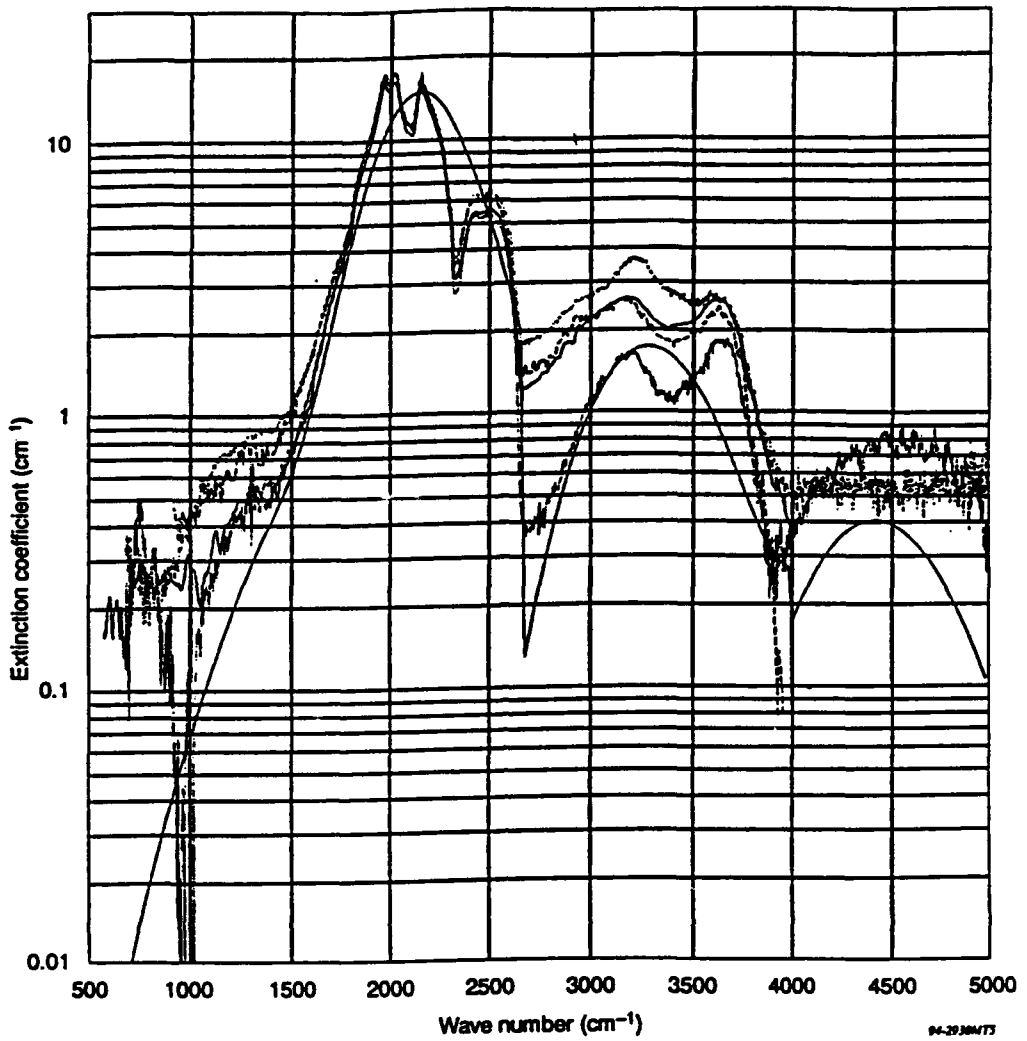

Figure 5. Comparison of spectrometer measurements by JHU/APL (dash-dot line, 788 K), Rockwell (dashed line, 748 K), and TI (solid line, 743 K) of the extinction coefficient of a common CVD diamond sample. The coefficient for experimental natural type IIa diamond (dotted line, 771 K) and the APL multiphonon model absorption coefficient (solid, smooth curve) are also shown.

Figure 5 compares JHU/APL, Rockwell, and TI measurements of the extinction coefficient at temperatures around 770 K. The values of the APL and Rockwell measurements in the two-phonon region are very close; the TI results are slightly lower. The peak value is approximately 17.5 cm^{-1}. In the three-phonon region, the Rockwell and TI data agree closely and the JHU/APL data are slightly higher. This trend was also observed at room temperature. The figure also shows the experimental absorption coefficient of natural type IIa diamond measured at JHU/APL. The type IIa diamond absorption coefficient data form a lower bound to the CVD results, as expected. The JHU/APL multiphonon model for diamond absorption[3] is shown by the solid, smooth curve in the figure. It underpredicts the experimental attenuation of CVD diamond, partly because the model does not include scatter.

5. CONCLUSIONS

Transmittance measurements on a common CVD diamond sample by different facilities were in good agreement, establishing the high-temperature (up to 800 K) infrared extinction coefficient of CVD diamond. These measurements are difficult because of background noise in the 10-μm region.

6. ACKNOWLEDGMENTS

The authors wish to thank Dr. John Trombetta of Texas Instruments, Inc., for providing data on sample D383-02.

7. REFERENCES

1. S. P. McGeoch, D. R. Gibson, and J. A. Savage, "Assessment of type IIa diamond as an optical material for use in severe environments," *Proc. SPIE–Window and Dome Technologies and Materials III*, Vol. 1760, pp. 122-142, 1992.
2. Private communication with Dr. Daniel Harris, Head, Optical & Electronics Materials Branch, Naval Air Weapons Center, China Lake.
3. M. E. Thomas, "Multiphonon model for absorption in diamond," *Proc. SPIE–Window and Dome Technologies and Materials IV*, this proceedings (Vol. 2286), 1994.

Appendix 18

Investigations of Stress in Polycrystalline Diamond

NISTIR 5418

Workshop on Characterizing Diamond Films III

February 23-24, 1994
Gaithersburg, MD

Albert Feldman
National Institute of Standards
and Technology

Sandor Holly
Rockwell International

Claude A. Klein
C.A.K. Analytics

Grant Lu
Norton Diamond Film

U.S. DEPARTMENT OF COMMERCE
Technology Administration
National Institute of Standards
and Technology
Ceramics Division
Materials Science and Engineering Laboratory
Gaithersburg, MD 20899

NIST

INVESTIGATIONS OF STRESS IN POLYCRYSTALLINE DIAMOND

A. B. Harker
Science Center
Rockwell International
P.O. Box 1085
Thousand Oaks, CA 91358

ABSTRACT

Relationships between growth conditions, microstructure and residual stress in microwave plasma assisted CVD grown polycrystalline diamond are being studied by a range of techniques. Characterization tools include angle resolved x-ray diffraction, channeling electron microscopy, convergent beam electron diffraction, and stimulated fluorescence. Thick and thin film samples with one dimensional crystalline orientation are being characterized to isolate microstructural effects.

Abstract submitted for presentation in the NIST Workshop on Stress in Polycrystalline Diamond in February, 1994.